Probing Nanoscale Electronic and Magnetic Interaction with Scanning Tunneling Spectroscopy

Jakob Bork

PhD Thesis at the Department of Physics and Nanotechnology, Aalborg University.

In collaboration with the Nanoscience Department - Klaus Kern, Max Planck Institute for Solid State Research.

Supervisor Lars Diekhöner
Aalborg University.

October 2006 - February 2010

Aalborg University
Department of Physics and Nanotechnology

PROBING NANOSCALE ELECTRONIC AND MAGNETIC INTERACTION WITH SCANNING TUNNELING SPECTROSCOPY

NANOSKALA ELEKTRONISK OG MAGNETISK VEKSELVIRKNING UNDERSØGT MED SKANNENDE TUNNEL SPEKTROSKOPI

1st edition.

Published and distributed by
Department of Physics and Nanotechnology, Aalborg University
Skjernvej 4A, DK–9220 Aalborg Øst.
Phone +45 99 40 92 15. Fax +45 99 40 92 35.
`www.nano.aau.dk`

Typeset in LaTeX2$_\varepsilon$ by the author.

ISBN 978-87-89195-28-5

Abstract

Keywords: *Ultra high vacuum, Scanning tunneling microscopy, Metallic heterostructures, Moiré pattern, Split Kondo resonance, Gold-coated tip, Freely positionable Kondo system, Two-impurity Kondo system, Crossover, Antiferromagnetic coupling*

This thesis is concerned with fundamental research into electronic and magnetic interaction on the nanoscale. From small metallic and magnetic islands and layers to single atoms. The research revolves around magnetic interaction probed through the spectroscopic capabilities of the scanning tunneling microscope (STM). Especially at low temperatures the Kondo resonance is used to probe magnetic interaction with ferromagnetic islands and between two atoms. The latter showing a crossover between Kondo screened atoms and antiferromagnetically coupled atoms close to the quantum critical point. This is related to research in correlated electron materials such as studies of phase transitions in heavy fermion compounds and magnetic interaction in spintronic research.

The capping of cobalt islands on Cu(111) with silver is investigated with STM and photoemission spectroscopy. It is shown that at low coverage the silver preferably nucleates on top of the bilayer high cobalt islands compared to directly on the Cu(111) substrate. Furthermore, the silver forms a combination of a reconstruction and a Moiré pattern which is investigated with low-energy electron diffraction and spectroscopic STM mapping at 6. The heterostructure is found to have very interesting electronic properties. The *d*-related state from the now buried cobalt island is visible through the silver capping layer, but the silver Moiré pattern modulates the spin-polarized cobalt *d*-related state in amplitude, energy position and width. This is related to the *d*-band model for catalytic reactions. The largest change is in the amplitude of the state, however the "reversed" structure of cobalt on Ag(111) show similar properties, but with a large shift in energy instead of amplitude.

The Kondo effect is used to probe magnetic interaction between the aforementioned silver-capped cobalt islands (and additionally gold-capped cobalt islands) and single cobalt atoms positioned on the Moiré pattern. A split Kondo resonance due to the exchange interaction between the island and the atom is observed.

In a more technical section of the thesis, it is shown how a gold-coated STM tip will make the tip apex susceptible to a single cobalt atom. The tip is indented either directly in a Au(111) surface or gold flakes are picked up from cobalt islands on Cu(111). A change in the local barrier height (work function) of the tip-sample junction indicates that the apex is gold-coated and a single cobalt atom can be pickup up. The cobalt atom attached to the tip displays a Kondo resonance formed between the atom and the tip similar to the resonance displayed when the atom is on the surface with a clean tip.

Here, this is used to show how a two-impurity Kondo system consisting of two cobalt atoms, one on the tip and one on the Au(111) sample, is undergoing a continuous crossover from Kondo screened atoms to antiferromagnetically coupled atoms when the atoms are moved from non-interacting to strongly interacting. In the Kondo screened regime, the Kondo temperature is believed to be constant, but the Fano line shape changes continuously from a dip to a peak. In the antiferromagnetic regime, inelastic spin-flip excitations reveal a splitting with a continuous increase in energy levels when pushing the atoms further together. This is supported by numerical renormalization group calculations. The crossover between the two regimes is furthermore interesting because it occurs in an area of the phase diagram close to the elusive quantum critical point, where the phase transition line meets absolute zero temperature.

This freely positionable Kondo system on the tip represents a novel way to probe magnetic interaction with the possibility to continuously change the position of the probing Kondo system. The experiment is believed to be one of many applications possible and the method opens up for a new field within STM. We expect that our work has direct impact in other research areas, such as for heavy fermion materials, a class of materials whose properties are governed by the competition between Kondo screening and local moment antiferromagnetism or for quantum information processing.

Preface

This thesis entitled ”Probing Nanoscale Electronic and Magnetic Interaction with Scanning Tunneling Spectroscopy” summarizes my work done partly at the Department of Physics and Nanotechnology at Aalborg University, Denmark, and partly at the Nanoscale Science Department (Dept. Klaus Kern) at the Max Planck Institute for Solid State Research (MPI-FKF - Festkörperforschung) in Stuttgart, Germany. The PhD work started in October 2006 ending in February 2010 with 18 month spent in Aalborg and 23 month in Stuttgart. The work was funded by a grant from the Danish Agency for Science, Technology and Innovation (Forsknings- og Innovationsstyrelsen) for international PhD work to increase collaboration between Danish and foreign research institutes or universities. The PhD student should spend approximately half the time at the Danish institute and half the time at the foreign institute.

The work has been mainly experimental, but including collaboration with theoreticians from the Laboratoire de Physique des Solides, Université Paris-Sud, Paris-Orsay, France, as well as from the Physikalisches Institut at Universität Bonn, and the Andersen department at MPI-FKF.

This thesis is based partly on published or submitted articles and partly on still unpublished material. The thesis consists of introductions and explanations of the relevant subjects, a short introduction to the articles with their main results where relevant and the addition of the unpublished material. The full articles are added as appendices and the reader is referred to read the articles when relevant.

Acknowledgements

Many people deserve great acknowledgements for their contribution to my work and time spent during my PhD thesis, both in Aalborg and in Stuttgart. First of all, I would like to thank my supervisor Associate Prof. Lars Diekhöner for the enthusiasm and steady support throughout the joint project. In Stuttgart, especially Prof. Klaus Kern for giving me the opportunity to work in his group with such truly competent and helpful people. Most importantly the always omniscient Peter Wahl which knowledge and curiosity lifted this project. Also mainly Robin Ohmann for help in the laboratory and fruitful discussions, together with Dr. Lucia Vitali and Yong-Hui Zhang.

At the synchrotron in Aarhus I am in dept to Prof. Jens Onsgaard, Dr. Zheshen Li and Dr. Jan Godowski for untiringly giving me insight into the large world of synchrotron physics.

On the theoretical side, I would like to acknowledge collaboration with Dr. Ove Jepsen at the MPI-FKF in Stuttgart, with Dr. Pascal Simon from Université Paris-Sud in Paris-Orsay and with Dr. László Borda and Prof. Hans Kroha from Universität Bonn.

At Aalborg University, my colleagues and good friends, especially Tobias Holmgaard Stær and Jesper Jung with their positive and creative minds, have made my

time there a time worth remembering. I would also like to thank the secretaries Ulla Ponsaing and Jette L. Christensen and the technical staff Hans Nilsson and Kim H. Jensen for always being friendly and helpful.

At MPI-FKF in Stuttgart, many people have contributed to a great and fun atmosphere both at work and in my spare time, especially Dr. Alex Langner, Theresa Lutz, Dr. Sebastian Stepanow, Dr. Violetta Sessi, Adarsh Sagar, Jens Dorfmüller, Dr. Thomas Weitz and many more. What a great group of people!

Finally I would like to thank Lars Diekhöner, Peter Wahl, Klaus Kern and secretary Sabine Birtel for making the collaboration across borders and institutions work seamlessly - they see opportunities and not hindrances.

Last but not least, I would like to thank my family and friends for their support and patience over the years.

My sincere thanks to all of you!

Aalborg, Denmark, February 2010 **Jakob Bork**

Contents

Appendix

List of used acronyms

1D:	One-dimensional
2D:	Two-dimensional
3D:	Three-dimensional
ARPES:	Angle resolved photo emission spectroscopy
DOS:	Density of states
fcc:	Face-centered cubic
hcp:	Hexagonal close-packed
LDOS:	Local density of states
LEED:	Low-energy electron diffraction
ML:	Monolayer
MPI-FKF:	Max Planck Institut für Festkörperforschung
PES:	Photo emission spectroscopy
RG:	Renormalization group
RKKY:	Ruderman-Kittel-Kasuya-Yosida
RT:	Room-temperature
SNR:	Signal-to-noise ratio
STM:	Scanning tunneling microscopy
STS:	Scanning tunneling spectroscopy
UHV:	Ultra high vacuum
QCP:	Quantum critical point

Introduction

1

1.1 Nano!

Since Feynman's famous talk "There's Plenty of Room at the Bottom" [1], Binnig and Rohrer's invention of the scanning tunneling microscope (STM) [2], and Eigler's first article on moving single atoms with the STM tip [3], the expectations to nanoscience and nanotechnology have been tremendous. As Eigler wrote in the abstract of his article; "*...the possibilities for perhaps the ultimate in device miniaturization are evident*". And even more evident than the impact on applications and technology is actually the possibilities in fundamental science that open up when we are able to control single atoms to create and characterize almost any conceivable structure. The possibilities to create structures beyond what nature builds automatically, give us unique ways of creating and investigating new material properties. This leads to a greater understanding of the fundamental properties of nature and how to utilize them to improve the technological world we live in.

A driving factor in both science and technology are companies trying to increase the efficiency and decrease the power consumption of integrated circuits by decreasing the size of the individual components in the integrated circuit. The continued miniaturization has so far been based on the top-down approach where lithographic techniques are used to print transistors and other components at an ever-decreasing size. As of 2007 the industry used the so-called 45 nm technology node and in the beginning of 2010 the 32 nm node[1]. With the 16 nm technology node scheduled for 2019 the transistor channel length will be around 5 nm and quantum tunneling directly over the transistor channel will become an inherent problem [5].

Reaching and going beyond this point, what scientist now describe as fundamental science will become useful knowledge in the continued process of increasing the efficiency and decreasing the power consumption – or creating a fundamentally different application based on new technology (such as e.g. spintronics [6, 7], fast non-volatile racetrack memory [8], implementation of the memristor [9] or quantum computing [10]).

In the process of trying to discover and understand new physical effects, influence from the surroundings should be minimized in order to see the physical effects clearly. This has several implications to the science done also in this thesis. Most prominently, different temperatures are needed to observe different effects. Growth, diffusion, catalytic properties and electronic correlations are among the effects that depend strongly on temperature. The work shown in this thesis has been carried

---

[1] The process scale is often erroneously reported to be the transistor channel length, but in fact the number refers more generally to the specific production process used. Historically it refers to the average of half the width and the space in between metal lines connecting transistors, normally in DRAM [4], but different companies stretch the definition at will. The smallest lateral feature size in the individual transistors is considerably smaller.

out mainly at either room-temperature (RT) or 6 K, depending on the relevance and availability.

Next, structures made and manipulated are all located on the surface of a material, in this work on a metallic (111) crystal surface. Impurities, oxides and dirt on this surface can disturb or completely inhibit nucleation, growth, and interaction between the materials of interest. The consequence is that most surface science is done in ultra high vacuum (UHV) conditions in order to drastically reduce the amount of particles that get in contact with the surface. The details of the setups used in this thesis can be found in Appendix E.

With these necessities in mind it is possible to perform "surface science" where the controlled fabrication of nanostructured islands, layers, molecules and single atoms leads to new and sometimes unique control over electronic, optical and magnetic effects.

This thesis focuses on magnetic interaction on the nanoscale. How single atoms interact with each other and with small magnetic islands. Metallic heterostructures made from 1-2 monolayers (MLs) of materials such as copper, silver, gold, and cobalt are investigated in order to use their properties to influence and control the magnetic properties of single cobalt atoms. All experiments are done at the surface and characterized with various surface science techniques.

1.2 Motivation

The motivation for this thesis work is found in the work done by Wahl, Diekhöner and colleagues [11–17] at the MPI-FKF when trying to reach a better understanding of the Kondo effect and how it is influenced by magnetic and electronic interaction of its surroundings. The Kondo effect is the result of a magnetic impurity with an unpaired spin in a non-magnetic, metallic host material forming a many-body ground state. This ground state arises below a certain Kondo temperature specific to the material combination and causes a resonance at the Fermi level of the material. Technologically, the Kondo resonance affects the resistance of the material at low temperatures and scientifically, it is a unique way to describe and characterize magnetic effects in correlated electron materials.

In the last 12 years research into the Kondo effect has revived due to the discovery of the resonance in single magnetic impurities at the surface by scanning tunneling spectroscopy (STS) [18] or in a quantum dot [19], both in 1998.

The Kondo resonance can be influenced by several things among those are the electronic structure of the substrate, the coordination number, and it can be split in a magnetic field. So far, results with Ruderman-Kittel-Kasuya-Yosida (RKKY) interaction between atoms and islands both on a surface [20], and exchange interaction between single atoms [17] both on a surface have been reported to show a change in the exchange interaction with varying distance. In both cases the single Co atoms are locked to the lattice sites of the substrate and can only be moved in steps on the order of 1 Å on the surface. This thesis improves these techniques by showing how the Kondo resonance of a single magnetic Co atom can be influenced by either a magnetic Co island or continuously tuned by approaching another Co atom attached to the tip of an STM.

Especially the latter subject we expect to have a substantial impact on the scientific research area of phase transitions in heavy fermion compounds. The Kondo problem is basically believed to provide clues for understanding the electronic properties of materials with strongly interacting electrons, such as heavy fermion materials and high-temperature superconductors [21]. These materials are investigated in the scientific community to find new and interesting phases occurring in the low temperature regime. This can be magnetic phases such as ferromagnetic and antiferromagnetic, but also superconducting phases or spin-glasses [22]. The phase diagrams are a function of temperature and a tunable external parameter such as doping level or magnetic field. By changing the doping level in e.g. $\mathrm{CeCu}_{6-x}Au_x$ the internal pressure in the crystal is changed and it can be perceived as if the distance between the atoms changes (although other parameters such as density, band structure, Fermi wavelength etc. also change). To understand the interaction between the charge-carrying electrons in these materials, the two-impurity Kondo problem is mentioned as the simplest conceivable structure [23, 24] where a magnetic phase transition can occur. When the temperature is low enough, the phase transition is driven by quantum fluctuations and called a *quantum phase transition*. If the temperature is absolute zero, a quantum critical point arises where the phase transition line meets $T = 0$ K in the phase diagram. The properties of this quantum critical point (QCP) extends also into finite temperatures and affects the properties of the very low-temperature phase diagram [25]. Examples of heavy fermion compounds that have these properties could be the material $\mathrm{Sr_3Ru_2O_7}$ which shows a QCP in a magnetic field of $\sim$7.8 T [26].

Magnetic properties and phases are determined from a collection of effects related to the electronic structure of the material and most fundamentally from the electron spin. In this thesis the magnetic properties are deduced only from measuring the electronic properties of the materials in question. This can be done due to the strong link between electronic and magnetic structure through the spin of the electron. Therefore, the first part of the thesis is about electronic structure and the second part is about the magnetic properties measured through the Kondo effect.

1.3 Overview

Magnetic Co islands on Cu(111) are used extensively throughout this thesis due to their well-known single domain out-of-plane ferromagnetism [11, 12, 27–31]. In order to measure interaction between these islands and a single cobalt atom displaying the Kondo effect, the cobalt atom can be placed on the Cu(111) surface next to the island or on top of the island. On the Cu(111) surface the cobalt atom is locked to the lattice sites of the surface and on top of the island the Kondo effect is quenched by the ferromagnetism.

Instead, the cobalt islands can be capped with a non-magnetic metal and the cobalt atom placed on top of the capping layer. This was first tried with copper as the capping layer[2], but the cobalt atoms on top of the copper showed either no or an unaffected Kondo resonance with 1 or 2 ML of copper, respectively. This digital situation of all-or-nothing was of limited use and other paths needed to be examined. This thesis starts from this point by substituting the copper capping layer by first

---

[2] unpublished work by Diekhöner

silver and later gold. The change in lattice constants[3] gives different ML heights and as will be shown also a combined Moiré pattern and reconstruction of the capping layer.

First, the peculiar growth of the Ag capping layer is investigated, which shows that Ag actually tends to accumulate on top of the bilayer high Co islands even at low coverage. This situation is optimal for creating the Ag-capped Co islands. Angle-resolved photoemission spectroscopy (ARPES) show a surface state on these islands and STS measurements at 6 K shows that the Moiré pattern in the Ag capping layer modulates the Co d-related state in energy, width and intensity. This is envisioned to have not only a magnetic effect, but also a catalytic effect on adsorbates that will be evaporated on top of the structure. This constitutes the first part of the work in this thesis on electronic properties of these multilayer islands.

Next, single magnetic cobalt atoms are evaporated at low temperature on top of these structures to measure the change in the Kondo resonance in the different positions of the Moiré pattern. While doing these measurements, it was realized that cobalt atoms could be picked up by a gold-covered STM tip and that the cobalt atoms show a Kondo resonance formed between the tip and the atom picked up. This Kondo system placed at the tip apex is used to show how magnetic coupling between two cobalt atoms (one on the surface and one on the tip) can be continuously driven from a Kondo ground state to an antiferromagnetic ground state by simply changing the Co-Co interatomic distance through a tip displacement. This experimental implementation of the two-impurity Kondo problem in readily available materials is the first of its kind to continuously and reversibly drive a crossover between two phases with an STM. It is envisioned that this tip Kondo system can be used as a magnetometer to measure magnetic properties of not only atoms, but also islands and molecules with magnetic centers.

The work in this thesis is build mainly on co-authored articles which can be found in the appendices. Chapter 2 contains short general introductions to surface science and the characterization techniques used in this thesis along with technical sections on how the STM tip is coated with gold and used to pick up cobalt atoms. Chapter 3 presents the results obtained based on the previous chapter, and chapter 4 introduces the Kondo effect and presents the results based on measuring magnetic interaction on the nanoscale through the Kondo resonance. Where relevant, work from the articles in the appendices is shortly introduced and the reader should then consult the article for the majority of the work.

---

[3] The lattice constants change from 2.56 Å of Cu to 2.89 Å for Ag and 2.88 Å for Au

Surface Science: Fundamentals and Methods

2

2.1 Fundamentals

Surface science is a large field at the interface between physics and chemistry [32] and has laid down the foundations for the fields of nanoscience and technology since our ability to control and manipulate structures is often limited to the surface. Nanotechnology can be defined in various ways, but is normally described as structures with at least one dimension sized below 100 nm [33]. This is often the length scale where the de Broglie wavelength of the electron starts to become comparable to the structure size of the material. This causes the wave-nature of the electron to become the deciding factor for the surface properties of the material. The electronic states for these electrons in bulk or at the surface make up the band structure and decide many of the properties of the material in general. An understanding of the physics behind this is the first step in controlling and forming these properties into applications. The field of surface science has been driven in large parts by the surface chemistry of catalysis. To name an example, a pioneer among many within this field is the 2007 Nobel prize winner in Chemistry, Gerhard Ertl, who explained hydrogen adsorption on a palladium surface with LEED [34,35], but most famously explained the catalytic synthesis of ammonia [36–39] over iron and oxidation of CO over platinum [40] used in e.g. car catalysts. Surface science is highly dependent on the characterization techniques available where mainly the invention and use of scanning probe microscopy and photoemission spectroscopy (PES) have had the greatest impact on the field.

In this thesis a variety of different surface characterization techniques is used, including low-energy electron diffraction (LEED), Auger spectroscopy (not shown), ARPES, and STM/S in order to visualize and understand the properties of the materials investigated. The following is a brief introduction to this large field, starting with the underlying physics of surface states, diffusion, nucleation, and growth of metallic structures (based on [41]) and then describing the characterization techniques used (ARPES and STM/S). In the end of the chapter, techniques for coating the STM tip with gold and picking up cobalt atoms to form a Kondo resonance at the tip is described.

2.1.1 Surface states

The surface of a material is special in the way that the bulk symmetry is broken. This leads to a different electronic structure at the surface compared to the bulk. For the valence electronic structure of a material the electronic states are normally split into three classes; (i) bulk states are extended over the entire sample and relevant for the bulk properties of the material, (ii) surface resonances are extended states with an increased probability to be found at the surface, and (iii) surface states localized at the surface and decaying exponentially into both the bulk and the vacuum. Surface states were first described mathematically by Tamm [42] and later in a different way by Shockley [43] as the result of the material being cut in a certain crystallographic direction causing Bloch states to be forbidden at the Fermi energy in the direction normal to the surface (and a range of angles around the normal) [44]. In this band gap, solutions to the Schrödinger equation exist that decay exponentially into both the bulk and the vacuum, thereby being confined to the surface. For Cu, Ag, and Au these surface state in the gap arise from *sp*-electrons, which are still free to move parallel to the surface and form a 2D electron gas with a nearly free electron-like parabolic dispersion.

The localized surface bands arising from the *d*-surface states are well below the Fermi level in these metal, but as it will be seen in the following, *d*-related surface states can become relevant close to the Fermi level in e.g. Co.

Surface states often dominate the electronic structure at the surface of a material close to the Fermi level and are easily accessible by the fact that the characterization techniques used i.e. ARPES and STM/S are extremely surface sensitive.

2.1.2 Diffusion, nucleation, and growth

Deposition of metallic material on a noble metal (111) surface is essential throughout the work in this thesis. The topic has been studied extensively [45–47] for decades. Generally, growth is described as illustrated in figure 2.1 by one of three modes of crystal growth which is depending on the surface energy of the materials involved; (i) island growth (Volmer-Weber growth) which is relevant for the Co islands on Cu(111), Au(111), and Ag(111), and (ii) layer growth (Frank-van der Merwe growth) which is relevant for Ag and Au at low coverage on Cu(111), and (iii) layer plus island growth (Stranski-Krastanov growth) which is relevant for Ag deposition at higher coverage in the ARPES measurements on Co/Cu(111).

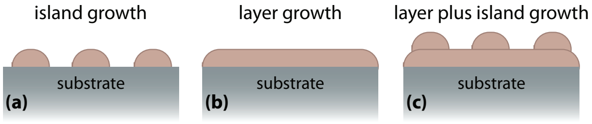

Figure 2.1: Illustration of the three common growth modes (a) island growth, (b) layer growth, and (c) layer plus island growth.

Material evaporated from a metal evaporator, see appendix E, arrives from the vapour phase at the surface and will either weakly interact through physisorption or more strongly interact through chemisorption (covalent bond) with the surface. Depending on the crystal surface index and the material combination atoms or molecules can now move in a two-dimensional (2D) surface diffusion according to the Arrhenius equation for the diffusion rate D

$$D = D_0 e^{-\frac{E_{\mathrm{dif}}}{k_{\mathrm{b}}T}}, \tag{2.1}$$

where D_0 is the diffusion prefactor, E_{dif} is the activation energy for the diffusion, $k_{\mathrm{b}}T$ is Boltzmann's constant times the temperature. The Arrhenius equation shows that diffusion is a temperature-activated process. The process is illustrated in figure 2.2. Diffusion can contain a rate-limiting step, which means that diffusion in different sites, directions, or steps can have different rates, where a slow rate can limit the overall process.

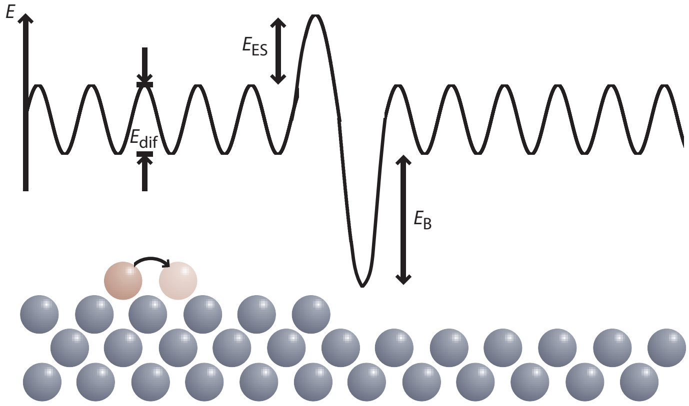

Figure 2.2: Atomic arrangement and sketch of associated energy barrier in a simplified one-dimensional (1D) model [41]. The diffusion barrier E_{dif} controls in-plane diffusion, the additional barrier for moving across a step is called the Ehrlich-Schwoebel barrier E_{ES}, and the binding energy to a step site is E_{A}. Care should be taken when comparing atomic sites to the energy since the situation actually has to be considered in a three-dimensional (3D) model.

The atoms can also inter-diffuse with atoms in the surface (to form an alloy) or diffuse across a step-edge if adequate energy is available, see figure 2.2. The additional barrier for diffusion over a step edge, called the Ehrlich-Schwoebel barrier E_{ES}, is normally larger than that of surface diffusion and furthermore, the barrier for diffusing up from a lower terrace is normally higher than vice versa [48]. If a particle adsorbed in the deepest well in figure 2.2 at the lower step edge gains energy (from e.g. thermal activation) to move again, it only needs $E_{\text{B}} + E_{\text{dif}}$ to hop away from the step edge, but more energy $E_{\text{B}} + E_{\text{dif}} + E_{\text{ES}}$ to hop up the terrace step.

To understand island formation it is necessary to look at how diffusion can be slowed down and stopped, which leads to nucleation. During diffusion, two atoms can meet on the surface, temporarily forming a cluster, in this case a dimer. A dimer diffuses (hops) less often on the surface and depending on temperature and deposition flux, this may already be stable enough to stop diffusion and thereby nucleate at the current position of the dimer. The criterion for further growth of the cluster is that the mean time until the next atom arrives to the cluster is shorter than the decay time of the cluster. If this criterion is true, another atom will attach to the dimer and form a trimer, which can still diffuse. This is determined not only by temperature giving hopping energy, but also by the deposition flux determining the mean time until the next atom arrives. At some cluster size, called the *critical cluster size*, the addition of another atom will stop the diffusion and nucleation will occur. Nucleation can also occur earlier at step edges or impurities due to the temperature not being high enough to overcome the increased energy barrier in these sites.

2.2 Angle resolved photoemission spectroscopy

Photoemission spectroscopy is a well established and widely used technique within the field of surface science. The process involved was discovered by Hertz [49] and explained by Einstein in 1905 [50] as the photoelectric effect. Monochromatic light (photons) is shined on a surface and depending on the energy of the photons, electrons at different energy levels can be emitted. The photon source in PES can be a laser, a gas-discharge lamp, an X-ray tube, or a synchrotron-radiation source. An X-ray tube has a fixed photon frequency with a high intensity, whereas photons from a synchrotron contain a broad continuous spectrum where a specific photon frequency can be chosen with a monochromator. An illustration of the setup in ARPES is shown in figure 2.3.

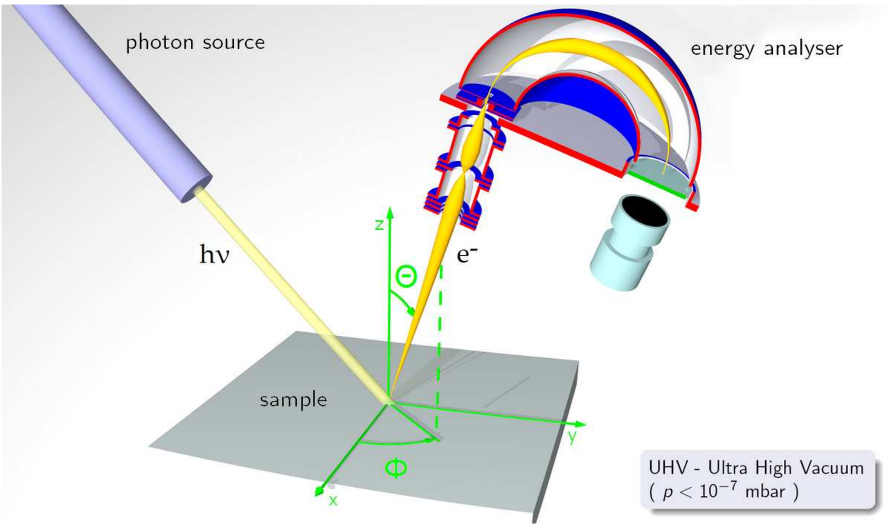

Figure 2.3: Principles of ARPES with incoming and outgoing electron beam [51]. The photon source can be e.g. a synchrotron radiation source and the detector normally uses an electric field to single out electrons with a specific energy. The sample is rotated in order to vary Θ.

Energy-wise, electrons anywhere from the valence band to the core levels of the sample band structure can be reached by using photons with energy $\hbar\omega$, follow the density of states (DOS) in figure 2.4. Electrons that leave the sample will have to overcome their binding energy E_B plus the work function of the sample ϕ_sample and the remaining energy is the kinetic energy of the electrons E_kin when they leave the sample. When the electrons enter the detector, the work function of the detector $\phi_{detector}$ is added to the energy of the electrons. This yields the energy relation

$$E_\text{kin} = \hbar\omega - \phi_\text{sample} + \phi_\text{detector} - |E_\text{B}| \,. \tag{2.2}$$

By fixing $\hbar\omega$ and measuring E_kin, the binding energy of electronic states in a material can be determined, as shown in figure 2.4. The binding energy of the core levels in a band structure of a transition metal will shift slightly depending on the bonding of the atoms to their surroundings. This is called a core-level binding energy

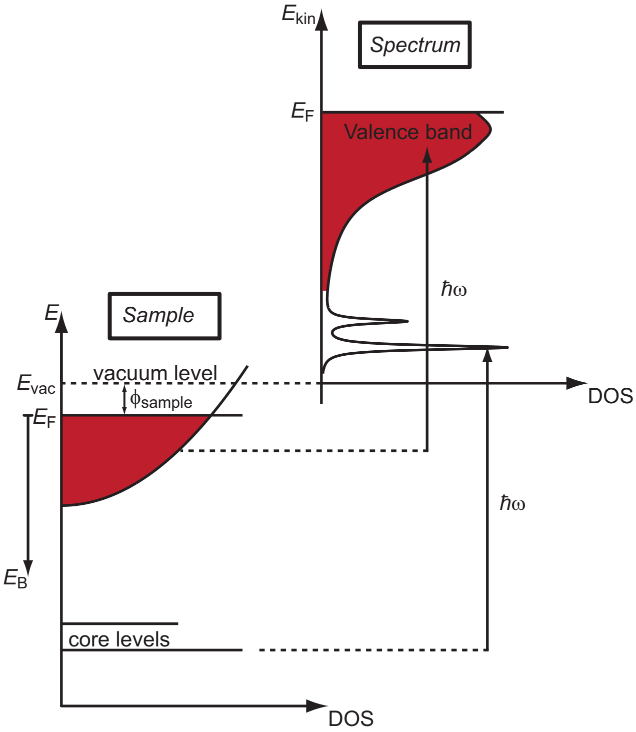

Figure 2.4: Schematics the energies involved in the PES process. The sample on the lower left is probed with photon energy $\hbar\omega$ and results in the spectrum on the upper right. Freely after [52].

shift and can be very accurately detected in PES. This is used to determine the neighbouring environment for evaporated layers.

The detector can be equipped with an aperture, whereby the user can choose to measure with a wide opening (to achieve high intensity) in normal emission corresponding to $\Theta = 0$ in figure 2.3 or with a small opening to measure angle-resolved with varying Θ. Since the electron wave vector parallel to the surface $k_{||}$ inside the sample is conserved when the electron is emitted, the momentum of the wave vector can be related to the detection angle Θ as

$$k_{||} = \sqrt{\frac{2m_e}{\hbar^2} E_{\text{kin}}} \sin\Theta, \tag{2.3}$$

where m_e is the mass of an electron, $\hbar$ is the reduced Planck constant and the kinetic energy E_{kin} is taken at the state under investigation.

By measuring the binding energy as a function of momentum, it is possible to determine the band structure of the material under investigation in one direction in momentum space.

Finally, it should be mentioned that the probing depth is depending on the electron mean free path. This length scale varies with materials and the kinetic energy of the electron but is normally between a few Å and 50 Å. At an electron energy of e.g. 40 eV the probing depth is typically 2-4 atomic monolayers.

2.3 Scanning tunneling microscopy and spectroscopy

Pioneered by Binnig and Rohrer at the IBM lab in Rüschlikon-Zurich [2] in the early 1980s, STM/S can be used to measure topographic images on the atomic scale with sub-Ångström resolution and determine the local density of states (LDOS) by use of spectroscopy. Beyond measuring, the STM tip can also be used to manipulate atoms by pushing or pulling atoms around on the surface, and pick up or put down single atoms or molecules with the tip. All of this will be explained in the following. The theory is mainly based on [53].

2.3.1 Basic usage

An STM is most commonly used as a form of microscope to take topographic images. This is done by bringing an atomically sharp metallic tip in close proximity (∼5 Å) to a metallic surface. When applying a bias voltage between tip and sample (voltages mentioned are normally with respect to the sample) a small current in the nA range will tunnel across the small vacuum gap between tip and sample. Tunneling of electrons is a quantum mechanical effect since classically no current would flow before the tip and sample are truly contacted. As shown later, the current in the tunneling region decays exponentially with increasing distance between tip and sample, therefore this current can be used to measure the height of the surface when scanning the tip laterally across the surface, see figure 2.5 for an illustration.

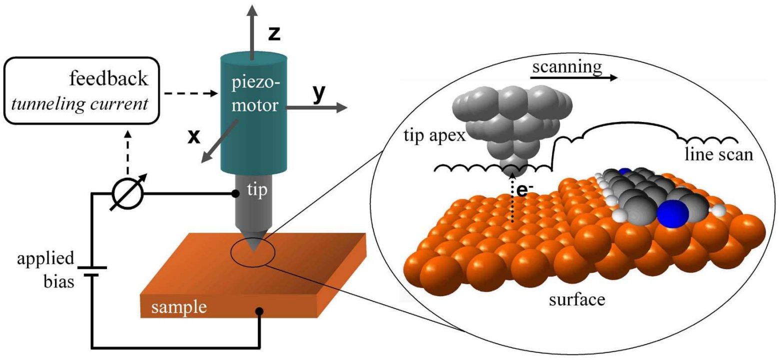

Figure 2.5: Schematics of the constant current operation of an STM. Reproduced with permission from [54].

Bringing the tip in proximity to the surface is done by a coarse approach motor over a range of some millimeters. The tip movement in the tunneling regime is controlled by piezoelectric elements, which are polar crystals that move precisely and over a small length scale when a high voltage is applied. The piezo elements are programmed to keep the height constant or controlled by a feedback loop that keeps the current constant when scanning the surface. When the surface is very flat the tip can be moved in constant-height mode where the current is measured and converted into a height. Normally, an STM is instead operated in constant-current mode, where the feedback loop works to keep the error between the set and measured current as low as possible by adjusting the distance between tip and sample, called the z height.

STM can be performed in various environments from ambient conditions, at liquid-solid interfaces and as here in vacuum. The vacuum prevents the surfaces from becoming contaminated or oxidized and clean metallic surfaces can be examined.

2.3.2 Microscopy

STM is based on the fact that electrons are quantum objects that can tunnel through an energy barrier. The electrons are described by the solution $\psi(z)$ to the Schrödinger equation. Inside the material $\psi(z)$ is called a wave function and is a complex exponential function describing a wave, but at the surface the electron wave function decays exponentially into the vacuum

$$\psi(z) = \psi(0)e^{-\kappa z}, \tag{2.4}$$

where this is the 1D case with z perpendicular to the surface ($z = 0$) and

$$\kappa = \frac{\sqrt{2m_e(U - E)}}{\hbar}, \tag{2.5}$$

where U is the height of the vacuum barrier, and E is the energy of the electron.

The probability density to find the electron in the vacuum is the square of the wave function and therefore non-zero in the vacuum. This tail with exponential decay exist from both "electrodes", the tip and the sample, and when they are sufficiently close it is the overlap of the tails that leads to electrons tunneling between the tip and the sample. The overlap of the wave functions is proportional to the current and it can therefore be seen that the current decays exponential as a function of distance in a tunneling junction. If the applied bias energy eV_{bias} is much smaller than the work function ϕ of the material, then $U - E = \phi$ and a general term for the current I is therefore

$$I(z) = I(0)e^{-2\kappa z}, \tag{2.6}$$

where

$$\kappa = \frac{\sqrt{2m\phi}}{\hbar}, \tag{2.7}$$

which can be used by the feedback loop to convert current to height z.

Care should be taken when interpreting STM topographic images, because eq. (2.6) is a simplified expression – as it will be shown in the next section, e.g. the LDOS of the sample should also be included in the expression. Thereby, according the Tersoff-Hamann model [55–57] what is measured is actually a contour of equal Fermi level LDOS of the sample. This means that different materials or atoms will be displayed with different height according to their LDOS at the Fermi level. This will cause some adatoms to show up as depressions in a topographic STM image even though the atoms are physically on top of the surface. This can for example be seen in [58,59].

2.3.3 Spectroscopy

An STM can also be used for spectroscopy to probe the electronic structure of the sample. There are many different modes in which spectroscopy can be performed, in this thesis it is mainly done at a single point by placing the tip at the area of interest, opening the feedback loop to maintain a constant distance between tip and sample, and then sweeping the bias while measuring the current ($I(V)$ can yield information about the LDOS [60]). Alternatively, the distance can be changed while measuring the current ($I(z)$ can yield information about the local barrier height [61]) or the feedback loop can remain closed while sweeping the bias ($z(V)$ can yield information about the image states [62]).

The theory of tunneling spectroscopy was developed in the 1960s especially by Bardeen [63] by assuming two planar, infinitely large tunneling electrodes after Giaever [64,65] showed experimentally that tunneling was possible between two metallic (superconducting) electrodes separated by a thin oxide layer. Bardeen's approach was to solve the Schrödinger equation for each electrode separately. Here we shall assume that one of the electrodes is a sample and one is a tip, as implemented by Binnig and Rohrer and theoretically shown by Tersoff and Hamann [56] to be equivalent to the planar tunneling junction.

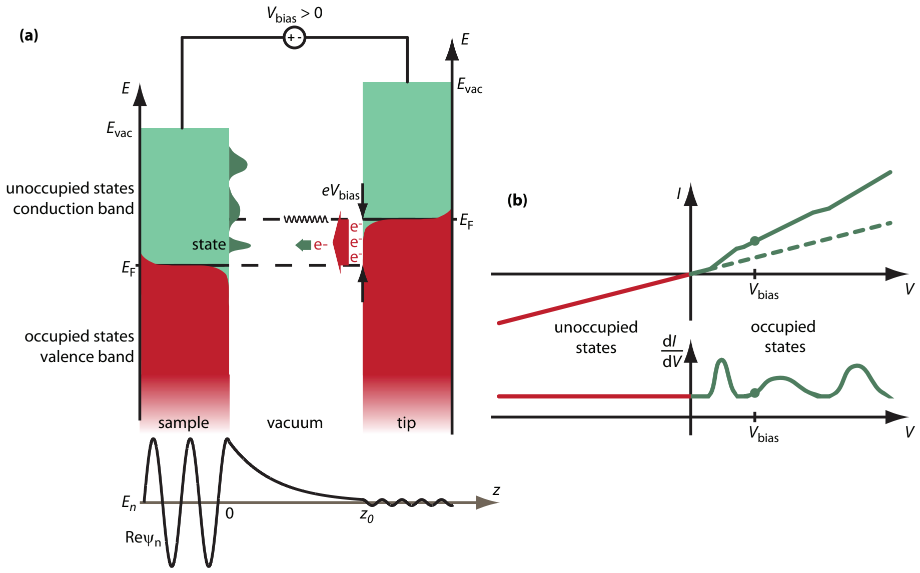

Figure 2.6: (a) The LDOS of a sample and a tip in STS. At a positive bias as shown here the Fermi levels of the sample and tip are displaced by the bias applied and the electrons tunnel from the tip into the unoccupied states of the sample conduction band. As the lock-in technique measures the change in current as the bias is swept, it is the temperature in the Fermi distribution function of the tip that determines the energy resolution of the experiment. (b) The current and the derivative of the current shown correspond to the LDOS of the sample shown in (a) with the green dot marking the applied bias.

Eq. (2.6) shows the exponential decay of the current into the vacuum, but it neglects the details of the material which is a simplification because of several things, which are illustrated in figure 2.6(a). First, the electrons tunnel elastically between tip and sample, which means they enter and leave the tip and sample with the same energy. Therefore an electron leaving the tip must tunnel into an empty state in the sample and vice versa. The only electrons allowed to tunnel are therefore the ones in the energy interval between $E_\mathrm{F} - eV_\mathrm{bias}$ and E_F. Second, the *rate* of electrons tunneling can be determined through Fermi's golden rule and Bardeen solved this by introducing a tunneling matrix M_ST that describes how well electrons tunnel between tip and sample at the different energies.

Taking this into account the tunneling current at a fixed tip-sample distance can be written as

$$I = \frac{4\pi e}{\hbar}\int_{-\infty}^{\infty}[f_\mathrm{T}(E_\mathrm{F} - eV_\mathrm{bias} + \varepsilon) - f_\mathrm{S}(E_\mathrm{F} + \varepsilon)]\cdot\rho_\mathrm{T}(E_\mathrm{F} - eV_\mathrm{bias} + \varepsilon)\cdot\rho_\mathrm{S}(E_\mathrm{F} + \varepsilon)\cdot|M_\mathrm{ST}|^2\,\mathrm{d}\varepsilon, \tag{2.8}$$

where $f_\mathrm{S}(E_\mathrm{F})$ and $f_\mathrm{T}(E_\mathrm{F} - eV_\mathrm{bias})$ are the Fermi distribution functions of the sample at the Fermi level E_F and of the tip displaced by eV_bias, respectively. It is the integral of this difference of the two Fermi distribution functions that governs the elastic tunneling of electrons. ρ_T and ρ_S are the LDOS of the tip and sample. $\rho(E)$ is a sum of the probability density over a small energy interval around E giving the LDOS per energy unit volume.

Several assumptions can be made in order to simplify eq. (2.8); (i) first, ρ_T can be considered a constant if the LDOS of the tip is featureless. This can be improved by using materials with a flat DOS in the relevant area as well as cleaning the tip by field emission and soft indents into the sample. The latter approach normally ensures that the tip material is equivalent to the surface material, which for most noble metal surfaces means a flat DOS at the tip apex.

When sweeping the bias (displacing the LDOS of the sample with respect to the tip in figure 2.6(a)), then the ${}^{\mathrm{d}I}/_{\mathrm{d}V}$ signal consists of the change measured at the two Fermi levels. And since the LDOS of the tip is considered flat, no change is detected at the Fermi level of the sample. Hence, it is only the change detected at the Fermi level of the tip that contributes to the ${}^{\mathrm{d}I}/_{\mathrm{d}V}$. (ii) When the temperature is lower than the required energy resolution, the Fermi distribution functions in eq. (2.8) can be reduced to step functions which limits the integral to 0 and eV_bias. The "sharpness" of the Fermi level directly influences the energy resolution of the experiment and is given by the temperature in the Fermi distribution function of the tip. In order to increase the energy resolution lower temperatures are needed. This is why most of the experiments in this thesis (involving spectroscopy) are carried out at low temperatures (~ 6 K), while the growth and structure topographic images are carried out at room temperature. (iii) Furthermore, the tunneling matrix element can be considered constant at low bias.

Given these assumptions the current at a fixed distance is proportional to the integral of sample LDOS between 0 and the applied bias

$$I \propto \int_0^{eV_\mathrm{bias}} \rho_\mathrm{S}(E_\mathrm{F} + \varepsilon)\mathrm{d}\varepsilon, \tag{2.9}$$

and the derivative of I with respect to the bias is proportional to the LDOS of the sample

$$\frac{\mathrm{d}I}{\mathrm{d}V} \propto \rho_\mathrm{S}(E_\mathrm{F} + eV_\mathrm{bias}). \tag{2.10}$$

This is a very important relation in STS and it is illustrated in figure 2.6(b).

When sweeping the bias to measure a spectrum as shown the feedback loop has to be deactivated so the tip is at a fixed distance throughout the measurement.

Normally, the $\mathrm{d}I/\mathrm{d}V$ is measured with a lock-in amplifier, which adds a small sinusoidal modulation to the applied bias voltage, as illustrated in the middle of figure 2.6(a). The lock-in amplifier uses this modulation to measure the $\mathrm{d}I/\mathrm{d}V$ with a very high signal-to-noise ratio (SNR), because frequencies differing from the modulation frequency are damped. If the frequency is chosen much higher than what the feedback loop can follow, it can be filtered out in the topographic current. An increase in the amplitude of this lock-in modulation will increase the SNR, but as it can be seen in figure 2.6(a) it also leads to additional broadening in the measured signal which turns into a decrease in energy resolution. Therefore, it is desirable to keep the lock-in modulation amplitude as low as possible.

In some cases the tip LDOS cannot be considered flat and it therefore contributes to the final spectrum measured. In simple cases, the background spectrum on the bare substrate can be measured and subtracted from the measured spectrum with the background subtraction method [66], but also other techniques exist to minimize the effect of the tip LDOS [67] [53, pp. 340-344].

2.3.4 Inelastic tunneling

When certain molecules are included in the tunneling junction a sharp kink (step) can occur in the differential tunneling conductance $\mathrm{d}I/\mathrm{d}V$ at a bias voltage of $V_{bias} = \pm\frac{\hbar\omega}{e}$, where ω is a frequency of a vibrational mode in the molecule. This kink is because electrons tunneling through this molecule now have an extra channel to tunnel through. They give $\hbar\omega$ of their energy to the molecule bond vibration and can then move to the tip with their reduced energy, thereby having tunneled inelastically [58, 59]. The kink is seen in the second derivative of the current $\mathrm{d}^2I/\mathrm{d}V^2$ as a sharp peak, which normally is detected directly by the lock-in technique to increase the SNR. This also works in the reversed case with reversed bias and will show up as (negative) increase in the current. The kinks in conductance are symmetric in energy around the Fermi level and this symmetry is a good experimental indication that the observed features stem from inelastic tunneling.

Tunneling electrons can also lose energy to spin-flip excitations in magnetic atoms or molecules [68]. This effect is seen by a step up in the differential conductance at an energy proportional to the applied magnetic field, hence the energy position of the step can be controlled by Zeeman splitting.

2.3.5 Tip preparation

As can be seen from the discussion above, the tip of the STM is a very important ingredient in the measurement. Hence, the fabrication and especially the cleaning of the tip before an experiment is critical. In the following is a practical explanation of the tip preparation procedures as done at the 4K-STM in Stuttgart.

Making the tip

The tip is made from a metallic wire of various different materials, e.g. PtIr or W. In this thesis tungsten (W) is used at the STMs both in Aalborg and Stuttgart. The wire is electrochemically etched in aqueous sodium hydroxide (NaOH), checked with an optical microscope for overall cleanliness and then dipped in hydrofluoric acid to remove the oxide layer just before inserting the tip into the UHV chamber.

Field emission

Once inserted, the tip is cleaned by field emission. The tip is retracted slightly from the tunneling range, a high voltage of a few 100 V is applied between the tip and sample until a field emission current of 40 μA is detected. The voltage can be increased up to $\sim$ 500 V while the tip is stepped back with the coarse approach motor to keep a field emission current of 40 μA.

Normally, several large drops in the current can be detected (especially in the beginning before even reaching a current of 40 μA) which is an indication that loose material is removed from the tip and the tip restructures into clean facets with a low surface energy [53, pp. 334–336]. The relatively high current heats the tip and makes the restructuring easier. After a field emission cleaning of the tip, the surface is dirty and should be cleaned if it should be used for experiments.

Soft indentation (dipping of the tip)

Finally, in the beginning of each experiment, the tip is checked to make sure that it is free of double tip features and that it images single atoms as spherical protrusions. For spectroscopic measurements, a spectrum is taken on the clean, bare substrate far away from a step edge to see if the surface state is imaged sharply and correctly and the spectrum is otherwise featureless in the relevant energy range, see figure 2.7 for an example.

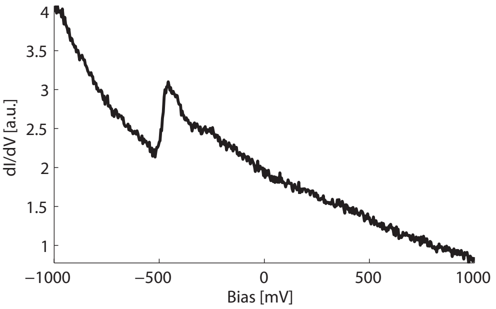

Figure 2.7: dI/dV spectrum of a clean Au(111) surface clearly showing the onset of the surface state at -460 mV. The remaining part of the spectrum is almost featureless except from a slope. This indicates a clean, metallic tip.

If these requirements are not met, which they normally are not at the beginning of an experiment, then the tip is dipped softly into the surface. The procedure is as follows: The voltage applied is raised to a value between 1 and 10 V and the tip is moved from 5 to 50 Å into the surface. When the tip contains double features, the experience is that a low voltage (1–2 V) and an indentation depth beginning at 15 Å can be used with steps forward of 5 Å until the tip is free from the double tip features (checked between each dip).

Then the spectroscopic features of the tip should be made acceptable. This is done with a smaller indentation depth (5–10 Å) and depending on the severity of the change requested to the spectrum a voltage between 2 and 10 V should be used. An example of a large change to the tip can be seen in figure 2.8 where 7 Å and 10 V are used. Using such a high voltage increases the chances of a double tip, as can also be found in this image[1]. Normally, a smaller voltage should be used and a correspondingly smaller "crater" will appear.

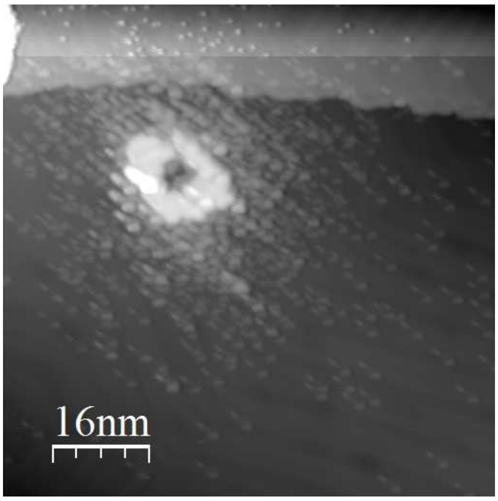

Figure 2.8: An STM image of the area around the center of a soft indentation. The parameters used were 7 Å into the surface and 10 V.

When seeking to slightly change the spectrum in the Kondo resonance regime (±50 mV) it is normally sufficient to continuously put down the outmost tip atom by briefly going into contact (3-5 Å) with a small bias (< 100 mV) until the desired featureless spectrum is achieved [69].

The end result of all these tip preparations is that the tungsten tip is covered with a thick layer of the substrate material from the dipping. Therefore it is often necessary to make low-coverage preparations of the materials investigated in order to have free, bare substrate areas to dip the tip in.

Dipping with 10 V and 50 Å is a "complete reset" of the tip and an area as large as 650×650 Å^2 can be destroyed.

Indenting the tip into the surface often creates a hole in the surface indicating that the surface material is now attached to the tip. In the following, a novel way of coating the tip with flakes of subML material deposited on the surface is presented.

---

[1] The upper part of this image actually shows no double tip, which indicates that the dip itself did not create the double tip (scan direction horizontal from upper left corner), but a tip change just before the step edge caused the rest of the image to be imaged with a double tip.

2.4 In-situ coating of the STM tip

The tip material is of the utmost importance not only to the convoluted LDOS of the tip/sample as described in section 2.3.3, but also to the attachment of single atoms to the tip apex. During the work of this thesis it was found that single Co atoms only attach to the very apex of a *gold*-coated tip. Furthermore, the single Co atom at the tip apex shows a Kondo resonance with the tip material (similar to that of a Co atom on the Au(111) surface). The gold-coating can be realized by soft-indents into a Au(111) sample as shown in the previous section. It has also been investigated extensively for copper-coating on Cu(111) and silver-coating on Ag(111), but never found to work with Co atoms; the Co atoms can be picked up, but does not show a Kondo resonance with the tip, presumably because the Co atom is not attached to the very apex of a copper- or silver-coated tip.

Having a Kondo system on the tip is an interesting property which can be freely positioned to measure interaction with other magnetic systems. In order to generalize the property beyond gold surfaces there are several ways to achieve a gold-coated tip. The easiest suggestion would be to use a gold wire as tip, but as the tip is dipped into the surface to make the tip sharp (and remove double-tip features), the material of the sample surface is transferred to the tip. By this reasoning, the sample should then be Au in order for the tip to end up as Au-coated. This is shown with a Au(111) crystal in section 4.6. In the following it will be shown that it is also possible to achieve a gold-coated tip on a Cu(111) surface without changing crystal, just by picking up layers of gold evaporated on cobalt islands on the Cu(111) surface. In

2.4.1 The technique

The Cu(111) sample is prepared with subML coverage of bilayer high Co islands and then Au is evaporated on the structures. The Au will cover both the Cu surface and the Co islands. Experiments have shown that it is easier to pick up the Au from the Co islands than from the Cu surface[2]. The pickup procedure is reproduced in figure 2.9(a) and is as follows; the tip is taken from tunneling conditions ($V = 200$ mV, $I = 0.48$ nA, $R = 417$ MΩ) to 3 Å closer and a bias voltage of 1 V. From there, the bias and Z extension is slowly increased resulting in a transfer of material from the surface to the tip. This can be seen as a sudden drop in the current trace, see figure 2.9(b). The first transfer happens at a bias of 1.26 V and a current of 100 μA ($R = 12.6$ kΩ), which is close to 1 quantum conductance $G_0 = {}^{2e^2}\!/_{h} = {}^{1}\!/_{12.9}$ kΩ^{-1}.

Depending on the surface structure, the size of the flake being picked up, and the tip structure the parameters for a successful pickup procedure can vary. To transfer a larger amount of material normally takes a higher voltage. The resistance in the tip-sample junction during the pickup procedure can be down to 2 kΩ, indicating that several conductance channels are open during the transfer of material.

In figure 2.10 a sequence of STM images are shown before and after these pickup procedures. The images show a part of a triangular Co island below and a bright Au layer on-top. The initial Au flake is visible in figure 2.10(a). By moving the STM

---

[2] A Au-coated tip has also been achieved by evaporating 2-4 ML Au on a Cu(111) sample and then dipping the tip into the Au layers, but since Au grows layer by layer on Cu(111), this technique will render the Cu(111) surface inaccessible.

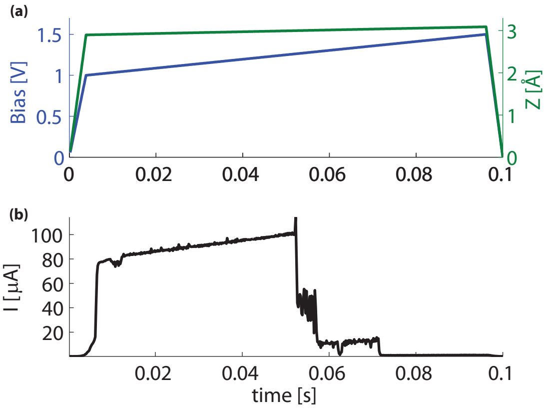

Figure 2.9: (a) The bias (blue) and the distance, Z (green) from tunneling $Z = 0$, during the 0.1 s the pickup procedure lasts. Initially, the bias and the distance from tunneling towards the sample is ramped up rapidly. Then the main period follows, where the bias and the distance is increased slowly. (b) The current trace shows several clear drops in current after 0.05 s. The first drop presumably represents transfer of Au material and the following steps a restructuring of the tip and sample.

tip to the small star (beginning of blue arrow) and performing the pickup procedure described above, Au can be removed from the surface and placed on the tip. The next image (b) shows that a small part of the Au is missing from the surface where the blue arrow ends. The diameter of the missing part is ~ 4 nm, which is a considerable amount of Au atoms.

The difference from figure 2.10(b) to (c) shows that also the Au material can be lost from the tip and go to the surface. Notice that the Au is completely restructured and does not fall back to the surface as a monolayer. The volume of the deposited material roughly corresponds to the volume of the Au flake picked up between (a) and (b). By applying a higher voltage, it is also possible to pick up this lump of gold (including some of the Au layer below), as seen from (c) to (d). Notice also that Au material can be scattered away from the center of the pickup place as seen already on the left side of (a) to (b). The smaller individual pieces can be picked up as it can be seen from (e) to (j). Two or more arrows indicate that two or more pickup procedures were carried out and the intermediate images are not shown.

2.4.2 Change in local barrier height

The real indication that the Au is not just removed from the surface, but also actually coats the tip apex is seen in a change of the measured local barrier height. This is a measure for the work function of the entire surface. The local barrier height ϕ can be found by the current $I(z)$ in the tunneling regime where $z = 0$ is tip-sample contact as

$$I(z) = I(0)e^{-2\kappa z}, \tag{2.11}$$

where

$$\kappa = \frac{\sqrt{2m_e\phi}}{\hbar}. \tag{2.12}$$

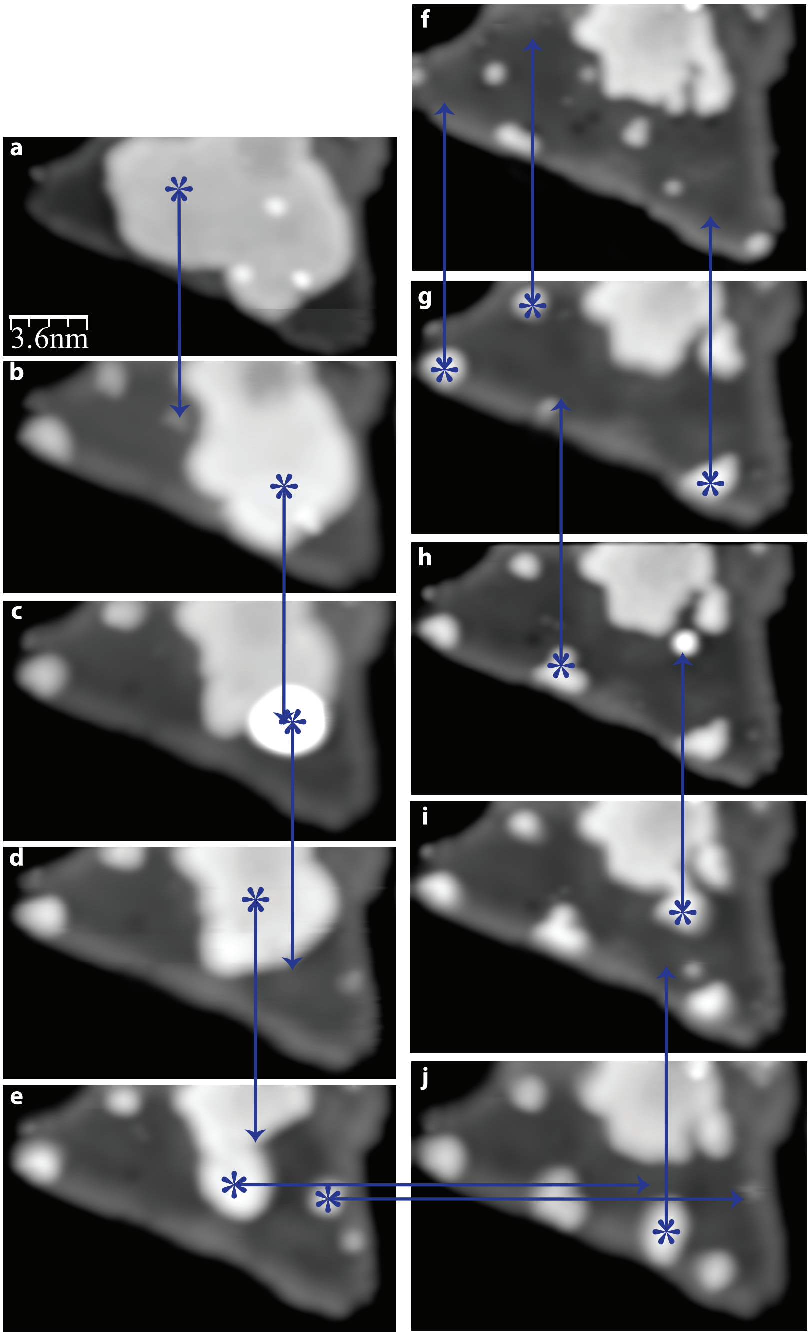

Figure 2.10: Series of STM images (200 mV bias) of the coating procedure. The initial image is seen in (a). The lowest visible layer is a cropped, triangular Co island. On top of this (brightest) is a layer of Au. The blue arrow indicates where the tip is approached with a star $*$ and the identical position in the next image with the arrow. When several arrows are present, several pickup attempts where done between the images shown.

Experimentally, the local barrier height can be measured in STS by keeping the bias constant and low (e.g. 50 mV) and then measure the current when ramping z. The resulting $I(z)$ can be fitted with an exponential and the local barrier height determined. The work function depends on the material, the surface orientation and the surface roughness or steps. It can be considered as an average of the tip and sample work functions. Literature values are for Cu(111): 4.2±0.1 eV and for 1 ML of gold on Cu(111): 4.5±0.2 eV measured with the same tip [70]. The local barrier height is then a slightly lower value than the bulk work function mostly due to the sharp form of the tip.

The local barrier height before these experiments, with a clean tungsten tip dipped in a Cu(111) surface is measured to $\phi = 4.0 \pm 0.05$ eV. When picking up Au flakes from the surface, the local barrier height increases slowly in steps of ~ 0.1 eV per successful pickup. After several successful pickups the local barrier height saturates at $\sim 4.4 \pm 0.05$ eV. The total increase of 0.4 eV of the local barrier height fits well with the increases in literature values.

Experiments have shown that there is an interesting difference between the clean Cu tip with $\phi = 4.0$ eV and Au-coated tip with $\phi = 4.4$ eV. When using these tips to pick up a Co atom, in the former case (Cu tip) the Co disappears from the surface, but the spectral feature of the tip does not change. In the latter case (Au-coated tip) the Co atom also disappears from the surface, but here the ${}^{\mathrm{d}I}\!/_{\mathrm{d}v}$ measurement shows a Kondo feature on a clean background after such an atom-pickup procedure. This leads to the conclusion that the Au makes it possible for the Co atom to sit as the outmost atom at the tip apex. This will be further discussed in the next section.

2.5 Picking up Co atoms with the STM tip

Manipulating atoms on a surface [3, 71, 72] as well as picking up and putting down single atoms with the STM tip [69, 73] has been achieved by many groups around the world . The purpose was normally to move atoms freely or to achieve better resolution in the STM topography. Here we report the possibility to pick up a Co atom with the STM tip and see a Kondo resonance formed at the tip. The Kondo resonance can be measured on the clean Au(111) substrate with no other Co atoms in the vicinity.

2.5.1 The technique

Single Co atoms are evaporated from a cobalt filament wound around a tungsten wire directly onto a Au(111) sample at 15–20 K. Figure 2.11 shows an example of such a sample preparation. As mentioned in the previous section, it is important that the tip is gold-coated, but apart from that the procedure has been tested with cobalt atoms on Au(111), Cu(111) and a few MLs of Au on Cu(111). Several techniques seem to work for the pickup procedure, but they all contain the two elements of approaching the tip to the Co atom and increasing the voltage in order to transfer the atom. In figure 2.12 three different examples are shown where the first example (a+b+c) approaches the tip 2.0 Å from tunneling set point (8 mV, 0.5 nA) on top of a Co atom and increases the voltage to 1.0 V as seen in figure 2.12(b). The current seen in (c) indicates a restructuring of the tip or a movement of the atom on the surface. As seen in the before/after images (a) the atoms look sharper after, which points to a tip

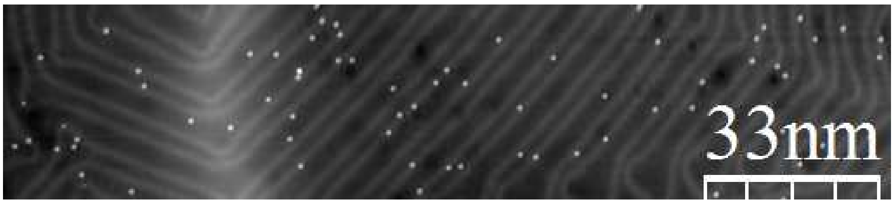

Figure 2.11: Individual cobalt atoms on a Au(111) surface.

restructuring. The differential conductance after the restructuring is seen in (d) with minor features related to the surface state scattering off the atoms on the surface.

This restructuring of the tip also indicates that the gold-coated tip is very soft and can easily adapt to a new configuration. The exact voltage and z-extension is not identical from experiment to experiment, so the parameters are slowly increased. In figure 2.12(f) the z is increased to 2.5 Å while the bias is kept at 1.0 V, which now shows no change in the current in (g) indicating that the tip is more stable now. This does not change the differential conductance spectrum.

Finally in (i) the voltage is increased to 1.2 V while keeping the distance at 2.5 Å and a characteristic signature of an atom being transferred from the sample to the tip is seen in (j). The subsequent image in (h) now shows no Co atom at the blue arrow and a measurement of the differential conductance on the bare substrate now shows the signature of a Kondo resonance as seen in (k). In this example the Kondo temperature is 126 K, but the line shape, the amplitude and the Kondo temperature can vary slightly depending on the atomic configuration of the apex of the tip. The process is only considered successful when the amplitude, width, and line shape of the Kondo resonance on the tip are similar to that on the surface.

The generally important factors in the pickup procedure are that the voltage should be kept below 20 mV when moving in z. A higher voltage can cause the atom to jump/fluctuate too early in the process and end up being further away from the tip apex. The Z-extension should be increased to the desired value close to contact (done in (b), (f), and (i) at time<0) and from this position, the bias should be ramped up to the desired value.

As mentioned, the tip might restructure instead of picking up an atom, so the procedure is not 100% reproducible, but so far works in 1 out of 5 attempts. The procedure can probably be further optimized for a better yield, either by use of local barrier height measurements described in section 2.4.2 or by stabilizing the tip further by putting down gold atoms before picking up the cobalt atom. It is beyond the scope of this thesis to discuss why exactly gold is easily mouldable to accept a Co atom placed at the very apex.

As mentioned in the previous section, this technique does not work for a Cu- or Ag-coated tip. The Co atoms can be removed from the surface, but do never show a Kondo resonance with the tip on the bare substrate. This is presumably due to the Co atoms not attaching at the apex of the tip, but further up along the side of the tip. On a related note, it has so far not been possible to find a reproducible reversible technique to put down a Co atom from a Au-coated tip. On the contrary, it has been

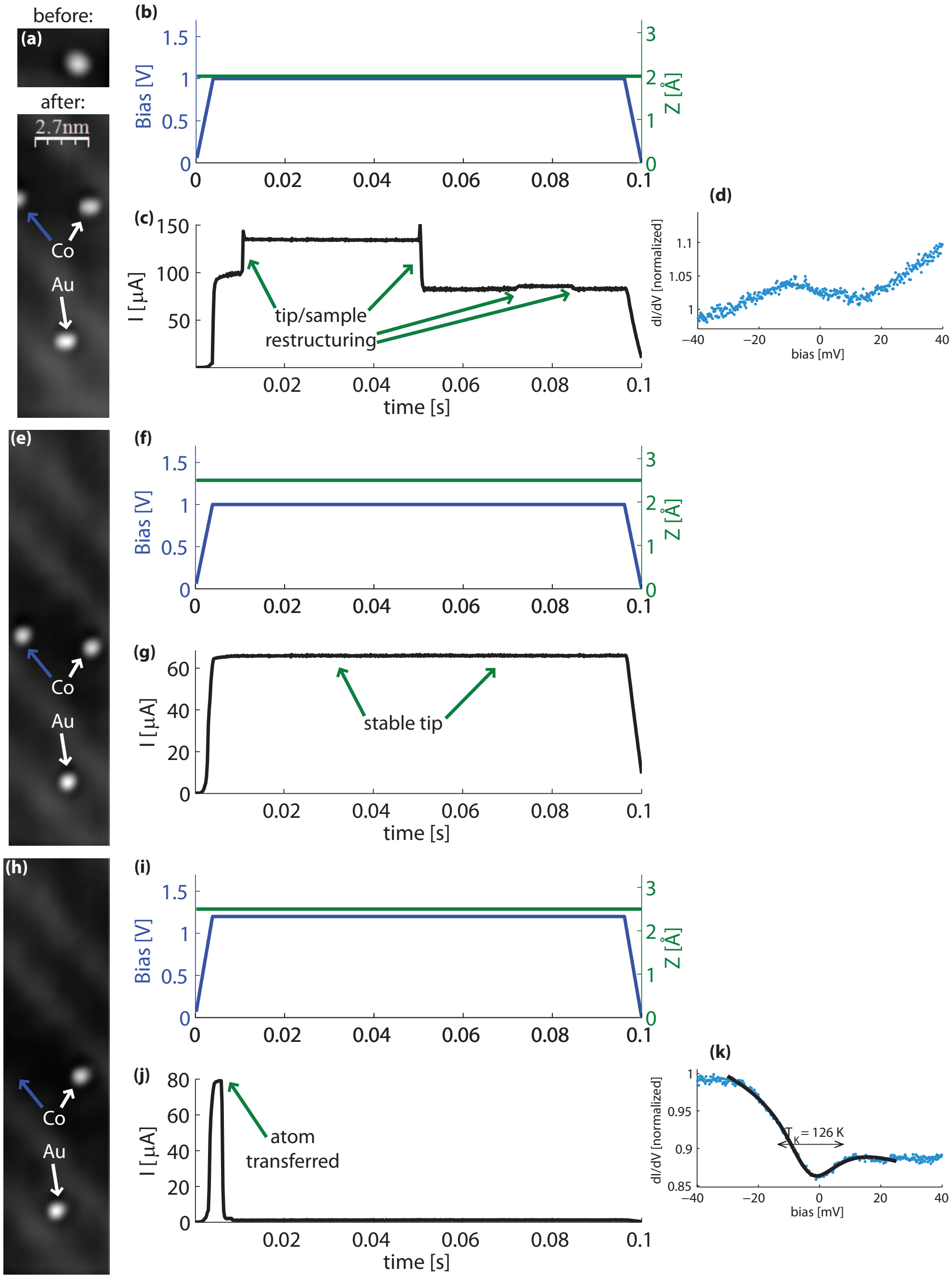

Figure 2.12: (a+b+c) showing a pickup process where the tip and/or sample atom restructures multiple times (seen in the current in (c)) during the 0.1 s when the tip is moved from tunneling (8 mV, 0.5 nA) to 2.0 Å closer at 1.0 V. (d) showing the differential conductance after restructuring. The pickup procedure is attempted on the left atom marked with a blue arrow. Lowest is one Au atom (shows no Kondo resonance) previously put down from the tip. The images are taken *after* the respective pickup procedures on the right. In (f) the tip is moved to 2.5 Å / 1.0 V but is now stable since there is no additional change in the current in (g). Pickup of the Co atom happens in (h+i+j) when the voltage during pickup is increased to 1.2 V and the distance is kept at 2.5 Å. The tip now shows a Kondo resonance (k).

shown in a few events that the Kondo resonance on the tip could be preserved while putting down an atom from the tip, which strongly suggests that the atom put down was not the outmost apex atom. Instead a looser attached atom from the side of the tip (presumably still close to the apex) was put down. These observations might also provide a clue to why it is only a gold-coated tip that is susceptible to a cobalt atom and creates a stable configuration at the tip apex.

One method to observe a successful atom pickup is to look for the absolute height change on the z-piezo, where the piezo extension should decrease roughly with the height of the atom. This seems to work for some atomic pickup processes[3], however, with the Au-coated tip this method is not applicable due to restructuring of the Au tip atoms when the Co attaches. The absolute height change is not representative of an addition of an atom to the tip as it has been observed so far.

In conclusion, the pickup procedure with a gold-coated tip is a fantastic tool to drastically change the properties of a normal, metallic tip into a Kondo system that can be freely positioned horizontally and laterally with very high precision. This method has the potential of opening up the scientific field of Kondo interactions and specifically the two-impurity Kondo problem as it shall be seen in section 4.6. Functionalization of the tip could also yield better control of spin-polarized tips due to different coupling mechanism for other atoms on the tip. Furthermore, it has already been shown that molecules such as C60 can change the tip to probe surface structures in new ways [74].

---

[3] private communication with Sebastian Loth, IBM Almaden

Growth and Electronic Structure of Capped Cobalt Islands

3

3.1 Growth and structure of Ag on bilayer Co nanoislands on Cu(111)

3.1.1 Introduction to the article in appendix A

In order to investigate magnetic interaction with STM and other relevant surface techniques, the onset for the work in this thesis was to look at the growth of magnetic islands and include a non-magnetic capping layer in order to magnetically isolate them from other materials. In the article in appendix A, it is shown how Ag nucleates and grows on a Cu(111) surface prepared with bilayer high Co islands. Interestingly, the silver preferably nucleates on top of the two ML high cobalt islands and almost completely covers the islands with a single, completed layer of silver. Due to the lattice mismatch between the cobalt island and the silver layer, a Moiré pattern appears similar to the pattern seen with Ag directly on Cu(111). The silver capping on the cobalt islands is studied by measuring the partial Ag coverage of the Co islands in the STM images as a function of total Ag coverage.

For all the details, the reader should read the article in appendix A before continuing.

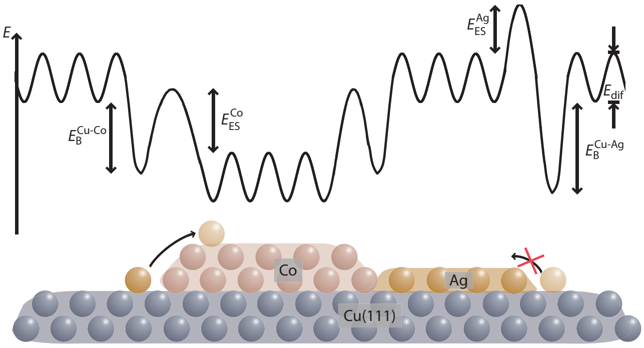

Figure 3.1: A qualitative suggestion to an extended version of figure 2.2. Here, the suggested energy barriers for diffusion and hopping on the Ag on Co islands and for Ag directly on Cu(111) are indicated and related to the layers shown below. The atomic arrangement is not to scale and the energy barriers are all relative to each other. The energy barriers are of course not the only factors involved in the diffusion process, but the illustration is a qualitative sketch of the Ag/Co/Cu(111) system.

Many factors can lead to this enhanced capping probability as discussed in the article, but generally equation 2.1 and figure 2.2 govern diffusion on the surface and at the step edge. In the article it is shown how silver preferably nucleates on top of the bilayer cobalt islands, which questions the general statement made above saying that less energy is needed to hop away from a step edge (lower step at an island) than to hop up the terrace (the island). It should be mentioned that it is not only the energy barriers involved but also e.g. the deposition flux and the diffusion prefactor that determines the final behaviour of the diffusion and growth.

In figure 3.1 a qualitative suggestion to modified sketch of the energy barriers in the situation of silver covered cobalt islands is shown. This model considers only energy barriers in a 1D model and does as mentioned not include other relevant factors such as the diffusion prefactor in equation 2.1. The energy scale on top describes the energy wells that the silver atoms/molecules sees when diffusing over the Cu(111) surface with the cobalt islands. We have not measured any absolute values for the energy barriers, so the barriers shown are only an example of how the situation might look like.

From left to right, the first larger energy well describes a silver atom attached to the lower step edge of a cobalt island held by the additional binding energy $E_{\mathrm{B}}^{\mathrm{Cu-Co}}$. In this situation there is an increased barrier in both directions, however hopping up seems more favourable than detaching from the step edge which is indicated by the lower barrier towards the island. When the silver atom is located on the cobalt island, diffusion is possible (to fill the island completely), but there is a substantial Erhlich-Schwoebel barrier to hop down from the island $E_{\mathrm{ES}}^{\mathrm{Co}}$.

From right to left, the situation is the classical situation also found in figure 2.2, with a relatively high binding energy $E_{\mathrm{B}}^{\mathrm{Cu-Ag}}$ which keeps the silver atoms on the Cu(111) surface growing in layer-by-layer growth mode. As mentioned, this model gives a qualitatively simple presentation of the situation by only considering energy barriers and not including the diffusion prefactor or molecule site which can play a major role in the full picture.

3.2 Photoemission spectroscopy of multilayered systems

3.2.1 Introduction to the articles in appendix B and C

In this thesis PES has been used to measure the growth conditions and electronic structure of two different systems. First, of a mainly catalyst-relevant material combination of Pt layers on Ru(0001) and second PES and ARPES of the previously mentioned silver-capped cobalt islands on Cu(111), both at the ASTRID synchrotron in Aarhus (see appendix E for setup). The measurements were carried out at RT and with the same evaporator as in the Aalborg STM, making a direct comparison of layer coverage possible.

In the first article with the title "*Study of the Pt/Ru(0001) Interface*" it is confirmed that Pt can be grown without intermixing at RT. The surface core level binding energy shift is followed for the Ru $4d_{5/2}$ and the Pt $4f_{7/2}$ and detected to be approx. 0.10 eV for the surface ruthenium when Pt is added and ≥ -0.476 eV between the $4f_{7/2}$ core levels of the two individual Pt layers deposited on Ru(0001). The details can be found in the article in appendix B.

In the second article using measurements made at the ASTRID synchrotron in Aarhus with the title "*Electronic structure and ordering of multilayers of Co and Ag on Cu(111) investigated by photoelectron spectroscopy and LEED*", the heterostructure $(\mathrm{AgCo})_{\mathrm{n}}\mathrm{Cu}(111)$ is investigated and compared to the STM study of the growth mentioned in section 3.1. The study with ARPES shows that the silver on top of the Co islands does not intermix and there is a surface state with a binding energy at 0.20 eV in normal emission.

The studies shown here with ARPES and previously with STM show that the Ag/Co/Cu(111) heterostructure is stable at RT as a model system for further magnetic studies. Before continuing below, the reader is now referred to the article in appendix C for all the details.

3.3 Potential energy landscape of metallic Moiré patterns

3.3.1 Introduction to the article in appendix D

After the growth of silver on Co/Cu(111) has been investigated, a low-temperature study of the electronic structure of the silver layer has been carried out and published as the article shown in appendix D. The article shows how the *d*-related state of the Co island is visible even through the Ag capping layer in the differential tunneling conductance maps. What is important to realize is that the Co islands grow pseudomorphic on the Cu(111) surface, which leads to almost identical lattice constants. Therefore, the Ag forms an almost identical Moiré pattern on both the Cu(111) surface and on the Co islands, but the Co islands introduce an extra *d*-related surface state in an otherwise identical system. The Moiré pattern is responsible for a spatial modulation of this *d*-related state – a modulation that is not seen with e.g. the onset of the *sp*-related surface state in the Ag/Cu(111). It is important to emphasize that this is not an additional *d*-related state brought in by the silver, but a modulation of the already existing state of the cobalt islands.

The measurements of the differential conductance are linked with the *d*-band model for catalysis, and although this model was originally designed for energies around 1-2 eV from the Fermi level, it still explains the observed spatial modulation and makes a very interesting link to catalysis. The catalytic properties of the surface can be controlled by adding an incommensurate metal layer that forms a Moiré pattern, thereby slightly shifting the catalytic properties of the original material.

Apart from the catalytic opportunities, the *d*-related state is know from the clean cobalt island to be spin-polarized [12], which could have an impact on magnetic structures placed on top of the Ag/Co/Cu(111) Moiré, thereby creating a magnetically selectable surface.

Before continuing below, the reader is now referred to the article in appendix D for all the details.

3.3.2 Comparison to Au/Co/Cu(111) and Co/Ag(111)

To further understand the spectroscopic features seen here, different experiments were carried out where a few elements were changed. First, the silver capping layer was changed to gold. The difference in lattice constants also yields a Moiré pattern, but with a periodicity of ~38 Å compared to the ~24 Å of the Ag/Co/Cu(111). The gold Moiré seems not to have the same strength as the silver Moiré, since domains of different orientations and even cracks and half-filled islands can appear, see figure 3.2(a). This rotation of the Moiré pattern indicates the coalescence of nuclei with different orientations.

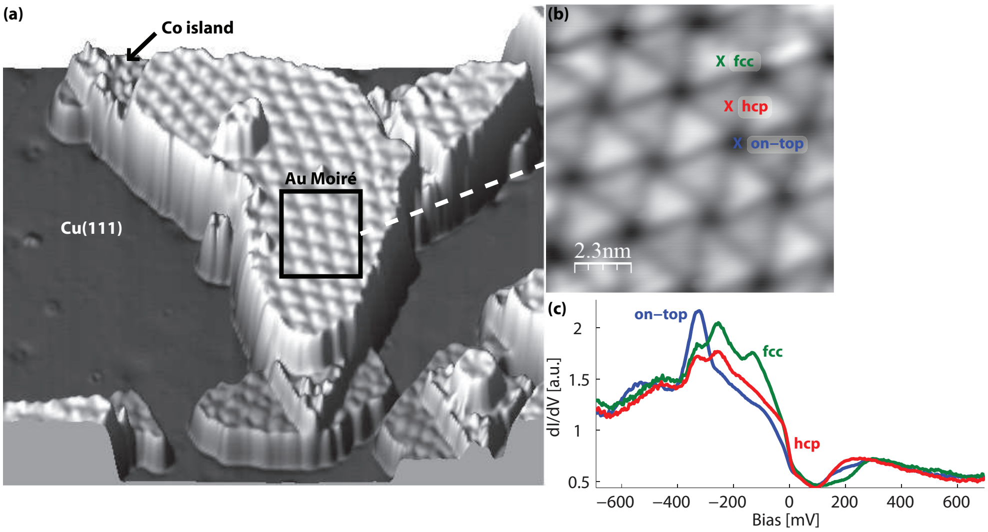

Figure 3.2: (a) Topography of a gold-capped cobalt island on Cu(111) (image size 73×73 nm, 1.4 nA, 1.0 V). The large island in the center is one island with a crack in the gold Moiré on the right-hand side. Small patches of gold are also visible directly on the Cu(111) surface. (b) A close up of the Moiré pattern and (c) the corresponding differential conductance curves for the three relevant regions.

The Moiré pattern from on top of the island is seen in the close-up in figure 3.2(b). Except for the periodicity, the overall symmetry of the Moiré pattern looks similar to Ag/Co/Cu(111). There are three regions which we assigned to fcc, hcp, and on-top regions, in descending apparent height, by analogy to the Ag/Co/Cu(111) assignments. The differential conductance spectra for the three regions are shown in figure 3.2(c), where some similarities to the spectra for Ag/Co/Cu(111) can be found (compare with figure 1(a+b) and 2(b) in the article in appendix D). The similarities are a dominant feature in the on-top region (here at −325 mV) and other features higher in energy with a comparable amplitude in the fcc/hcp regions, but the number of features in the range −600 to 100 mV and their spatial modulation cannot be resolved in a satisfying way.

In an attempt to simplify the structural composition and thereby hopefully also the differential conductance spectra, the structures of 3 ML cobalt islands on Ag(111) [75] has been investigated. This can be thought of as the "reversed" structure with respect to Ag/Co/Cu(111), especially when it is known that cobalt grows pseudomorphically on Cu(111). An STM topography can be seen in figure 3.3(a), where the formed Moiré pattern with a periodicity of ∼19 Å is visible in (b) and the corresponding differential conductance spectra in (c).

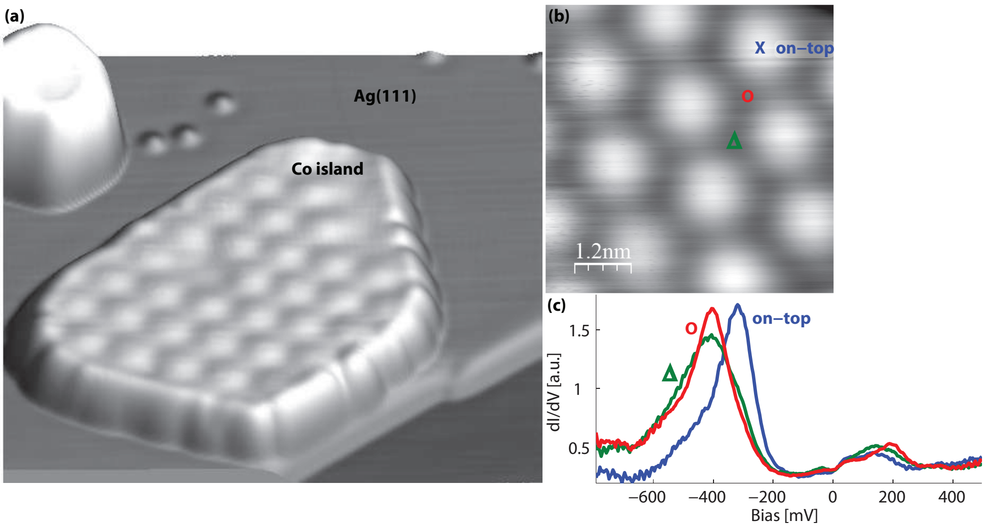

Figure 3.3: (a) Topography of a cobalt island on Ag(111) (image size 73×73 nm, 0.7 nA, 300 mV). (b) A close up of the Moiré on the cobalt island and (c) the corresponding differential conductance curves for the three relevant regions.

By symmetry arguments only the on-top position in the Moiré pattern can be assigned as the apparently highest protrusion. Although STM images at −400 mV bias show different apparent height of the fcc and hcp regions as expected from figure 3.3(c), it is not possible to assign which region is fcc and which is hcp without further information. Here it is important to notice that the height contrast is inverted compared to the Ag/Co/Cu(111) and Au/Co/Cu(111) Moiré patterns. The on-top region appears high for Co/Ag(111) which points to the fact that here the hybridization is also inverted and thereby making hcp/fcc regions the ones with strongest hybridization.

In this case, the features in the differential conductance spectra are easier decomposable than for Au/Co/Cu(111). A main feature below the Fermi level located at −320 mV in the on-top region and moved to −400 mV in the hcp/fcc regions is clearly seen in figure 3.3(c). The shift is larger than for Ag/Co/Cu(111), but the amplitude of the feature stays almost the same from on-top to fcc/hcp. On the contrary, for Ag/Co/Cu(111) the amplitude changes by a factor 7. This interesting difference might cause a larger change in reactivity for the Ag/Co/Cu(111) surface if the adsorbent is sensitive to a change in intensity instead of energy relative to E_F. This would depend on the adsorbate.

During these studies, we became aware of similar work [76] on the same structure, where similar spectra arise and differential conductance mapping is used to show the variation across a cobalt island. In [76] the lowest island is taken to be a monolayer island whereas in [75] this is taken as a bilayer island with reference to their figure

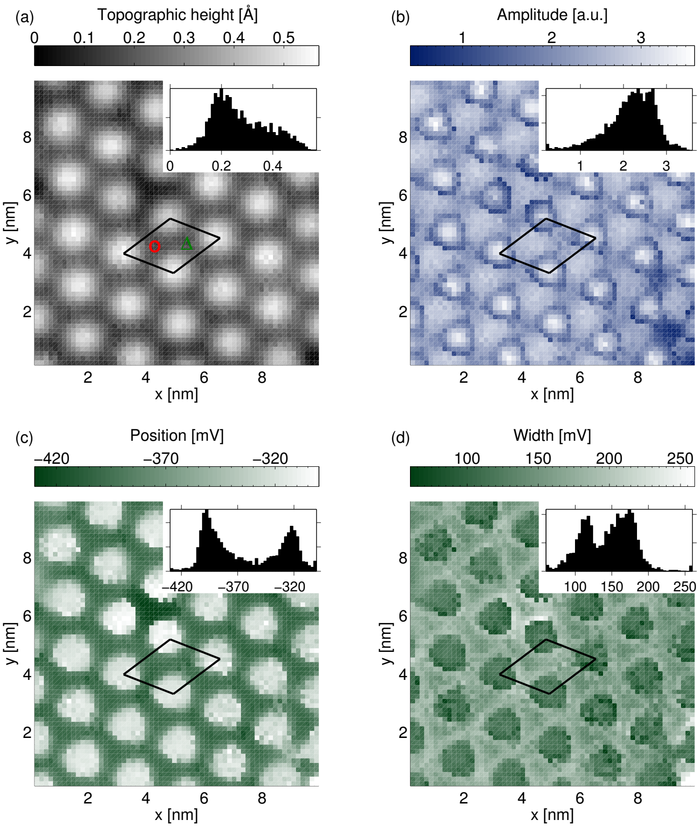

Figure 3.4: (a) Topographic image of the area in which the spectroscopic map has been acquired from which the following maps have been extracted; (b) map of the amplitude, (c) map of the energy position, and (d) map of the full width at half maximum. The inset in each panel shows a histogram of the respective quantity. All data maps consist of 64x64 points.

4b histogram of island heights showing peaks at 4, 6, and 8 Å thereby indicating 2 Å per ML and a growth behaviour like cobalt on Cu(111) where the minimum at RT deposition is also bilayer islands. This interpretation is also chosen here although it cannot be excluded that an electronic effect causes the first monolayer to have an apparent height double that of the consecutive layers. This could be tested by deposition of cobalt at lower temperatures than the 180 K done in [75] to look for a 2 Å monolayer.

In this work, differential conductance spectra are taken in each point in the topography in figure 3.4(a), and fitted with two Lorentzian functions in the range −700 to −100 mV. A main feature located between −320 and −400 mV and a shoulder to this feature around -500 mV. In the following, only the main feature will be mentioned and the shoulder can be seen as stabilizing the fit of the main feature. Figures 3.4(b), (c), and (d) show the amplitude, energy position and width of the main feature and can be compared with the article in appendix D, figure 3 – peak A. It is clear that for Co/Ag(111) the amplitude change is comparatively small, but the energy shift is

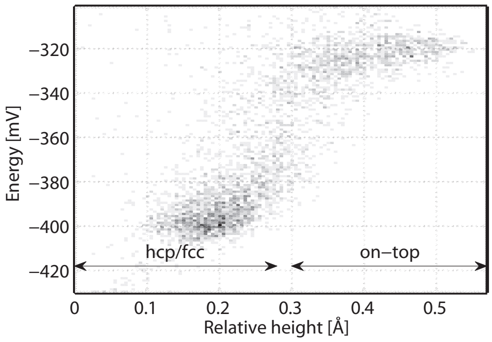

Figure 3.5: 2D histogram of the energy position against the height extracted from figures 3.4(a) and (c).

much larger. To show this energy shift more clearly, figure 3.5 contains a 2D histogram comparable to figure 4(a) in the article in appendix D. As mentioned in the article, lower apparent height translates into stronger hybridization between the cobalt atoms and the silver atoms and the situation here also complies with the *d*-band model [77] used to describe the observations in the article in appendix D.

The large shift in energy and small change in amplitude of the Co/Ag(111) structure is interesting in comparison with the small shift in energy and large change in amplitude of the Ag/Co/Cu(111) structure. Depending on whether the catalytic selectivity is governed by the energy position of the *d*-related state or the presence of additional DOS, the selectivity in the two cases could be very different. In [76] the work is extended to show site-specific adsorption of FePc molecules in the Moiré pattern of the 4 ML cobalt islands (3 ML in [76]) on Ag(111). In figure 3.6 the growth of additional cobalt on the original Ag/Co/Cu(111) is shown. The Moiré pattern on the island is visible and it can be observed that the additional cobalt grows in very small islands and that they have all nucleated in the on-top region of the Moiré pattern. This is the region with the largest amplitude of the *d*-related state.

These results show that both the energy position and the amplitude of the *d*-related state can govern the catalytic properties. Selective adsorption has been shown which indicates an electronic template effect that shapes the potential energy landscape of a metallic Moiré pattern. With two examples from Ag/Co/Cu(111) and Co/Ag(111) it is suggested that this is a general effect for Moiré patterns which can be utilized as a template to control and assemble patterned clusters and molecules.

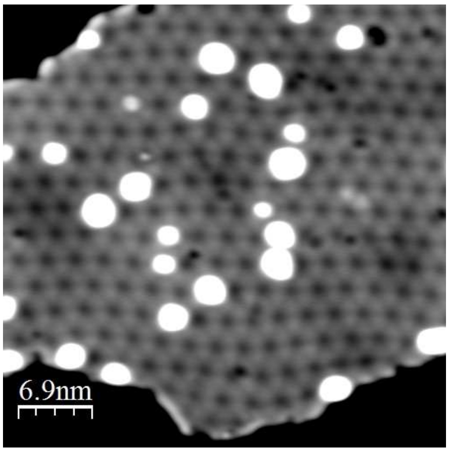

Figure 3.6: 40×40 nm topography (1.5 nA, 600 mV) of small cobalt clusters grown at RT on the silver-capped cobalt islands on Cu(111). All Co clusters nucleated in the on-top region of the Moiré pattern.

The Kondo Effect

4

4.1 Background

The resistance of a pure metal decreases with decreasing temperature due to suppression of lattice vibrations. But in the 1930s it was found that some metals showed an increase in resistance below a certain temperature [78, 79]. This is shown in figure 4.1 with the real data from [78], where the overall trend of decreasing resistance with decreasing temperature is shown in the main panel and the inset shows a zoom-in on the low-temperature part of the same curve. In the original article it is already speculated that the increase in resistance might be related to impurities, but the authors were not aware that the production process left magnetic impurities in their sample. In 1964 Jun Kondo was the first to give an explanation of the effect [80]. Jun Kondo showed that when the temperature is lowered in a metal with diluted magnetic impurities, an additional scattering of the conducting electrons in the metal occur. When the temperature is low enough, the magnetic atoms also act as impurities for the spin-part of the electron, giving rise to spin-flip scattering.

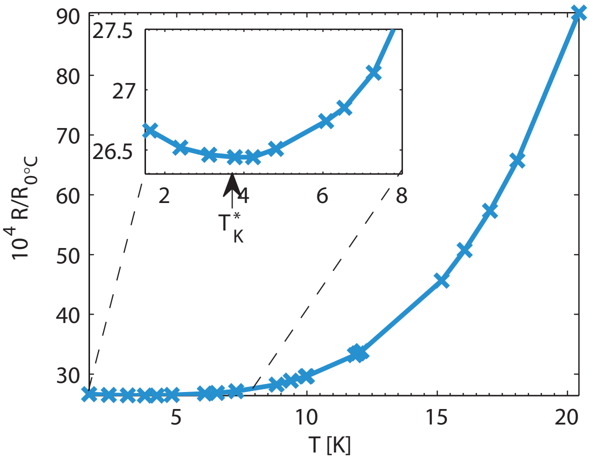

Figure 4.1: The first data from 1934 showing resistance measurements as a function of temperature in a Au wire with $T_K = 3.70$ K. This is a plot of the original data given in [78].

The Kondo temperature T_K^* is defined as the resistance minimum, but in STM the Kondo temperature T_K is defined as the energy scale (temperature regime) where the Kondo results are valid. Jun Kondo showed that the resistivity $R(T)$ should be written as

$$R(T) = R_0 \left[1 + 2\rho J \log\left(\left|\frac{k_\mathrm{b} T}{\epsilon_\mathrm{k} - E_\mathrm{F}}\right|\right)\right], \tag{4.1}$$

where R_0 is the resistance when only including first order scattering processes (not spin-related), ρ is the density of states at the Fermi level E_F, ϵ_k is the energy of the scattered electron, and $k_\mathrm{b}T$ is Boltzmann's constant times the temperature. J is an exchange interaction between the s-state conduction electrons and the d or f level impurity that causes the conduction electrons around the impurity to align with the magnetic moment in the impurity. The sign of J determines the s-d (or s-f) coupling. If $J > 0$ the spin of the conduction electrons will align parallel to the spin of the magnetic impurity (ferromagnetic case) and if $J < 0$ the spins will align antiparallel (antiferromagnetic case). Only in the antiferromagnetic case, the second term in equation (4.1) yields a resistance increase with decreasing temperature and this is the case that will be used throughout this thesis.

Jun Kondo's model explains the resistance minimum, but the logarithmic term will also make the resistance diverge to ∞ as $T \to 0$, which is not correct. The work for a correct theoretical description of the $T < T_\mathrm{K}^*$ regime is called the Kondo Problem and was solved for the single impurity case by Wilson in 1975 [81] by introducing renormalization group (RG) theory. It is worth noticing, that the Kondo effect is a many-body phenomenon, where one magnetic impurity (in the bulk or on the surface) causes many conduction electrons to screen the magnetic moment in an entangled Kondo cloud, see figure 4.2(a). The net magnetic moment of the impurity and the cloud is 0 when the screening is antiferromagnetic – this is called a spin singlet state.

4.2 The Kondo effect in STS

In 1998 the interest in Kondo systems was revived by the discovery of the Kondo effect in a tunable quantum dot [19] and in STS [18,82]. In the decade that followed, single-impurity Kondo systems quickly gained more interest and lately also the two-impurity Kondo systems have been investigated [17,83].

The Kondo resonance has been shown to exist for Co atoms on different metallic surfaces [16] and for different atoms on the same surface, such as e.g. Ti, Co, and Ni on Au(111) [84]. Furthermore, the Kondo resonance has been detected in molecules [13,85] and carbon nanotubes [86].

The Kondo effect can be measured in STS by placing the tip over an impurity on or in the surface as shown in figure 4.2(a) and sweeping the bias in the low-energy range. The impurity can be a single atom, a dimer, or a larger molecule, but must contain a localized d- or f-level that hybridizes with the metallic substrate. In the following, the d-level of Co on Au(111) will be used as an example.

With the local spin-density approximation it can be calculated [87] that the average impurity occupation number for Co on Au(111) is $n_d \simeq 8.8$ instead of the $n_d = 7$ expected from the electronic configuration [Ar]4s^{2}3d^7. This increase is mainly due to the sp-d hybridization between the bulk Au and the Co impurity, which shifts the Co d-level downward and thereby increasing the occupation number. This leaves only the last three, $Z = 8, 9, 10$, of the 11 possible charge states of the Co d-level, $Z = 0, 1, ..., 10$, free. From Hund's rule, these states can be determined within the effective spin $1/2$ Anderson impurity model as the empty ($Z = 8,\ \sigma = 1$), the singly ($Z = 9,\ \sigma = \pm 1/2$), and the doubly ($Z = 10,\ \sigma = 0$) occupied state without orbital degeneracy.

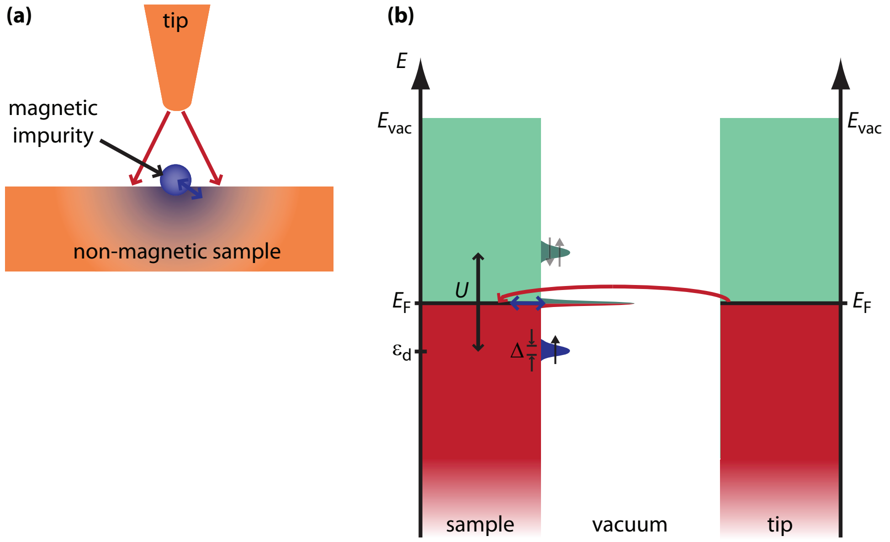

Figure 4.2: (a) Illustration of a single magnetic impurity on a metallic surface. Electrons from the tip tunnel into the substrate surrounding the magnetic impurity and here the electrons spin-flip scatter with the magnetic moment of the impurity, hereby creating the Kondo resonance. (b) Energy diagram of a *d*-state impurity Kondo system.

It can be shown [87] that a 3*d* or 4*f* impurity with an effective spin higher than $S = 1/2$ can be converted in to a single orbital impurity with $S = 1/2$, i.e. with 0, 1 or 2 electrons. This means that the impurity can be described by the Anderson single-impurity model [88].

An Anderson single-impurity adsorbed on a metal surface will hybridize its local 3*d* or 4*f* state with the continuum in the bulk metal, leading to a broadening of Δ of the state located ε_d below the Fermi level, as illustrated in figure 4.2(b). The state is singly occupied and the energy cost due to Coulomb repulsion U of adding a second electron is $\varepsilon_\mathrm{d} + U$, which will move the state above the Fermi level. The Kondo resonance only occurs when the singly occupied state is below the Fermi level and the doubly occupied state is above. Anderson showed [88] that local moment formation only occurs when $\Delta \approx 2\pi V^2 \rho_0 \ll |\varepsilon_\mathrm{d}|, \varepsilon_\mathrm{d} + U$ as shown in figure 4.2(b). Here, V is the hopping matrix element connecting the electrons of the Fermi sea to the localized impurity level and ρ_0 is the DOS of the Fermi sea at the energy ε_d [44]. The physical meaning of this is that the *d*- or *f*-level has to be well separated and not overlap with the Fermi level.

The interaction of the localized *d*-level with the substrate introduces a sharp resonance-like peak pinned at the Fermi level. This Kondo peak is the many-body resonance and it arises from calculations beyond mean-field calculations such as Hartree-Fock. The width of this feature is $2k_\mathrm{b}T_\mathrm{K}$ and this can be detected in STS to determine the Kondo temperature of an impurity.

When the STM tip is placed over a magnetic Kondo impurity as illustrated in figure 4.2(a), electrons tunnel into the Fermi sea around the impurity. Earlier models [89,90] suggested that a non-negligible amount of the electrons tunnel directly into the

Kondo state located at the Fermi level (even at tunneling set points several Å above the atom). Due to experiments showing no line shape change when moving the tip away from the impurity, this is neglected in most current models [87,91,92]. Instead, the electrons can interact or resonate with the local impurity once they have entered the substrate at the Fermi sea. This is illustrated by the blue arrow in figure 4.2(a) and (b) as the interaction between the local impurity state at the Fermi level and the continuum Fermi sea of the substrate.

Mathematically, a Kondo impurity is one special case which is well described by the Fano formalism [93], in which the low-energy excitations arising from the spin scattering at the local moment are described by the Fano line shape

$$f(\omega, q) = a\frac{(\omega+q)^2}{\omega^2+1}, \tag{4.2}$$

where a is the amplitude, q is a line shape parameter and

$$\omega = \frac{eV_{\mathrm{bias}} - E_0}{k_{\mathrm{b}}T_{\mathrm{K}}}, \tag{4.3}$$

where E_0 is position of the resonance with respect to the Fermi level, which is slightly offset from the Fermi level due to repulsion from the localized d-states at ε_{d}. Equation (4.2) is fitted to an STS spectrum of a Co atom on Au(111) in figure 4.3, where all the relevant parameters are shown.

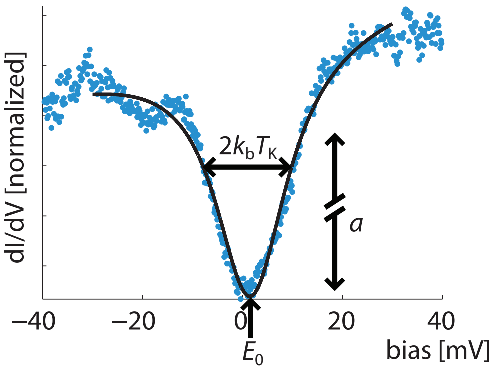

Figure 4.3: STS data for a Co atom on Au(111) with the corresponding Fano line shape fit. Also indicated are the parameters from equation (4.2) and (4.3).

The main thing one notices in the figure is that the resonance line shape (a dip) does not follow the DOS shown close to the Fermi level in figure 4.2(b) (a peak). The transport into the Kondo resonance at the Fermi level is governed by the Fano line shape parameter q, which specifies the shape of the resonance as shown with examples in figure 4.4. q is the ratio of the real part to the imaginary part of the Green's function for the tunneling electron [87]. The Green's function describes how electrons propagate in the Fermi sea and interact with the localized magnetic moment to change the q parameter. This is more extensively reviewed by Plihal and Gadzuk [90], but with mainly the same conclusions; the Fano line shape is governed by the electronic

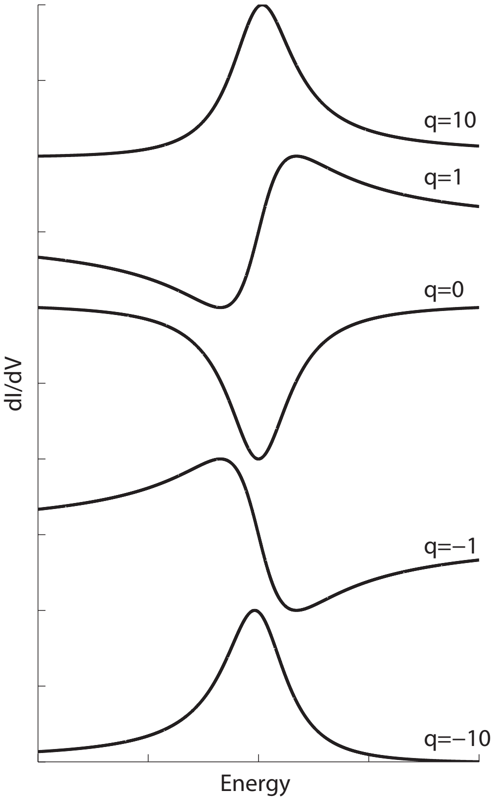

Figure 4.4: Examples of the Fano line shape parameter q. When q approaches $\pm\infty$ the Fano line shape approaches a Lorentzian line shape. At ± 1 the line shape is asymmetric and at 0 a symmetric dip.

structure at the surface of the substrate and the interaction with the Fermi level localized impurity state.

To emphasize the effect of the substrate, the quantum mirage experiment should be mentioned [94], where a Kondo resonance is observed in one empty focus point of an elliptic quantum corral, when the other focus point contains a Kondo impurity. This is explained in detail by Fiete and Heller [44] and shows how the Kondo resonance can be mediated by the substrate surface state while completely separated from the localized d-level state.

4.3 Magnetic influence on the Kondo effect

As shown in the previous section, electronic effects can change the Kondo resonance, but also magnetic effects can have an influence. The influences from a magnetic field, from an exchange field, and from another Kondo impurity are reviewed in the following.

4.3.1 Applied magnetic field

In a magnetic field, the unpaired localized impurity level will split up by an energy $\epsilon_Z = g\mu_B B$, where g is the g-factor, μ_B is the Bohr magneton, and B is the applied field [95]. This causes the Kondo resonance at the Fermi level to split by the double voltage $V_{\text{split}} = \pm g\mu_B B/e = \pm 0.12\text{mV/T}$ if $g = 2$ is taken as the free electron g-factor. This was predicted theoretically [96] and shown in quantum dots [19, 95], single atom or molecule transistors [97, 98] and in STM [68, 99] – all with an external magnetic field. In a 15 T field the Kondo resonance will be split by ±1.8 mV which demands a good energy resolution, a low Kondo temperature and low temperatures in general to measure. More recently, it has also been shown experimentally that another embedded impurity affects the original Kondo system and a so-called two-impurity Kondo system can also show a splitting of the resonance [99–102].

The splitting can be described [17] with the sum of two Fano line shapes as

$$g(\epsilon) = a_1 f(\frac{eV_{\text{bias}} - {}^{J}\!/_{2}}{k_b T_K}, q_1) + a_2 f(\frac{eV_{\text{bias}} + {}^{J}\!/_{2}}{k_b T_K}, q_2), \tag{4.4}$$

where $f(\omega, q)$ is the Fano line shape from equation (4.3) and the total splitting between the two peaks is $J = eV_{\text{split}}$.

4.3.2 Exchange interaction

Exchange interaction is a quantum mechanical effect and a consequence of exchange symmetry between indistinguishable particles. Changing the label of two such particles infers that the wave function describing the two particles must be either unchanged or inverted in sign. For anti-symmetric wave functions (fermions) this can (due to the Pauli exclusion-principle) in some cases lead to ferromagnetism [103].

The exchange interaction can be split into several subgroups, such as *direct exchange* related to the direct overlap of atomic orbitals, *indirect exchange* polarizing non-magnetic conduction electrons to transfer the exchange, *superexchange* between next-nearest neighbour atoms and *double-exchange* between neighbouring atoms of different species.

Normally, the exchange interaction is orders of magnitude stronger than the competing dipole-dipole interactions between two ferromagnetic objects. For the case of a Kondo impurity influenced by a ferromagnetic cobalt island it is therefore relevant to focus on the exchange interactions.

This has been calculated with a Cu spacer layer on a monolayer high Co island by Brovko et al. [104]. The calculations yield exchange coupling energies J between an island and an atom as a function of Cu monolayers and a reproduction of the results shown in the article is given in figure 4.5. It is seen that the coupling energy has an oscillatory decay with a maximum energy of -780 meV (ferromagnetic) for the Co atom directly on the island and 40 meV (antiferromagnetic) for two layers of Cu spacer. This would in principle result in the equivalent splitting of the Kondo resonance of the single Co atom into ±40 mV for the latter case. Experiments using the exchange interaction will be shown in section 4.4.

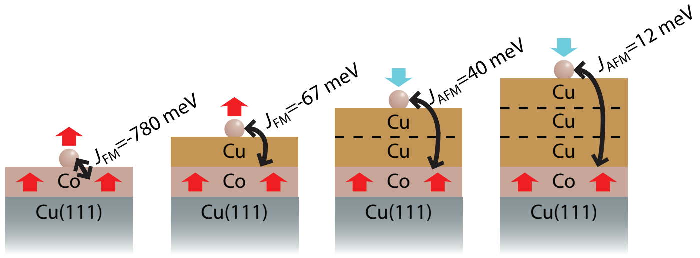

Figure 4.5: A cobalt atom placed either directly on a layer of cobalt or with an increasing number of copper spacer layers in between. Calculations of the exchange interaction between the cobalt atom and the cobalt layer yields ferromagnetic interaction, J_{FM}, for no and 1 ML spacer and antiferromagnetic interaction, J_{AFM}, for 2 and 3 ML spacer. Reproduction of figure 1a+b in [104].

4.3.3 Two-impurity Kondo system

The two-impurity Kondo problem has been studied extensively theoretically [23, 105, 106] and the general idea of two Kondo impurities with a varying distance has until now only been implemented with two atoms on the surface [17, 83]. Normally the distance between the two atoms is the variable parameter. Three regimes then dominate the coupling of the two atoms depending on the exchange interaction strength J versus the single-impurity Kondo temperature; (i) if $J \gg k_{\mathrm{b}}T_{\mathrm{K}}$ (J is large and positive) the two atoms are coupled ferromagnetically with each other and form a spin triplet state; (ii) if $-J \gg k_{\mathrm{b}}T_{\mathrm{K}}$ (J is large and negative) the interaction is antiferromagnetic meaning that the magnetic moments of the two atoms couple antiferromagnetically and form a spin singlet state; (iii) if $k_{\mathrm{b}}T_{\mathrm{K}} \gg |J|$ (J is small) the single impurity Kondo temperature is the dominant energy scale, the single atoms interact weakly and they are each screened by individual Kondo clouds (individual spin singlets).

In section 4.6 it will be shown how continuously varying the distance between two Co atoms creates a controlled crossover between a Kondo compensated state and an antiferromagnetically coupled state and how this unique possibility to traverse a crossover in a two-impurity Kondo system between two quantum phases reversibly with the STM tip could become an important tool for research in quantum phase transitions.

4.4 Exchange interaction in Kondo impurities on capped cobalt islands

As described in the Introduction in section 1.2, the initial onset for this PhD thesis work were experiments done by Wahl, Diekhöner and colleagues [11–17] with individual cobalt atoms in the vicinity of larger magnetic structures, such as magnetic cobalt islands. Varying the distance between the Co atoms and the magnetic island should be reflected in the Kondo resonance and thereby indicating the magnetic interaction between the island and the atom [20]. Moving individual atoms on a surface is limited by the facts that the atoms will stick to predefined lattice sites which limits the freedom and the distance resolution of the measurement. When getting within a few Å of another atom or island, the atoms will hop to the other object making measurements in the sites in between impossible [107].

This problem was sought to be solved in the 3rd dimension by adding a non-magnetic layer on top of a magnetic island, thereby creating magnetic isolation for the cobalt atoms now evaporated on top of this sandwich structure, see figure 4.6 for an illustration of the setup.

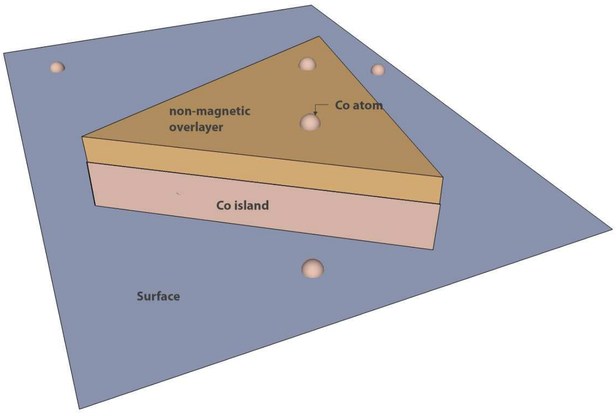

Figure 4.6: Model of the system in question.

The non-magnetic spacer layer can be one of several metals; we have tried Cu, Ag, and Au. Since the Co islands grow pseudomorphic on Cu(111), adding additional Cu will result in nucleation around the Co islands and eventually also pseudomorphic growth on top of the Co islands[1]. With a single Co atom on top of 1 ML Cu spacer (on a Co island), no Kondo resonance is detected, indicating that the spin-flip scattering of the Kondo resonance is not energetically favourable and the moment of the Co atom is fixed. When increasing the Cu spacer layer to 2 ML or more, the Kondo resonance reappears as completely restored to that of a Co atom on clean Cu(111), due to a very small exchange interaction to the underlying Co island. The calculations by Brovko et al. [104] shown in section 4.3.2 did therefore not hold true for the bilayer cobalt islands with a Cu spacer layer.

Due to the difference in lattice constants and electronic structure, different effects could appear when adding 1 ML of Ag or Au as the non-magnetic spacer instead of Cu. As shown in our article in appendix D, Ag forms a combination of a buckling layer and a Moiré pattern where the apparent height is varied across the unit cell of the Moiré and Au has similar properties as a capping layer. Atomic manipulation is used to place Co atoms in the different lattice areas of the Moiré.

For the experiments, the Co islands are grown on Cu(111) and capped with Ag or Au as it is also described in the article in appendix D. Single atoms are then evaporated directly on the sample in the cryostat at temperatures around 15 K.

The spectra for Co atoms on the Ag Moiré are seen in figure 4.7 and the spectra for Co atoms in the Au Moiré are seen in figure 4.8. First notice that the backgrounds

---

[1] unpublished work by Diekhöner

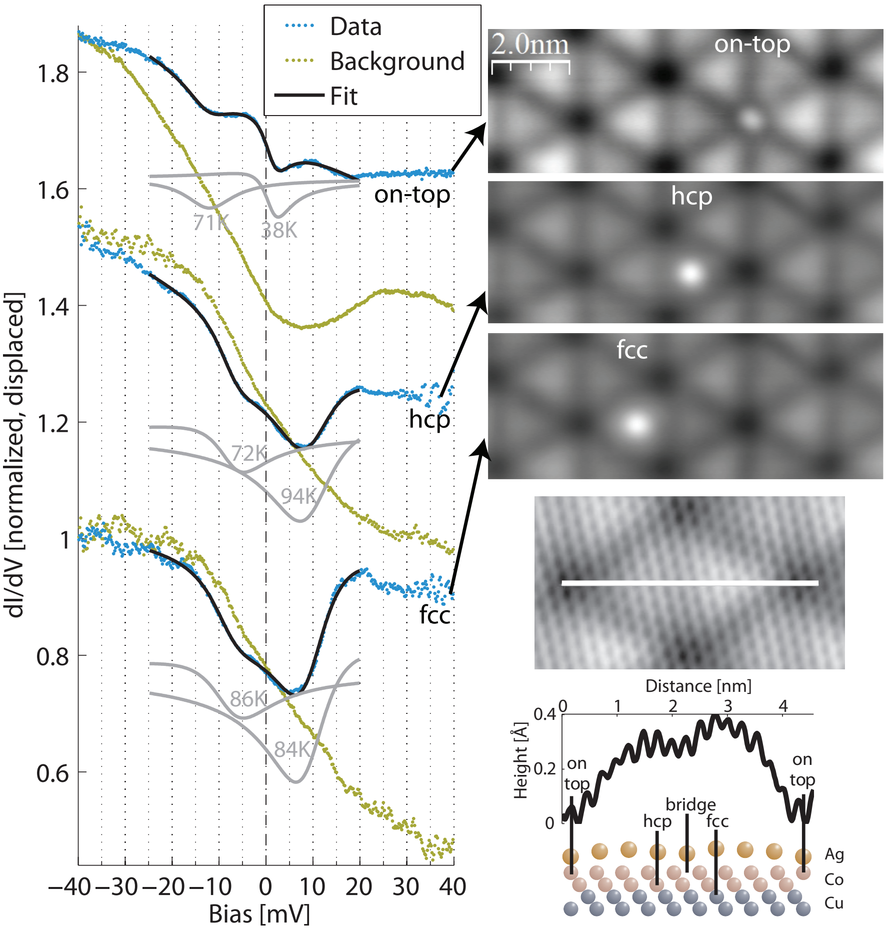

Figure 4.7: Kondo spectra, corresponding background spectra, and corresponding STM images (11 mV bias) of a Co atom on 1 ML of Ag on a bilayer Co island grown on Cu(111). The island edges are not visible. The total fits to a sum of two Fano line shapes are shown as black curves, whereas the individual Fano line shapes are shown as grey curves below the total fit with their individual T_{K}. The spectra are normalized at -40 mV and displaced vertically for readability.

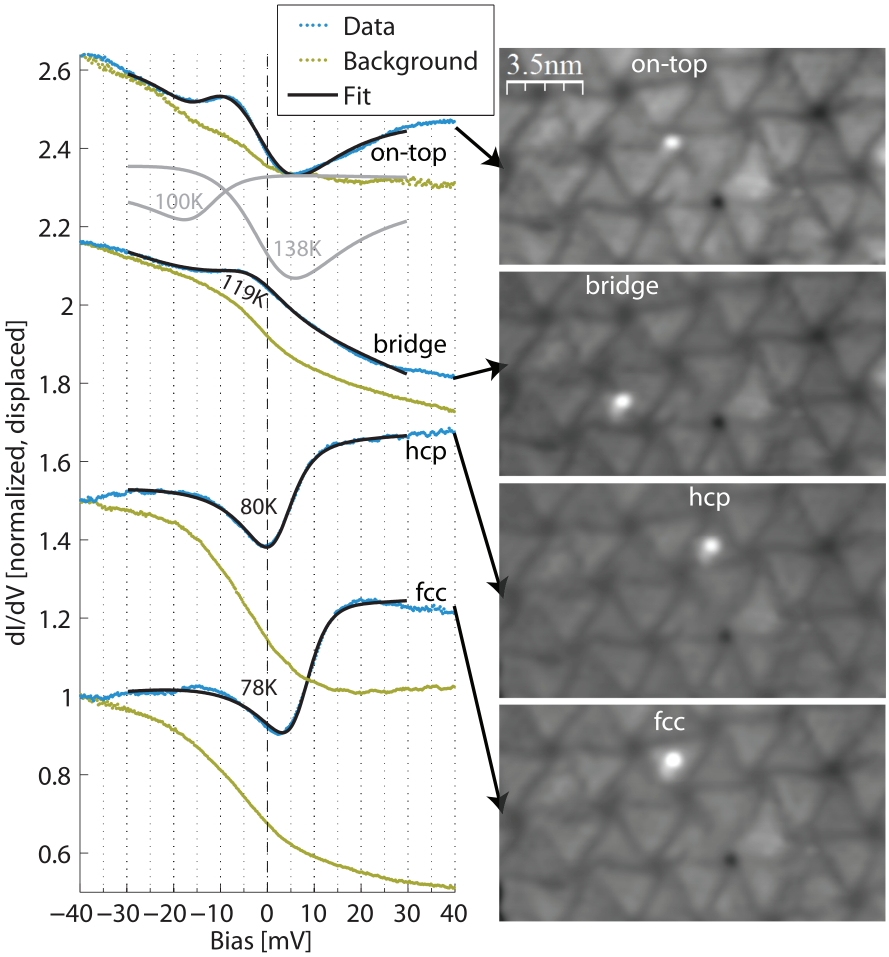

Figure 4.8: Kondo spectra, corresponding background spectra, and corresponding STM images (20 mV bias) of a Co atom on 1 ML of Au on a bilayer Co island grown on Cu(111). The island edges are not visible. The total fits are shown as black curves (single Fano line shapes for fcc/hcp/bridge and the sum of two Fano line shapes for the on-top curve) and the individual Fano line shapes are shown as grey curves below the total fit of the on-top curve. The spectra are normalized at -40 mV and displaced vertically for readability.

in all cases are not completely flat. This is due to the tail of the *d*-related states described in our article in appendix D, which is mainly located below the Fermi level. The slope of some of the Kondo spectra follow this background, but a general background subtraction according to the method described in [66] does not improve the readability of the spectra.

All spectra shown here for Ag are representative of several measurements made with different tips and sample preparations which all have shown similar features. For Au all spectra are taken within the same sample preparation and with the same tip.

The Kondo spectra of Co in the Ag Moiré all show additional features close to the Fermi level. The clearest, undisturbed Kondo resonance is found for the Co atom in the fcc region of the Moiré which is also the region with highest apparent height in the model in figure 4.7, i.e. furthest away from the underlying Co island. Even in this region, there is clearly a small feature just below the Fermi level at approx. -5 mV.

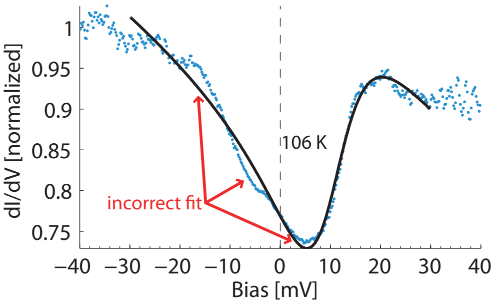

Figure 4.9: Kondo spectrum from a cobalt atom in the fcc region of the silver Moiré identical to lowest curve in figure 4.7 . A single Fano line shape is fitted to the data as an example.

If the spectrum in the fcc region is fitted with a single Fano line shape fit as shown in figure 4.9 the Kondo temperature regardless of the fitting range is found to be ∼106 K, which is slightly broader than the 92 K on Ag(111) [16, 108]. More importantly it is not possible to correctly fit the data with a single Fano line shape as can be seen at the red arrows in the figure. This indicates that the Kondo resonance is affected by its environment either by a broadening or a splitting.

If this is interpreted as a splitting of the Kondo resonance, the spectrum can be fitted with the sum of two Fano line shapes from equation (4.4) and the difference between the energy positions of the two line shapes in the fit will reveal the splitting energy for the fcc case as $\Delta E = 17.0$ mV as shown in figure 4.7.

When moving the Co atom to the hcp region, which is slightly lower in apparent height, the splitting stays almost the same at $\Delta E = 16.8$ mV, which indicates that the difference for the Co atom in these two sites is negligible. On the other hand, with the Co atom in the on-top region, it is noticed that the entire feature is moved down in energy, so the center passes below the Fermi level. The splitting is even more visible in this situation, where the two Kondo features are almost non-overlapping. Surprisingly, the splitting from the fit is only $\Delta E = 13.6$ mV which is however within the range of the hcp/fcc region. This would indicate that the observed difference in the spectra is mainly an electronic effect that does not depend on height difference due to the buckling, or simply that the actual buckling of the Ag atoms is negligible

	Ag [Å]	Au [Å]
empty on-top	2.47	2.00
Co on-top	2.86	2.73
Co bridge	×	3.19
Co hcp	3.28	3.28
Co fcc	3.34	3.36

Table 4.1: Apparent height measured with respect to the underlying Co island in the apparently lowest region of the Moiré pattern (empty on-top) and the top of a Co atom in the given region. All values are in Å and measured on STM images taken with low bias of 11 and 20 mV for Ag and Au respectively.

compared to the electronic variations of the Moiré (a large change in height for the different regions is equal to a change in distance between the atom and the island and this would result in a noticeable change in the exchange interaction and the accompanying splitting – this is not seen).

From the theory (equation (4.4)) the splitting is expected to be symmetric in energy, but the energy offset is not known and can vary in different positions. Symmetric amplitudes could also be expected ($a_1 = a_2$ in equation (4.4)), but probably due to an uneven background this symmetry cannot be observed.

The Kondo temperatures of the individual Fano fits shown in the figure are slightly lower because the resonances are still overlapping instead of being completely separated. Only the on-top resonance at 38 K is too low and might indicate that the fit does not describe the physics well enough.

The spectra for the fcc and hcp regions in the Au Moiré in figure 4.8 do not show the same split feature as in the Ag Moiré. The Kondo temperature for the fcc and hcp spectra on Au are 78 and 80 K, respectively when the normal Fano line shapes are fitted in the bias range ±30 mV, which indicates normal, unaffected behaviour of the Co atoms reported to be 75 K [18]. The split feature does however reappear in the on-top site of the Au spacer layer with a splitting of $\Delta E = 15.4$ mV. This is almost the same splitting as for Ag and a somewhat similar behaviour to the Ag on-top region, in the sense that the two individual features are almost non-overlapping and the resonance above the Fermi level is stronger than the resonance below.

For Au, the Co atom has also been positioned in the bridge site between fcc and hcp. Here it is impossible to identify two resonance dips, but instead the spectrum shows one broader resonance peak. This could be interpreted as a Kondo resonance split by the exchange field to the Co island below, similar to the situation found in [17, 99] and as shown later in section 4.6 Here the Kondo temperature extracted with a single Fano line shape fit is 119 K.

The apparent height of the Co atoms above the Co island is shown in table 4.1 measured at 20 mV for the gold and 11 mV for the silver Moiré. All apparent heights are given with respect to the top of the Co island, which is 3.9 Å above the Cu(111) surface. The first row shows the apparent height of the Moiré pattern measured from the top of the underlying Co island to the empty on-top region. The following apparent heights are from the top point of a Co atom placed in the relevant region, again with respect to the Co island. It is found that although the Ag Moiré pattern appears 0.47 Å higher than the Au, the atoms are positioned in almost identical distances above the Co island. This also leads to the conclusion that there is a small buckling effect from the reconstruction, but a much larger electronic effect from the Moiré pattern. The Co atoms change height due to the small buckling, but the electronic structure can furthermore influence the Kondo resonance.

In conclusion, a splitting of $\sim$15 mV is well within the range of the model proposed in [104] where a cobalt atom on two MLs of copper capping on Co/Cu(111) is calculated to give a maximum of 20 mV splitting, but the model is in no way adapted to this special case with Ag or Au as the spacer layer. To find the expected splitting in this case, the calculations from [104] would need to be repeated for these specific materials, which have not yet been done.

Being able to control the magnetic coupling of single atoms to a buried magnetic layer through the exchange interaction could be an essential tool in building future storage or spintronic devices based on single atoms. Here it is shown that it is possible to change the Kondo resonance of such atoms by only slightly changing the distance or electronic structure of the non-magnetic spacer layer between the magnetic layer and the magnetic atom.

To understand the spectra better in both the Ag and the Au case, it would be interesting to use the combination of density functional theory and RG theory proposed by Tosatti et al. [91] to model the STS spectra. This could give a better understanding of the separate effects of the electronic structure of the Moiré pattern and the magnetic exchange interaction induced by the Co island below.

Experimentally, the spacer layer could be increased to several MLs which have a similar Moiré pattern, but at double the distance to the buried cobalt island. This would give an indication whether the effect is related to the exchange interaction between the island and the atom. This will be a topic of further work in the future.

4.5 Phase transitions

4.5.1 Classical phase transitions

An important field within thermodynamics is the phase of matter and the changes between the different phases, the so-called phase transitions. Different phases of a material are characterized by the same atoms having a different structure or composition. This can be in the form of the solid/liquid/gas phases, but it can also be a ferromagnetic or superconducting phase, which can be caused by different electron binding, different distances between atoms, different crystal structure, etc. A phase transition can be driven by e.g. a change in temperature or pressure.

There are mainly two types of phase transitions. The first-order phase transition which include the addition or removal of a fixed amount of energy to or from the system. This process is characterized by the fact that the temperature stays constant while the energy is converted to or from latent heat. It is named a first-order phase transition in the Ehrenfest classification scheme [109] because the lowest derivative of the free energy with a thermodynamic variable that is discontinuous in the transition is the first. For solid/liquid/gas transitions the first derivative of the free energy with respect to the chemical potential is the density.

The second type of phase transition discussed here is the continuous phase transition which is, as the name suggest, continuous in the first derivative of the free energy. In e.g. the paramagnetic/ferromagnetic phase transition the first derivative of the free energy with respect to the applied magnetic field is the magnetization which is continuous when the temperature is lowered below the Curie temperature. Instead, the magnetic susceptibility (the second derivative of the free energy with respect to the applied magnetic field) is discontinuous; therefore, the transition is also called a second-order phase transition in the Ehrenfest classification scheme. Other examples of continuous phase transitions include the transition into the superconducting and the superfluid phase.

4.5.2 Quantum phase transitions

The classical phase transitions described above are driven by thermal fluctuations [110], but at the very bottom of the phase diagram at $T = 0$ K there are no thermal fluctuations and the system can therefore not undergo classical phase transitions. Instead, while changing another physical parameter such as pressure or magnetic field (not temperature), a quantum phase transition can be induced by the quantum fluctuations in the system. The point in a phase diagram where the phase transition line meets $T = 0$ K is called a quantum critical point (QCP) [111, 112]. It is of course impossible to put a material into this point at $T = 0$ K because of temperature, but the consequences and properties of the QCP extends upwards in the phase diagram away from absolute zero temperature. A quote from the introduction of the Science article by Rost et al. [113] highlights the importance of the topic:

> “ *Low-temperature phase transitions and the associated quantum critical points are a major field of research, but one in which experimental information about thermodynamics is sparse. ... Quantum critical points (QCPs) are continuous phase transitions at zero temperature, where quantum mechanical zero point fluctuations play the role assumed by thermal fluctuations in the classical case [110]. Their importance is not only academic because large portions of the low-temperature phase diagram can be affected by their presence, and the production of QCPs and the formation of new quantum phases in their vicinity has become a central theme of modern condensed matter physics.*”

In STM/S the electrons contributing to the transport are confined to the small ”channel” that constitutes the tunneling junction. This channel of electrons has to be considered representative for the electron transport on a larger scale. In the following section, it is shown how electron current can be drawn through two Co atoms, one on the surface of a Au(111) crystal and one on the Au-coated tip. By approaching tip to the surface we vary the distance between the two atoms and thereby simulate a pressure variation in a bulk crystal. The consequence is that the system of the two Co atoms can be tuned through a crossover from a regime where the individual atoms are Kondo screened to a regime where the two atoms couple antiferromagnetically. A crossover means that the two phases coexist as a superposition in the crossover regime.

4.6 Tuning a cobalt dimer between Kondo screening and local moment antiferromagnetism

4.6.1 Background

Correlated electron materials with their often puzzling properties and complicated phase diagrams [22] attract substantial interest both from fundamental research in trying to understand their properties and due to the hope connected to exploiting them for applications. The phase diagrams of heavy fermion compounds exhibiting typically a number of phases connected to different magnetic properties as a function of temperature and pressure. It had been recognized early that the balance between the formation of local magnetic moments and their quenching due to screening by conduction band electrons plays a key role in the behaviour of these materials. Basic features of the phase diagrams of heavy fermion compounds can be understood by considering the coupling J of neighbouring spins in a 1D chain of magnetic atoms to the conduction electrons [114]. A description of real materials however has still remained a formidable task because of the importance of electronic correlations whose theoretical treatment is highly non-trivial. This is why it is important to investigate model systems with a small number of well-controlled parameters which can be compared directly to theoretical predictions. A simple model system is the two-impurity Kondo problem, which can be driven between antiferromagnetism and Kondo screening by tuning the coupling between the two impurities [115].

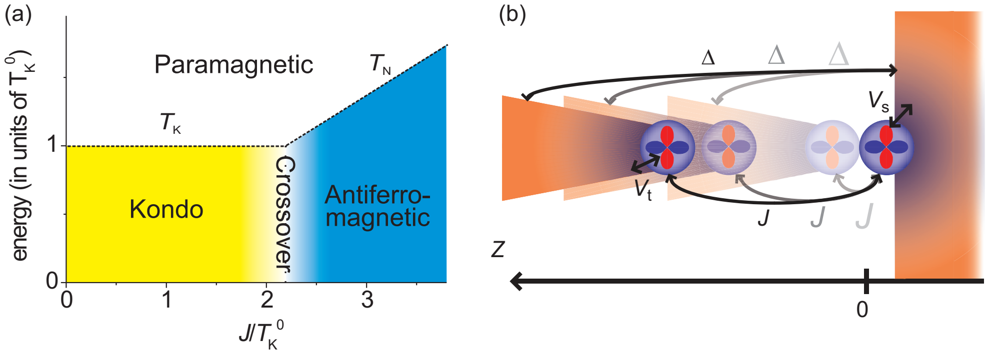

Figure 4.10: (a) Phase diagram of the two-impurity Kondo model showing the relevant energy scales (in units of the Kondo temperature T_K^0 with no interaction) and the phases: *Kondo* screening – the single impurity Kondo screening dominating and the Kondo temperature T_K is the characteristic energy scale; *Antiferromagnetic* behaviour – local moment antiferromagnetism dominated by the magnetic coupling between the two spins, the dashed line indicates the expected behaviour of the Néel temperature T_N of the two impurities; inbetween these two phases is a *Crossover*. (b) Illustration of the measurement setup with one cobalt atom on the STM tip and one on the surface. By changing the distance between the atoms, a crossover between two phases appears where the dominant coupling is changed from Kondo screening due to hybridization $V_{s,t}$ between the cobalt atoms and their respective electrodes to antiferromagnetic coupling J between the two cobalt atoms. The additional coupling Δ between the conduction electron baths suppresses the quantum critical point, resulting in a crossover between the two phases.

The two-impurity Kondo problem has been investigated theoretically for two coupled quantum dots [116] and soon after also experimentally [117,118]. The basic phase diagram for the two-impurity Kondo problem is shown in figure 4.10(a). For weak coupling J between the two impurities, the each spin is forming a Kondo system with its respective bath, while for strong coupling J, the spins become locked in an antiferromagnetic singlet. If the coupling Δ between the electron baths (electrodes) is negligible, a quantum phase transition will separate the two ground states, otherwise a crossover occurs. Experiments on quantum dots were only performed in the limit of strong and weak coupling between the impurities, but not in the regime where the two couplings compete.

In studies of magnetic adatoms on metal surfaces, a realization of the two-impurity Kondo problem has been attempted by putting two magnetic atoms next to each other, however as the interatomic separations are limited to the substrate lattice, the coupling can only be set to discrete values [17, 107]. Only recently it has been proposed that a model system for the two-impurity Kondo problem could consist of two magnetic atoms, one attached to the tip of an STM and the other sitting on a metal surface [119]. By positioning the tip including the magnetic atom on top of another magnetic atom on the surface and varying its height above the surface, the coupling can be tuned continuously and equally important the distance can be fixed at some arbitrary point which would not be possible with manipulation of atoms on the surface. An illustration of this with the relevant coupling terms can be seen in figure 4.10(b).

As shown in section 2.5 we have been able to do STM/S experiments with a Kondo compensated state on the Au coated STM tip. We have done measurements on clean surfaces, on cobalt islands on Cu(111) and Au(111), but the most prominent results so far have been with the simpler two-impurity Kondo problem of the distance dependence of two cobalt atoms. Fine tuning of the coupling between the two spins is accomplished by adjusting the tip-sample distance, allowing to drive the system under consideration – a cobalt dimer – continuously from Kondo behaviour to local moment antiferromagnetic coupling.

A relevant difference from previous measurements is that when the two atoms are on the surface, a large part of the coupling between the molecules is indirect exchange interaction (RKKY) through the substrate, whereas when the atoms are clamped between the substrate and the tip, the RKKY interaction is drastically reduced. As a consequence, the two cobalt atoms have to be moved much closer together than on the surface to see a comparable effect. An illustration of the coupling regimes for the exchange interaction in this situation is shown in figure 4.11.

4.6.2 Measurement procedure for spectroscopy

The STS spectra shown in the following are acquired two at a time unless otherwise noted. First, the tip is approached by a predefined distance d and after a few seconds of pause to get clear of piezo creep, the first spectrum is acquired. After another few seconds of pause to assess the resulting drift during acquisition of the spectrum, the tip is approached by a small distance Δd to the next position and a repeated pause/acquisition/pause sequence is performed before the tip is returned to tunneling conditions. A topography scan is then performed to confirm that the Co atoms (on the surface and on the tip) are at the same positions as before the spectrum. If this is not the case, the experiment is stopped. If they are in the same positions, the next

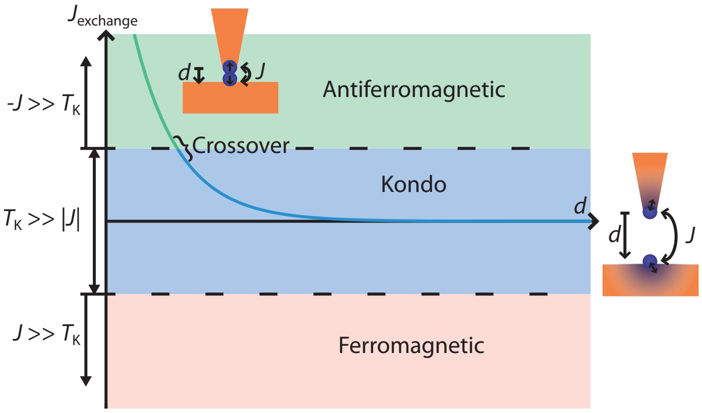

Figure 4.11: Schematic plot of the coupling J as a function of distance between the two cobalt atoms. When the interaction is small, the Kondo regime is dominating. When the interaction is larger, either antiferromagnetic or ferromagnetic coupling will occur between the atoms. The transition can be a quantum phase transition or a crossover. Ferromagnetic coupling is not seen in our experiment.

two spectra are acquired. This ensures reversibility and reproducibility of the entire process, we can go in and out of contact and obtain the features repeatedly.

There is a considerable amount of vertical piezo creep when approaching the tip to the surface by more than 3 Å (compared to the picometer precision of the experiment). The uncertainty resulting from the creep is avoided by measuring the current during the pauses before and after acquisition of the spectra. The stable current just before acquisition of each spectrum is used as a measure for the vertical position of the tip by converting the current to tip-sample distance through a measured approach curve as shown in figure 4.13(a). Close to point contact, the conductance trace becomes unstable due to mechanical instabilities and due to the large slope the conductance has close to contact as a function of distance making measurements in this regime extremely sensitive to external perturbations. In point contact, the conductance trace becomes stable again.

4.6.3 The experiments

The sample is prepared as described in section 2.5 and the single cobalt adatoms on the Au(111) surface (figure 4.12(a)), can be identified by their characteristic Kondo resonance [18] (figure 4.12(e)). The atom is transferred to the tip by applying a voltage pulse between tip and sample (figure 4.12(b)). After application of a successful voltage pulse the cobalt atom cannot be found any more on the sample surface (figure 4.12(c)) in close vicinity of its original position. In some cases, after the atom has been removed from the sample surface, the tip exhibits a resonance with very similar shape and width compared to the cobalt atom on the sample surface (figure 4.12(f)). In these cases, the atom stays attached to the apex of the STM tip and the spin of the cobalt atom forms a Kondo system with the conduction electrons of the tip. Not each pick-up results in a tip exhibiting a resonance as that shown in figure 4.12(f). Sometimes, no resonance appears or the resonance has a different shape and amplitude, presumably depending on the specific adsorption site of the cobalt atom on the tip. For the results shown

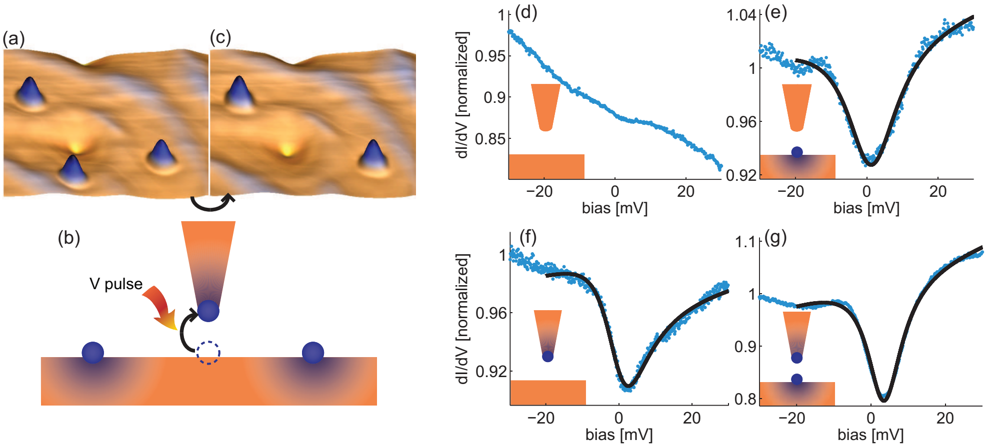

Figure 4.12: (a) Au(111) surface with three cobalt adatoms taken with a featureless tip (d) when measuring spectra on the Au(111) surface. The Co atoms show the well known Kondo resonance (e). By applying a voltage pulse (b), one of the cobalt adatoms in (a) is being picked up, placed at the tip and the Co atom is not seen in (c). The tunneling spectrum of the clean surface taken with an STM tip with a cobalt atom attached to it now shows a Kondo resonance (f), which is enhanced when moving the tip over another Co atom (g).

here, only experiments where the spectrum of the tip after pick-up closely resembled that of a cobalt atom on the surface are considered. This indicates that the atom has a similar environment as on the surface and a significant portion of the tunneling current is affected by the cobalt atom.

With the cobalt atom attached to the STM tip, the tip is positioned on top of a second cobalt atom (figure 4.12(g)). For a number of tip-sample distances, we have recorded tunneling or (in point contact) transport curves. The two regimes, the tunneling and the point contact regime, in which we have acquired I/V-spectra are shown in figure 4.13(a). In the tunneling regime the current increases exponentially when approaching the tip to the surface. The point contact regime is reached when the slope of the current trace reaches a plateau, only changing comparatively little upon further moving the tip towards the sample. Reversible formation of point contacts to single atoms on a metal surface with conductances up to one conductance quantum has been shown previously both for non-magnetic [120] and magnetic atoms [121,122].

Spectra acquired in the tunneling regime more than 2 Å away from point contact (see the identical spectra in figure 4.12(g) and in the top of figure 4.13(b)) show a similar resonance as is found with a single cobalt atom in the junction (compare with figures 4.12(e) and (f)). Shape and width of the feature change only little as long as the tip-sample distance stays comparatively large ($Z > 2$ Å). Once the two atoms are moved within 2 Å of point contact the width of the resonance decreases, as it can be seen by fitting Fano functions to the measured differential conductance in figure 4.13(b). The width of the resonance (equal to $2k_\mathrm{b}T_\mathrm{K}$) is shown in figure 4.14(a)). The reduction of the width amounts to 30%. In a continuation of the spectra below figure 4.13(b), after the transition to the point contact regime the picture changes dramatically. These spectra can be seen in figure 4.13(c). The resonance persists, but changes into a peak-like resonance in the differential conductance. The peak initially

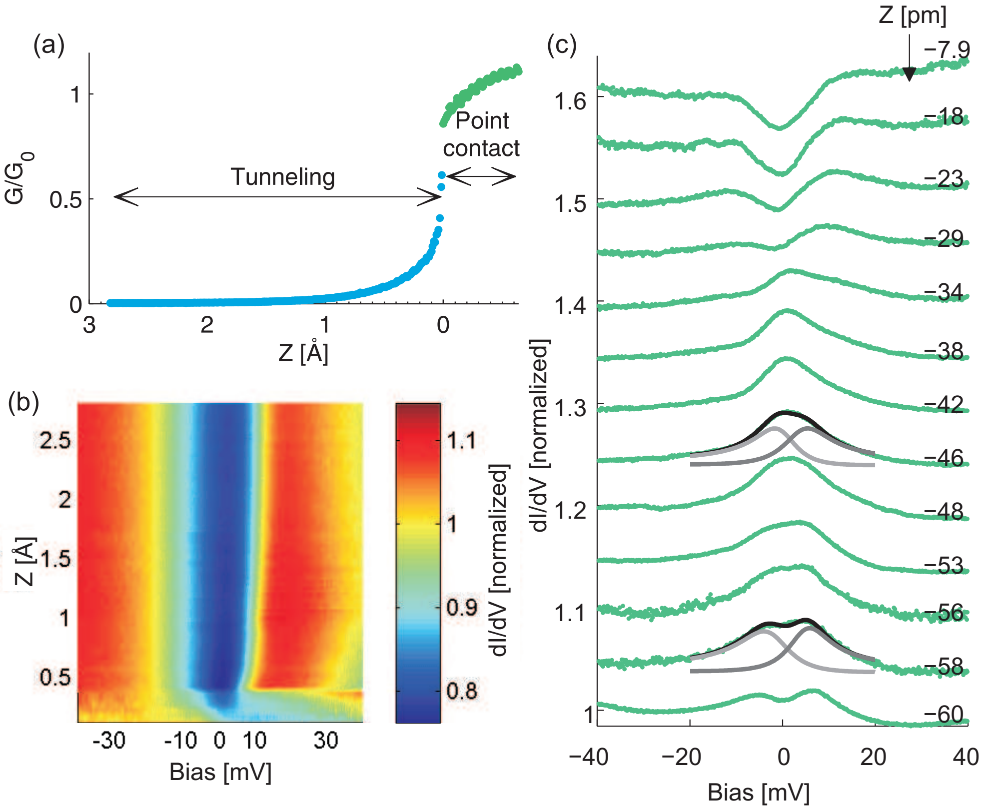

Figure 4.13: (a) Approaching a cobalt atom on the surface with a cobalt atom on the tip, shown is the conductance as a function of tip-sample distance at fixed bias voltage ($V_{bias} = 40$ mV), the transition from tunneling regime (blue) to point contact regime (green) can be clearly seen. (b) Spectra as a function of tip-sample distance (vertical axis) in the tunneling regime, (c) spectra as a function of tip-sample distance in the point contact regime. After the closest spectrum, we lost the tip atom. The data set shown has been obtained with one tip.

has a similar width as the dip. On pushing the tip further in the peak splits into two resonances at symmetric positions with respect to the Fermi energy.

Reference measurements with only one cobalt atom between the tip and the surface show no reduction of the width of the Kondo resonance, no change in the lineshape from dip to peak and no splitting of the resonance. Thus these effects must be related to the presence of two Kondo impurities in the tunneling junction.

For a quantitative analysis of the splitting, we have fitted the spectra with the sum of two Fano lineshapes shown in equation (4.4). The dependence of the splitting on the distance between the tip and the sample is plotted in figure 4.14(b). The splitting increases with decreasing tip-sample distance in an almost linear fashion.

4.6.4 Discussion

Thus we can identify of the cobalt dimer two clearly distinguishable phases as depicted in figure 4.10(a). Far out in the tunneling regime, the two cobalt atoms behave as

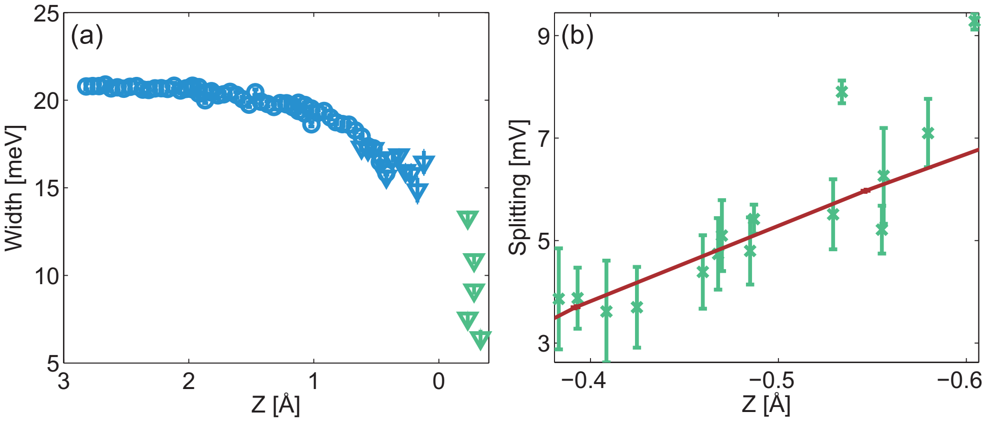

Figure 4.14: (a) Width of the resonances seen in figure 4.13(b) as a function of tip-sample distance where circles and triangles indicates measurements done at different sample preparations. (b) Splitting of the peaks seen in figure 4.13(c) as a function of tip-sample distance. The red line has been obtained from numerical RG calculations, with the assumption $z \sim \log \Delta$.

two weakly interacting Kondo impurities, each of which has its own Kondo resonance. The tunneling spectrum is composed of a superposition of the two resonances. While approaching the two atoms towards each other, the interaction grows stronger. The first indication of the interaction is a change in the overall width of the resonance and a change in its line shape, seen as a transition from a dip to a peak. Because the Kondo resonances of the two impurities are superimposed in the spectra, we cannot uniquely determine whether the reduction in width is due to the growing interaction, as e.g. discussed with the pertubative RG theory in [123] for the heavy fermion compound $\mathrm{CeCu}_{6-\mathrm{x}}\mathrm{Au}_x$ or whether it is only a secondary effect due to the change in line shape. It can be shown that the latter can lead to an apparent reduction of the width of the overall resonance at the transition of the line shape of the single impurity Fano resonances from a dip to a peak. This is confirmed by numerical RG calculations made specifically for this setup by L. Borda and P. Simon (not shown). These calculations show no change in the Kondo temperature in the entire Kondo regime. The Kondo resonance, which is governed by the hybridization $V_{\mathrm{s},t}$ between the cobalt atoms and their electrodes as shown in figure 4.10(b) is unchanged when the coupling between the cobalt atoms is increased. Instead, the increased cobalt-cobalt coupling changes the tunneling path from tunneling between the s-level Fermi seas of the tip and the sample (dip) to tunneling directly between the localized Kondo state of the cobalt atoms at the Fermi level (peak). This is an interesting result in itself, since this gives direct real-space access to probe the d-orbital.

The exact transition where the differential conductance spectra changes from an overall dip to an overall peak can occur in the tunneling regime or in the point contact regime, depending on the specific configuration of the Co atoms from experiment to experiment. There seems to be no strict correlation between the position of point contact and the position of this transition, however the transition appears close to point contact.

What follows when the tip is pushed further towards the substrate is that the magnetic interaction directly between the atoms can compete in magnitude with the Kondo screening. The atoms undergo a crossover from a ground state (phase) dominated by individually Kondo screened atoms to an antiferromagnetic ground state between the two atoms locked together with opposite magnetic moments. This is shown by theory [124] to be a continuous crossover instead of a sharply defined transition due to the lack of particle-hole symmetry and large electronic coupling between the tip and the sample in the two-impurity Kondo system[2].

In this regime the resonance becomes split by the exchange interaction, and upon further reducing the tip-sample distance, the separation between the two peaks increases. The local moments of the two cobalt atoms are locked into a singlet and the spectra exhibit a splitting of the inelastic spin-excitations as a function of tip-sample distance. This splitting is similar to the splitting of the Kondo resonance seen in magnetic field in quantum dots [19, 95] or for magnetic atoms [125] – in our case, the splitting can be thought of as being due to the effective magnetic field felt by one atom due to the presence of the other [99].

The residual peak which we observe in the antiferromagnetic regime can be understood as being due to the finite spin lifetime: Though it is still short due to scattering with the conduction band electrons, the antiferromagnetic interaction prohibits singlet formation of the impurity spins with the conduction band electrons.

Numerical RG calculations also correctly predicts the transition from the Kondo regime to the antiferromagnetic regime and the splitting seen. The resulting theoretical splitting is plotted as the brown line in figure 4.14(b).

4.6.5 Additional data

To show the general aspects of the data and a wider splitting, another dataset is shown here, where the overall transition from dip to peak is slightly displaced in z-distance compared to the results shown up to now. This illustrates the point that this transition is independent from the transition to point contact. The entire amount of spectra are shown in the 2D coloured plot in figure 4.15(a) and selected spectra close to the transition from dip to peak and further into the antiferromagnetic split peak regime is shown in figure 4.15(b). Notice the effect close to point contact ($z \approx 0$ pm in figure 4.15(b)), that the noise increase due to the proximity of the two Co atoms to each other and a large slope of the current. Several curves (only a few shown) prove that the transition from dip to peak is not related to the point contact since the transition here happens in the tunneling regime.

The splitting as a function of tip-sample distance in the antiferromagnetic regime is shown in figure 4.15(c) and is in this dataset larger due to a more stable configuration of Co atoms on the tip and sample. The splitting is maximum 42 mV when the tip is pushed furthest in (before losing the Co atom on the tip). This dataset illustrate the fact that the coordination of the cobalt atoms in the experiment is of vital importance to the distance offset of the two atoms. It is not possible to compare the splitting in this dataset directly with the splitting shown in figure 4.13 and 4.14 due to the fact that the splitting occurs already in the tunneling regime and the cur-

---

[2] An abrupt quantum phase transition could be found in a Kondo lattice or Kondo necklace problem, as well as in a two-impurity Kondo system that is structured in a way that particle-hole symmetry is conserved and the coupling between tip and sample is lowered.

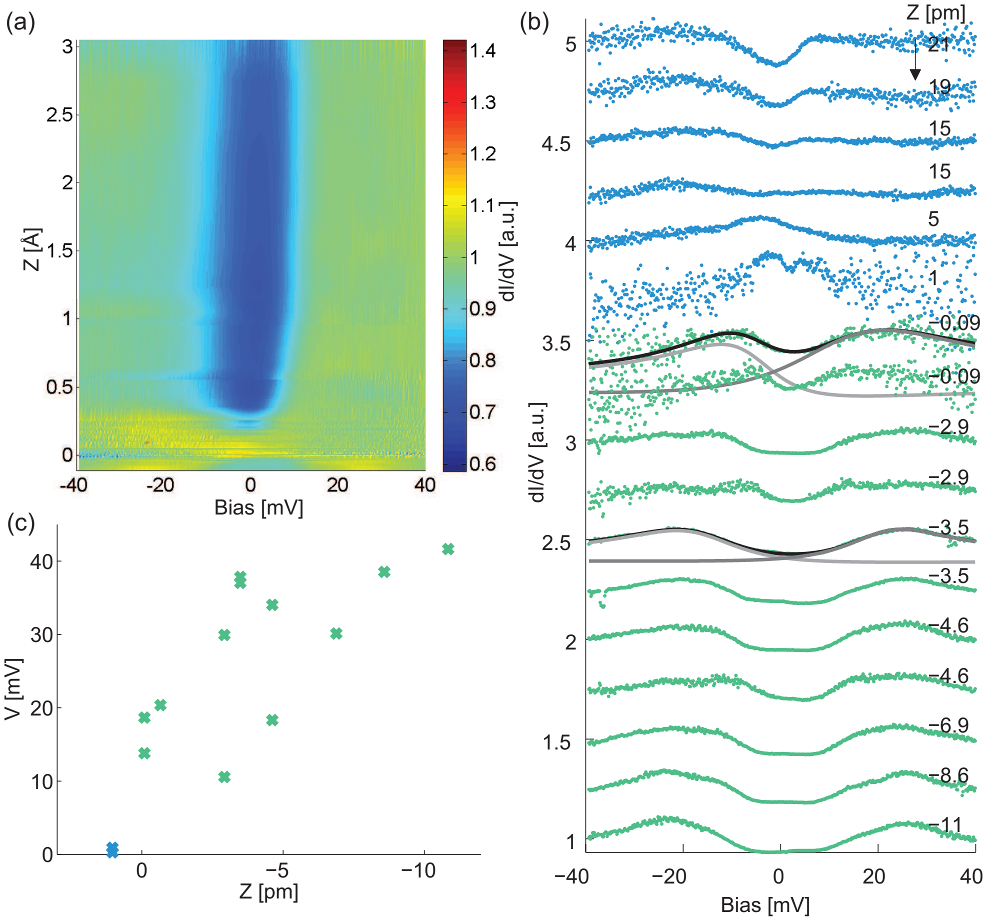

Figure 4.15: (a) Spectra as a function of tip-sample distance (vertical axis) in the tunneling regime at positive distances. Closely before contact (distance = 0 Å), yellow-coloured spectra indicate the transition from a dip to a peak and the subsequent splitting. (b) Differential conductance curves as a function of tip-sample distance shown on the right. Two examples are shown where the splitting is fitted with the sum (black) of two Fano line shapes (grey). The blue curves are from tunneling and the green curves are from point contact. (c) Value of the splitting of the two features seen in (b) fitted with the sum of two Fano line shapes showing a roughly linear increase in the splitting as a function of tip-sample distance. More curves are used for the fitting here than are shown in (b). The scattering seen in the data is mainly due to the current before the spectrum acquisition not being stable enough to sort the data better on the z-scale. This figure can be compared with figure 4.13 and 4.14(b).

rent and z-scale do not match the data in the article. Instead the dataset shown here underlines the generality of the physical effect independent of changes in the cobalt coordination.

We believe that the generality of the methods described here can be expanded to investigate many other systems. First of all, investigating other two-impurity Kondo problems would broaden the understanding of this phenomenon and it remains to be seen if the entire procedure of achieving a Kondo resonance at the gold-coated tip apex with e.g. Ce is possible. Varying the temperature might also give an indication of the shape of the phase diagram and the extent of the crossover region.

So far experiments trying to approach a Kondo system to a magnetic cobalt island on Cu(111) have not been successful. No reduction in width or splitting of the Kondo resonance has been seen before reaching point contact, where the cobalt atom is lost. This somewhat surprising result could be explained by the fact that the effect is only seen when two Kondo-impurities changes line shape at the same time. This further strengthens the interpretation that the Kondo temperature stays constant throughout the approach.

4.6.6 Reference experiments

As reference we have acquired spectra taken with a gold atom on the tip (clean tip softly indented in the Au(111) surface) on top of a gold atom on the surface shown in figure 4.16(a) and on top of a cobalt atom on the surface shown in figure 4.16(b) to have measurements where both or one of the cobalt atoms were exchanged with gold.

The spectra acquired on top of a gold atom on the surface do not reveal any significant changes in the spectroscopic features on approaching the tip from tunneling to point contact. Especially, the features seen in tunneling do not change their position nor their width in a systematic way.

In case of a cobalt adatom, the Kondo resonance can be seen until the tip jumps into point contact, where the resonance disappears and is replaced with a broad feature that is constant as a function of tip-sample distance (two lowest green curves in figure 4.16(b)). The Kondo temperature increases slightly by ∼17 K from the tunneling setpoint until the tip jumps to contact. The behaviour is somewhat different compared to what have been found for cobalt atoms on Ag or Cu single crystals [121,122]. These experiments have shown the modification of the Kondo resonance of the cobalt atom by the presence of the tip as well as due to the influence of relaxations of the tip-adatom-surface geometry.

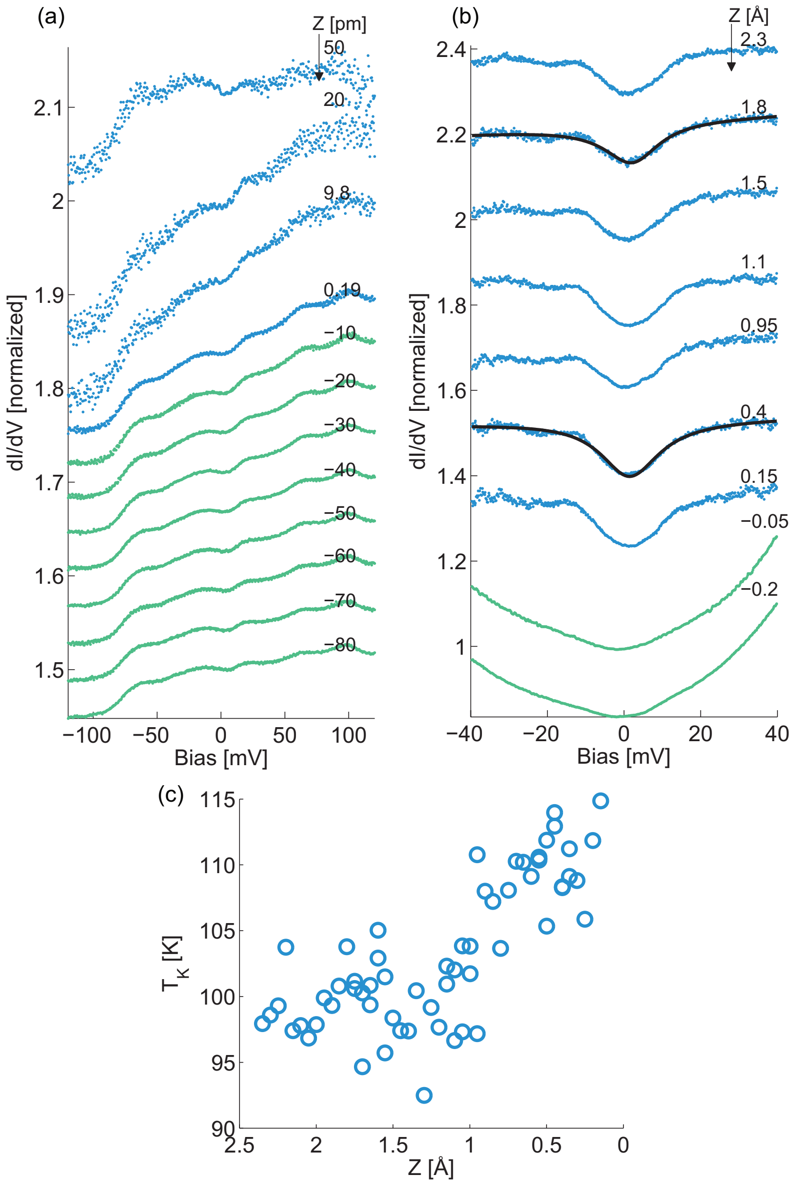

Figure 4.16: Transport measurements with a clean tip (presumably with a gold atom at the apex of the tip) while approaching (a) a gold atom on the surface and (b) a single cobalt adatom on the Au(111) surface. Blue is tunneling and green is point contact. (c) The Kondo temperature corresponding to the resonances in (b) in tunneling. The spectra in (b) are only 1 out of every 10th spectrum taken and used in (c). Spectra in (a) have been acquired one at a time, those shown in (b) in one sequence.

Conclusion and Outlook

The primary focus of this thesis is the control and characterization of the magnetic properties of single cobalt atoms through coupling to another cobalt atom or through the presence of metallic/magnetic heterostructures. This focus has been explored through capping of magnetic cobalt nanoislands on Cu(111) with a non-magnetic spacer layer and the electronic properties have been investigated before the magnetic interaction with single cobalt atoms on top was studied. Ultimately it has been shown how the phase of a two-impurity Kondo system can be tuned continuously from Kondo screening to antiferromagnetic coupling by simply changing the distance between the two atoms.

Initially, the nucleation and growth of a silver adlayer on cobalt nanoislands on the Cu(111) surface has been investigated with STM and LEED. This shows that the silver prefers to nucleate on top of the bilayer high cobalt islands at low silver coverage. The cobalt islands are furthermore either completely empty or almost completely filled with silver. This shows that the silver can traverse the 2 ML high step edge up to the cobalt islands and there coalesce with other silver molecules to nucleate.

The same structure is then investigated with ARPES measurements and it is confirmed that the silver and cobalt does not alloy when grown at RT. A surface state on the silver adlayer is found at 0.2 eV below the Fermi level.

To further clarify the electronic structure of the Moiré pattern formed between the silver and the cobalt islands, it has been investigated by spectroscopic mapping in a 6 K STM. The *d*-related state from the buried cobalt island is found to be visible through the silver capping layer with an overall shift from -0.31 eV to -0.19 eV. Apart from the overall shift, the Moiré pattern of the silver capping layer is found to modulate the energy position, the amplitude and the width of the state. The modulation has been related to the *d*-band model for *sp*-*d*–hybridization and the connections to catalytic and magnetic properties are shown. Other material combinations yielding a Moiré pattern were investigated and the largest shift in energy position was found for Co/Ag(111) while the largest shift in intensity of the state was found in the case of Ag/Co/Cu(111). It is believed that Moiré patterns in general have the ability to shape the potential energy landscape of a surface and thereby act as a template for assembly of molecules or magnetically/catalytically active clusters.

The structure with a capping layer of silver or gold on the cobalt nanoislands on Cu(111) has then been used influence the Kondo resonance of single cobalt atoms placed in the different regions of the Moiré pattern measured with STS. Signatures of a split Kondo resonance possibly due to the exchange interaction between the buried cobalt islands and the single cobalt atom has been shown and analyzed. The splitting is $\sim$15 mV in the regions where it is visible, but the line shape varies drastically within the Moiré pattern. The measurements clearly show that the Kondo resonance can be manipulated by exchange coupling to an underlying magnetic layer. This is a small step towards understanding how information can be stored in single magnetic atoms by controlling their magnetic properties.

A novel method for changing the tip of the STM into a Kondo system has been presented. The procedure consists of coating the tip with gold, either by soft indentation into a gold crystal or by controlled pickup of large flakes of gold from the surface. The pickup of single atoms with the gold-coated tip follows a standard procedure and places the cobalt atom at the very apex of the tip forming a freely positionable Kondo resonance with the tip.

In a first proof-of-concept, this has been used to create a two-impurity Kondo system with a cobalt atom on a Au(111) crystal. The distance between the two cobalt atoms can be continuously changed from tunneling to point contact, effectively forming a cobalt dimer. Supported by numerical RG calculations, the Kondo temperature is believed to be constant in the Kondo screened regime although a decrease in the effective width of the resonance is observed. Instead the Fano line shape parameter q is found to increase from close to zero (dip-like Fano line shape) to large values (peak-like Fano line shape). This is interpreted as a change in the tunneling path from tunneling between the tip/substrate Fermi seas to tunneling directly between the locally induced d-symmetric state of the cobalt atoms at the Fermi level.

The two-impurity Kondo system offers a direct way of probing magnetic interaction between single atoms. When pushing the atoms further together it is shown how the cobalt atoms change their ground state configuration from two individually Kondo screened singlets into a common antiferromagnetically coupled singlet. In this antiferromagnetic regime, inelastic spin-flip excitations are found to split as a function of interaction between the two atoms. The signatures of this crossover are measured in the differential conductance spectra and supported by theoretical calculations. The results are the first of their kind by STM and it is believed that the discovery of a freely positionable Kondo system formed at the apex of an STM tip can have a large impact on the research within magnetic interaction on the nanoscale.

4.7 Outlook

Being able to modulate the catalytic and magnetic properties of a substrate by adding a metallic Moiré pattern opens up for further experiments where additional metals or molecules are deposited onto the structure. Theoretical calculations combined with experiments of additional magnetic and non-magnetic materials could separate purely catalytic effects from magnetic effects. This can also be related to the splitting of single cobalt atoms placed in the Moiré pattern shown in section 4.4, where the magnetic exchange interaction should be separated from electronic properties of the Moiré pattern. Increasing the number of non-magnetic spacer MLs would also give an indication on whether the observed effect is electronically or magnetically related.

A Moiré modulated potential energy landscape can pave the way for forming self-assembled structures of material that would otherwise not self-assemble on an unstructured surface. This can be used for small storage clusters/molecules which are magnetically coupled to a buried layer and stable without contact to the neighbouring clusters/molecules. Ultimately, information would be stored in single atoms which are also investigated in this thesis. First attempts to change the magnetic coupling mechanism between two atoms or an atom and an island show great prospects. A better understanding of this phenomenon could be achieved by changing the atoms from cobalt to another atom with a lower Kondo temperature. This will result in a lower characteristic energy for the Kondo system and thereby an easier perturbed system. For the tunable dimer a lower Kondo temperature will make the crossover appear at an earlier position with the atoms further apart than for the cobalt dimer.

Changing the measurement temperature might also reveal more details leading to a phase diagram for the cobalt dimer. A variable low-temperature experiment could shed light on the extent of the crossover region and how far it extends upwards in the phase diagram.

The method of a tip Kondo system is also envisioned to probe magnetic interaction with molecules containing a magnetic center or magnetic islands, but experiments with the latter have so far been unsuccessful. Possibly, an atom with a lower Kondo temperature is needed in order to move the interesting transition region out into the tunneling regime. Alternatively, an externally applied magnetic field could give more information on the magnetic nature of the systems.

As mentioned earlier, the methods presented here could have a substantial impact on the heavy fermion material research, in which Kondo necklaces and lattices play an essential role. The possibility to freely tune the interaction strength is a promising tool within Kondo physics and magnetic interaction in general. We hope it can contribute to shed new light on the properties of the low-temperature phase diagrams for heavy fermion compounds and how single atom impurities can be influenced through magnetic interaction.

References

[1] R. P. Feynman, "There's Plenty of Room at the Bottom," Website (2009). `www.zyvex.com/nanotech/feynman.html`.

[2] G. Binnig, H. Rohrer, C. Gerber, and E. Weibel, "Surface Studies by Scanning Tunneling Microscopy," Phys. Rev. Lett. **49**(1), 57–61 (1982).

[3] D. M. Eigler and E. K. Schweizer, "Positioning single atoms with a scanning tunnelling microscope," Nature **344**, 524–526 (1990). `http://dx.doi.org/10.1038/344524a0`.

[4] ITRS, "The International Technology Roadmap for Semiconductors," Website (2009). `www.itrs.net`.

[5] Z. News, "Intel scientists find wall for Moore's Law," Website (2009). Short link: `www.bit.ly/2FibyA` (original: `www.news.zdnet.com/2100-9584_22-133066.html`).

[6] G. A. Prinz, "Magnetoelectronics," Science **282**(5394), 1660–1663 (1998). `www.sciencemag.org/cgi/content/abstract/282/5394/1660`.

[7] S. Wolf, D. Awschalom, R. Buhrman, J. Daughton, S. Von Molnar, M. Roukes, A. Chtchelkanova, and D. Treger, "Spintronics: A spin-based electronics vision for the future," Science **294**(5546), 1488 (2001).

[8] S. Parkin, M. Hayashi, and L. Thomas, "Magnetic domain-wall racetrack memory," Science **320**(5873), 190 (2008).

[9] D. Strukov, G. Snider, D. Stewart, and R. Williams, "The missing memristor found," Nature **453**(7191), 80–83 (2008).

[10] D. DiVincenzo, "Quantum computing," Science **270**, 255 (1995).

[11] N. N. Negulyaev, V. S. Stepanyuk, P. Bruno, L. Diekhöner, P. Wahl, and K. Kern, "Bilayer growth of nanoscale Co islands on Cu(111)," Physical Review B **77**(12) (2008).

[12] L. Diekhöner, M. A. Schneider, A. N. Baranov, V. S. Stepanyuk, P. Bruno, and K. Kern, "Surface States of Cobalt Nanoislands on Cu(111)," Phys. Rev. Lett. **90**(23), 236801 (2003).

[13] P. Wahl, L. Diekhöner, G. Wittich, L. Vitali, M. A. Schneider, and K. Kern, "Kondo Effect of Molecular Complexes at Surfaces: Ligand Control of the Local Spin Coupling," Phys. Rev. Lett. **95**(16), 166601 (2005).

[14] M. A. Schneider, P. Wahl, L. Diekhöner, L. Vitali, G. Wittich, and K. Kern, "Kondo Effect of Co Adatoms on Ag Monolayers on Noble Metal Surfaces," Japanese Journal of Applied Physics **44**(7B), 5328–5331 (2005). `jjap.ipap.jp/link?JJAP/44/5328`.

[15] N. Knorr, M. A. Schneider, L. Diekhöner, P. Wahl, and K. Kern, "Kondo Effect of Single Co Adatoms on Cu Surfaces," Phys. Rev. Lett. **88**(9), 096804 (2002).

[16] P. Wahl, L. Diekhöner, M. A. Schneider, L. Vitali, G. Wittich, and K. Kern, "Kondo Temperature of Magnetic Impurities at Surfaces," Phys. Rev. Lett. **93**(17), 176603 (2004).

[17] P. Wahl, P. Simon, L. Diekhöner, V. S. Stepanyuk, P. Bruno, M. A. Schneider, and K. Kern, "Exchange Interaction between Single Magnetic Adatoms," Physical Review Letters **98**(5), 056601 (pages 4) (2007). `http://link.aps.org/abstract/PRL/v98/e056601`.

[18] V. Madhavan, W. Chen, T. Jamneala, M. Crommie, and N. Wingreen, "Tunneling into a single magnetic atom: Spectroscopic evidence of the Kondo resonance," Science **280**(5363), 567 (1998).

[19] D. Goldhaber-Gordon, H. Shtrikman, D. Mahalu, U. Meirav, D. Abusch-Magder, and M. A. Kastner, "Kondo effect in a single-electron transistor," Nature **391**(6663), 156–159 (1998).

[20] F. Meier, L. Zhou, J. Wiebe, and R. Wiesendanger, "Revealing magnetic interactions from single-atom magnetization curves," Science **320**(5872), 82 (2008).

[21] L. Kouwenhoven and L. Glazman, "Revival of the Kondo effect," Nanotechnology pages 33–38 (2001).

[22] E. Dagotto, "Complexity in Strongly Correlated Electronic Systems," Science **309**, 257–262 (2005).

[23] C. Jayaprakash, H. R. Krishna-murthy, and J. W. Wilkins, "Two-Impurity Kondo Problem," Phys. Rev. Lett. **47**(10), 737–740 (1981).

[24] B. A. Jones, C. M. Varma, and J. W. Wilkins, "Low-Temperature Properties of the Two-Impurity Kondo Hamiltonian," Phys. Rev. Lett. **61**(1), 125–128 (1988).

[25] Z. Fisk, "The Thermodynamics of Quantum Critical Points," Science **325**(5946), 1348–1349 (2009). `www.sciencemag.org/cgi/reprint/325/5946/1348.pdf`.

[26] S. A. Grigera, R. S. Perry, A. J. Schofield, M. Chiao, S. R. Julian, G. G. Lonzarich, S. I. Ikeda, Y. Maeno, A. J. Millis, and A. P. Mackenzie, "Magnetic Field-Tuned Quantum Criticality in the Metallic Ruthenate Sr3Ru2O7," Science **294**(5541), 329–332 (2001). `www.sciencemag.org/cgi/content/abstract/294/5541/329`.

[27] J. de la Figuera, J. E. Prieto, C. Ocal, and R. Miranda, "Scanning-tunneling-microscopy study of the growth of cobalt on Cu(111)," Phys. Rev. B **47**(19), 13043–13046 (1993).

[28] K. Heinz, S. Müller, and L. Hammer, "Crystallography of ultrathin iron, cobalt and nickel films grown epitaxially on copper," J. Phys. Cond. Matt. **11**, 9437–9454 (1999).

[29] U. Alkemper, C. Carbone, E. Vescovo, W. Eberhardt, O. Rader, and W. Gudat, "Exchange-split electronic states of ultrathin Co layers on Cu(111)," Phys. Rev. B **50**, 17496–17501 (1994).

[30] J. de la Figuera, J. E. Prieto, G. Kostka, S. Müller, C. Ocal, R. Miranda, and K. Heinz, "Crystallography and morphology of the early stages of the growth of Co/Cu(111) by LEED and STM," Surface Science **349**, L139–L145 (1996).

[31] O. Pietzsch, A. Kubetzka, M. Bode, and R. Wiesendanger, "Spin-Polarized Scanning Tunneling Spectroscopy of Nanoscale Cobalt Islands on Cu(111)," Phys. Rev. Lett. **92**, 057202 (2004).

[32] C. Duke and E. Plummer, *Frontiers in Surface and Interface Science* (North-Holland, 2002).

[33] B. Bhushan, *Springer handbook of nanotechnology*, 2nd ed. (Springer, 2006).

[34] H. Conrad, G. Ertl, and E. Latta, "Adsorption of hydrogen on palladium single crystal surfaces," Surface Science **41**(2), 435 – 446 (1974). `www.sciencedirect.com/science/article/B6TVX-46X3RND-B/2/a729526547ea12862052a4dd700e29d9`.

[35] K. Christmann, G. Ertl, and T. Pignet, "Adsorption of hydrogen on a Pt(111) surface," Surface Science **54**(2), 365 – 392 (1976). `www.sciencedirect.com/science/article/B6TVX-46SWVPV-JG/2/8bd85a069575b6ed8d51e4557cba73c7`.

[36] F. Bozso, G. Ertl, M. Grunze, and M. Weiss, "Interaction of nitrogen with iron surfaces : I. Fe(100) and Fe(111)," Journal of Catalysis **49**(1), 18 – 41 (1977). `www.sciencedirect.com/science/article/B6WHJ-4CFVH59-RH/2/1309d88ab670a071956aa6d8f38b32f9`.

[37] R. Imbihl, R. Behm, G. Ertl, and W. Moritz, "The structure of atomic nitrogen adsorbed on Fe(100)," Surface Science **123**(1), 129 – 140 (1982). `www.sciencedirect.com/science/article/B6TVX-46SXN4Y-1CM/2/3c7c96de57f8266368546892eaa94326`.

[38] G. Ertl, S. Lee, and M. Weiss, "Kinetics of nitrogen adsorption on Fe(111)," Surface Science **114**(2-3), 515 – 526 (1982). `www.sciencedirect.com/science/article/B6TVX-46TY3P1-1RC/2/1427b608a4aacd2fbf92dd99fccbabf0`.

[39] G. Ertl, “Primary steps in catalytic synthesis of ammonia,” Journal of Vacuum Science & Technology A: Vacuum, Surfaces, and Films **1**(2), 1247–1253 (1983). `http://link.aip.org/link/?JVA/1/1247/1`.

[40] T. Engel and G. Ertl, “Elementary steps in the catalytic oxidation of carbon monoxide on platinum metals,” Advances in Catalysis **28**, 1–78 (1979).

[41] H. Ibach, *Physics of surfaces and interfaces* (Springer Verlag, 2006).

[42] I. Tamm, “A possible kind of electron binding on crystal surfaces,” Physikalische Zeitschrift der Sowjetunion **1**, 733–46 (1932).

[43] W. Shockley, “On the Surface States Associated with a Periodic Potential,” Phys. Rev. **56**(4), 317–323 (1939).

[44] G. A. Fiete and E. J. Heller, “Colloquium: Theory of quantum corrals and quantum mirages,” Rev. Mod. Phys. **75**(3), 933–948 (2003).

[45] J. Venables, G. D. T. Spiller, and M. Hanbrücken, “Nucleation and growth of thin films,” Rep. Prog. Phys. **47**, 399 (1984).

[46] H. Brune, “Microscopi view of epitaxial metal growth: nucleation and aggregation,” Surf. Sci. Rep. **31**, 121 (1998).

[47] C. Ratsch and J. Venables, “Nucleation theory and the early stages of thin film growth,” J. Vac. Sci. Technol. A **21**, S96 (2003).

[48] K. Kolasinski, *Surface science: foundations of catalysis and nanoscience* (John Wiley & Sons Inc, 2002).

[49] H. Hertz, “Über einen Einfluss des ultravioletten Lichtes auf die elektrische Entladung,” Annalen der Physik **31**, 983 (1887).

[50] A. Einstein, “Über einen die Erzeugung und Verwandlung des Lichtes betreffenden heuristischen Gesichtspunkt,” Annalen der Physik **322**(6), 132–148 (1905). `http://dx.doi.org/10.1002/andp.190532206073`.

[51] “Wikimedia Commons - ARPES general,” Website (2009). Short link: `www.bit.ly/1G7YX3` (original: `commons.wikimedia.org/wiki/File:ARPESgeneral.png`).

[52] S. Hüfner, *Photoelectron Spectroscopy*, page 4, third edition ed. (Springer, 2003).

[53] C. Chen, *Introduction to scanning tunneling microscopy*, 2nd ed. (Oxford University Press, USA, 2008).

[54] A. Langner, “Self-Assembly of Multiligand Supramolecular Architectures at Metal Surfaces,” Ph.D. thesis, EPF Lausanne, Switzerland (2009).

[55] P. K. Hansma and J. Tersoff, “Scanning tunneling microscopy,” Journal of Applied Physics **61**(2), R1–R24 (1987). .

[56] J. Tersoff and D. R. Hamann, “Theory and Application for the Scanning Tunneling Microscope,” Phys. Rev. Lett. **50**(25), 1998–2001 (1983).

[57] J. Tersoff and D. R. Hamann, “Theory of the scanning tunneling microscope,” Phys. Rev. B **31**(2), 805–813 (1985).

[58] B. Stipe, M. Rezaei, and W. Ho, “Single-molecule vibrational spectroscopy and microscopy,” Science **280**(5370), 1732 (1998).

[59] J. R. Hahn, H. J. Lee, and W. Ho, “Electronic Resonance and Symmetry in Single-Molecule Inelastic Electron Tunneling,” Phys. Rev. Lett. **85**(9), 1914–1917 (2000).

[60] R. Feenstra, J. A. Stroscio, and A. Fein, “Tunneling spectroscopy of the Si(111)2 1 surface,” Surface Science **181**(1-2), 295 – 306 (1987). `www.sciencedirect.com/science/article/B6TVX-46P3TFM-168/2/154f32463ffde15d521641984279e72d`.

[61] G. Binnig, H. Rohrer, C. Gerber, and E. Weibel, “Tunneling through a controllable vacuum gap,” Applied Physics Letters **40**(2), 178–180 (1982). `http://link.aip.org/link/?APL/40/178/1`.

[62] G. Binnig, K. H. Frank, H. Fuchs, N. Garcia, B. Reihl, H. Rohrer, F. Salvan, and A. R. Williams, “Tunneling Spectroscopy and Inverse Photoemission: Image and Field States,” Phys. Rev. Lett. **55**(9), 991–994 (1985).

[63] J. Bardeen, “Tunnelling from a Many-Particle Point of View,” Phys. Rev. Lett. **6**(2), 57–59 (1961).

[64] I. Giaever, “Energy Gap in Superconductors Measured by Electron Tunneling,” Phys. Rev. Lett. **5**(4), 147–148 (1960).

[65] I. Giaever, “Electron Tunneling Between Two Superconductors,” Phys. Rev. Lett. **5**(10), 464–466 (1960).

[66] P. Wahl, L. Diekhöner, M. A. Schneider, and K. Kern, “Background removal in scanning tunneling spectroscopy of single atoms and molecules on metal surfaces,” Review of Scientific Instruments **79**(4), 043104 (pages 4) (2008). `http://link.aip.org/link/?RSI/79/043104/1`.

[67] M. Ziegler, N. Néel, A. Sperl, J. Kröger, and R. Berndt, “Local density of states from constant-current tunneling spectra,” Phys. Rev. B **80**(12), 125402 (2009).

[68] A. Heinrich, J. Gupta, C. Lutz, and D. Eigler, “Single-atom spin-flip spectroscopy,” Science **306**(5695), 466–469 (2004).

[69] L. Limot, J. Kröger, R. Berndt, A. Garcia-Lekue, and W. A. Hofer, “Atom Transfer and Single-Adatom Contacts,” Phys. Rev. Lett. **94**(12), 126102 (2005).

[70] J. F. Jia, K. Inoue, Y. Hasegawa, W. S. Yang, and T. Sakurai, “Local work function for Cu(111)–Au surface studied by scanning tunneling microscopy,” Journal of Vacuum Science & Technology B: Microelectronics and Nanometer Structures **15**(6), 1861–1864 (1997).

[71] S.-W. Hla, “Scanning tunneling microscopy single atom/molecule manipulation and its application to nanoscience and technology,” Journal of Vacuum Science & Technology B: Microelectronics and Nanometer Structures **23**(4), 1351–1360 (2005). `http://link.aip.org/link/?JVB/23/1351/1`.

[72] B. Neu, G. Meyer, and K. Rieder, “Controlled Vertical and Lateral Manipulation of Single Atoms and Molecules with the Scanning Tunneling Microscope,” Modern Physics Letters B **9**, 963–969 (1995).

[73] D. Eigler, C. Lutz, and W. Rudge, “An atomic switch realized with the scanning tunneling microscope,” Nature **352**, 600–603 (1991).

[74] G. Schull, T. Frederiksen, M. Brandbyge, and R. Berndt, “Passing Current through Touching Molecules,” Physical Review Letters **103**(20), 206803 (pages 4) (2009). `http://link.aps.org/abstract/PRL/v103/e206803`.

[75] K. Morgenstern, J. Kibsgaard, J. V. Lauritsen, E. Lægsgaard, and F. Besenbacher, “Cobalt growth on two related close-packed noble metal surfaces,” Surface Science **601**(9), 1967 – 1972 (2007). `www.sciencedirect.com/science/article/B6TVX-4N49VFG-1/2/0a01a8c8d00f9c6ec6723013982aedaf`.

[76] T. Gopakumar, N. Néel, J. Kröger, and R. Berndt, “Spatial modulation of d states in a nanoscale Co island,” Chemical Physics Letters **484**(1-3), 59–63 (2009). `www.sciencedirect.com/science/article/B6TFN-4XNF6HD-1/2/8741f2ecf5a3ce6fcfe4006465c62e22`.

[77] A. Ruban, B. Hammer, P. Stoltze, H. Skriver, and J. Nørskov, “Surface electronic structure and reactivity of transition and noble metals,” Jrnl. Mol. Cat. A **115**, 421–429 (1997).

[78] W. de Haas, J. de Boer, and G. van dën Berg, “The electrical resistance of gold, copper and lead at low temperatures,” Physica **1**(7-12), 1115–1124 (1934). `www.sciencedirect.com/science/article/B6X42-4GSCH1F-2H/2/a1b7447943ee0ca20069711b3d132394`.

[79] W. Meissner and B. Voigt, “Messungen mit Hilfe von flüssigem Helium XI Widerstand der reinen Metalle in tiefen Temperaturen,” Annalen der Physik **399**(7), 761–797 (1930). `http://dx.doi.org/10.1002/andp.19303990702`.

[80] J. Kondo, “Resistance Minimum in Dilute Magnetic Alloys,” Progress of Theoretical Physics **32**(1), 37–49 (1964). `http://ptp.ipap.jp/link?PTP/32/37/`.

[81] K. G. Wilson, “The renormalization group: Critical phenomena and the Kondo problem,” Rev. Mod. Phys. **47**(4), 773–840 (1975).

[82] J. Li, W.-D. Schneider, R. Berndt, and B. Delley, “Kondo Scattering Observed at a Single Magnetic Impurity,” Phys. Rev. Lett. **80**(13), 2893–2896 (1998).

[83] E. Minamitani, H. Nakanishi, W. A. Dino, and H. Kasai, “Scanning tunneling spectroscopic evidence of crossover transition in the two-impurity Kondo problem,” arXiv.org – cond-mat arXiv:0910.3467v2 (2009). `www.citebase.org/abstract?id=oai:arXiv.org:0910.3467`.

[84] T. Jamneala, V. Madhavan, W. Chen, and M. F. Crommie, “Scanning tunneling spectroscopy of transition-metal impurities at the surface of gold,” Phys. Rev. B **61**(15), 9990–9993 (2000).

[85] V. Iancu, A. Deshpande, and S. Hla, “Manipulating Kondo Temperature via Single Molecule Switching,” Nano Letters **6**, 820–823 (2006).

[86] P. Jarillo-Herrero, J. Kong, H. van der Zant, C. Dekker, L. Kouwenhoven, and S. De Franceschi, “Orbital Kondo effect in carbon nanotubes,” Nature **434**, 484–488 (2005).

[87] O. Újsághy, J. Kroha, L. Szunyogh, and A. Zawadowski, “Theory of the Fano Resonance in the STM Tunneling Density of States due to a Single Kondo Impurity,” Phys. Rev. Lett. **85**(12), 2557–2560 (2000).

[88] P. W. Anderson, “Localized Magnetic States in Metals,” Phys. Rev. **124**(1), 41–53 (1961).

[89] V. Madhavan, W. Chen, T. Jamneala, M. F. Crommie, and N. S. Wingreen, “Local spectroscopy of a Kondo impurity: Co on Au(111),” Phys. Rev. B **64**(16), 165412 (2001).

[90] M. Plihal and J. W. Gadzuk, “Nonequilibrium theory of scanning tunneling spectroscopy via adsorbate resonances: Nonmagnetic and Kondo impurities,” Phys. Rev. B **63**(8), 085404 (2001).

[91] P. Lucignano, R. Mazzarello, A. Smogunov, M. Fabrizio, and E. Tosatti, “Kondo conductance in an atomic nanocontact from first principles,” Nature Materials **8**, 563–567 (2009). `http://dx.doi.org/10.1038/nmat2476`.

[92] M. Maltseva, M. Dzero, and P. Coleman, “Electron Cotunneling into a Kondo Lattice,” Physical Review Letters **103**(20), 206402 (pages 4) (2009). `http://link.aps.org/abstract/PRL/v103/e206402`.

[93] U. Fano, “Effects of Configuration Interaction on Intensities and Phase Shifts,” Phys. Rev. **124**(6), 1866–1878 (1961).

[94] H. Manoharan, C. Lutz, and D. Eigler, “Quantum mirages formed by coherent projection of electronic structure,” Nature **403**(6769), 512–515 (2000).

[95] S. Cronenwett, T. Oosterkamp, and L. Kouwenhoven, “A tunable Kondo effect in quantum dots,” Science **281**(5376), 540 (1998).

[96] Y. Meir, N. S. Wingreen, and P. A. Lee, “Low-temperature transport through a quantum dot: The Anderson model out of equilibrium,” Phys. Rev. Lett. **70**(17), 2601–2604 (1993).

[97] J. Park, A. Pasupathy, J. Goldsmith, C. Chang, Y. Yaish, J. Petta, M. Rinkoski, J. Sethna, H. Abruña, P. McEuen, *et al.*, “Coulomb blockade and the Kondo effect in single-atom transistors,” Nature **417**(6890), 722–725 (2002).

[98] W. Liang, M. Shores, M. Bockrath, J. Long, and H. Park, “Kondo resonance in a single-molecule transistor,” Nature **417**(6890), 725–729 (2002).

[99] A. F. Otte, M. Ternes, S. Loth, C. P. Lutz, C. F. Hirjibehedin, and A. J. Heinrich, “Spin Excitations of a Kondo-Screened Atom Coupled to a Second Magnetic Atom,” Physical Review Letters **103**(10), 107203 (pages 4) (2009). `http://link.aps.org/abstract/PRL/v103/e107203`.

[100] W. Chen, T. Jamneala, V. Madhavan, and M. F. Crommie, “Disappearance of the Kondo resonance for atomically fabricated cobalt dimers,” Phys. Rev. B **60**(12), R8529–R8532 (1999).

[101] N. Craig, J. Taylor, E. Lester, C. Marcus, M. Hanson, and A. Gossard, “Tunable nonlocal spin control in a coupled-quantum dot system,” Science **304**(5670), 565 (2004).

[102] H. B. Heersche, Z. de Groot, J. A. Folk, L. P. Kouwenhoven, H. S. J. van der Zant, A. A. Houck, J. Labaziewicz, and I. L. Chuang, “Kondo Effect in the Presence of Magnetic Impurities,” Physical Review Letters **96**(1), 017205 (pages 4) (2006). `http://link.aps.org/abstract/PRL/v96/e017205`.

[103] C. Kittel and P. McEuen, *Introduction to solid state physics* (John Wiley & Sons, 2005).

[104] O. O. Brovko, P. A. Ignatiev, V. S. Stepanyuk, and P. Bruno, “Tailoring Exchange Interactions in Engineered Nanostructures: An Ab Initio Study,” Physical Review Letters **101**(3), 036809 (pages 4) (2008). `http://link.aps.org/abstract/PRL/v101/e036809`.

[105] M. T. Béal-Monod, “Kondo Resistivity due to a Pair of Interacting Impurities,” Phys. Rev. **178**(2), 874–881 (1969).

[106] B. A. Jones and C. M. Varma, “Study of two magnetic impurities in a Fermi gas,” Phys. Rev. Lett. **58**(9), 843–846 (1987).

[107] W. Chen, T. Jamneala, V. Madhavan, and M. F. Crommie, “Disappearance of the Kondo resonance for atomically fabricated cobalt dimers,” Phys. Rev. B **60**(12), R8529–R8532 (1999).

[108] M. A. Schneider, L. Vitali, N. Knorr, and K. Kern, “Observing the scattering phase shift of isolated Kondo impurities at surfaces,” Phys. Rev. B **65**(12), 121406 (2002).

[109] B. N. Roy, *Fundamentals of Classical and Statistical Thermodynamics*, pages 239, 434–438, first edition ed. (Wiley, 2002).

[110] S. Sachdev, *Quantum phase transitions* (Cambridge University Press, 2001).

[111] Q. Si, S. Rabello, K. Ingersent, and J. Smith, "Locally critical quantum phase transitions in strongly correlated metals," Nature **413**(6858), 804–808 (2001).

[112] Q. Si, J. Smith, and K. Ingersent, "Quantum Critical Behavior in Kondo Systems," International Journal of Modern Physics B **13**(18), 2331–2342 (1999).

[113] A. W. Rost, R. S. Perry, J.-F. Mercure, A. P. Mackenzie, and S. A. Grigera, "Entropy Landscape of Phase Formation Associated with Quantum Criticality in Sr3Ru2O7," Science **325**(5946), 1360–1363 (2009). `www.sciencemag.org/cgi/content/abstract/325/5946/1360`.

[114] S. Doniach, "Phase Diagram for the Kondo Lattice," in *International Conference on Valence Instabilities and Related Narrow Band Phenomena*, R. Parks, ed., pages 169–176 (Rochester, NY, 1977).

[115] B. Jones, C. Varma, and J. Wilkins, "Low-Temperature Properties of the Two-Impurity Kondo Hamiltonian," Phys. Rev. Lett. **61**, 125–128 (1988).

[116] A. Georges and Y. Meir, "Electronic Correlations in Transport through Coupled Quantum Dots," Phys. Rev. Lett. **82**, 3508–3511 (1999).

[117] H. Jeong, A. Chang, and M. Melloch, "The Kondo Effect in an Artificial Quantum Dot Molecule," Science **293**, 2221–2223 (2001).

[118] N. Craig, J. Taylor, E. Lester, C. Marcus, M. Hanson, and A. Gossard, "Tunable Nonlocal Spin Control in a Coupled-Quantum Dot System," Science **304**, 565–567 (2004).

[119] E. Sela and I. Affleck, "Nonequilibrium Transport through Double Quantum Dots: Exact Results near a Quantum Critical Point," Phys. Rev. Lett. **102**, 047201 (2009).

[120] L. Limot, J. Kröger, R. Berndt, A. Garcia-Lekue, and W. Hofer, "Atom Transfer and Single-Adatom Contacts," Phys. Rev. Lett. **94**, 126102 (2005).

[121] N. Néel, J. Kröger, L. Limot, K. Palotas, W. Hofer, and R. Berndt, "Conductance and Kondo Effect in a Controlled Single-Atom Contact," Phys. Rev. Lett. **98**, 016801 (2007).

[122] L. Vitali, R. Ohmann, S. Stepanow, P. Gambardella, K. Tao, R. Huang, V. Stepanyuk, P. Bruno, and K. Kern, "Kondo Effect in Single Atom Contacts: The Importance of the Atomic Geometry," Phys. Rev. Lett. **101**, 216802 (2008).

[123] M. Klein, A. Nuber, F. Reinert, J. Kroha, O. Stockert, and H. v. Löhneysen, "Signature of Quantum Criticality in Photoemission Spectroscopy," Physical Review Letters **101**(26), 266404 (2008). `http://link.aps.org/abstract/PRL/v101/e266404`.

[124] J. B. Silva, W. L. C. Lima, W. C. Oliveira, J. L. N. Mello, L. N. Oliveira, and J. W. Wilkins, "Particle-Hole Asymmetry in the Two-Impurity Kondo Model," Phys. Rev. Lett. **76**(2), 275–278 (1996).

[125] A. Otte, M. Ternes, K. v. Bergmann, S. Loth, H. Brune, C. Lutz, C. Hirjibehedin, and A. Heinrich, "The role of magnetic anisotropy in the Kondo effect," Nature Physics **4**, 847–850 (2008).

[126] "SGM1 beamline at ASTRID," Website (2009). Short link: `www.bit.ly/NsopV` (original: `www.isa.au.dk/facilities/astrid/beamlines/sgm1/sgm1.asp`).

List of publications

Articles in or submitted to peer-refereed journals (included in appendix)

(A) Jakob Bork, Jens Onsgaard, and Lars Diekhöner, *"Growth and structure of Ag on bilayer Co nanoislands on Cu(111)"*, Accepted in Journal of Physics: Condensed Matter (2010)

(B) P. J. Godowski, Z. S. Li, J. Bork, and J. Onsgaard, *"Study of the Pt/Ru(0001) Interface"*, Surface Review and Letters, Vol. **14**, No. **5**, 911914 (2007)

(C) J. Bork, L. Diekhöner, Z. Li, and J. Onsgaard, *"Electronic structure and ordering of multilayers of Co and Ag on Cu(111) investigated by photoelectron spectroscopy and LEED"*, Submitted (2010)

(D) Jakob Bork, Peter Wahl, Lars Diekhöner, and Klaus Kern, *"Potential energy landscape of metallic Moiré patterns"*, New Journal of Physics **11**, 113051 (2009)

(E) Jakob Bork, Yong-hui Zhang, Lars Diekhöner, Pascal Simon, László Borda, Johann Kroha, Peter Wahl, and Klaus Kern, *"Tuning a Cobalt Dimer between Kondo Screening and Local Moment Antiferromagnetism"*, In preparation (2010)

Presentations

1. Poster presentation at the iNano Summerschool: Nanomaterials and Nanosynthesis, June 2007, Fuglsø centret, Aarhus, Denmark
2. Poster presentation at the Summer School on Modern Concepts for Creating and Analyzing Surfaces and Nanoscale Materials, May 2008, Sant Feliu de Guixols, Costa Brava, Spain
3. Oral presentation at the International Conference on Nanoscience + Technology (ICN+T), July 2008, Keystone, Colorado, USA
4. Poster presentation at the Max Planck Institute Beirat, November 2008, Stuttgart, Germany
5. Poster presentation at the iNano Annual Meeting, January 2009, Aarhus, Denmark
6. Poster presentation at the Trends in Nanoscience conference, February 2009, Kloster Irsee, Germany
7. Oral presentations at Ringberg and Lauterbad meetings, October 2006/April 2008/October 2009, Germany

Dansk resumé

Denne afhandling omhandler grundforskning indenfor elektronisk og magnetisk vekselvirkning på nanoskala. Fra små metalliske og magnetiske øer og lag til enkelte atomer på overflader. Magnetisk interaktion undersøges gennem de spektroskopiske muligheder ved et skannende tunnelmikroskop (STM). Især ved lave temperaturer bruges Kondoresonansen til at studere magnetisk interaktion med ferromagnetiske øer og mellem to atomer. Sidstnævnte viser et crossover mellem Kondo-skærmede atomer og antiferromagnetisk koblede atomer tæt på det kvantekritiske punkt. Dette relateres til forskningen indenfor korrellerede elektronmaterialer såsom studier af faseovergange i tunge fermion materialer og magnetisk vekselvirkning indenfor spintronik forskning.

Nøgleord: *Ultrahøjt vakuum, Skannende tunnel mikroskopi, Metalliske heterostrukturer, Moiré mønster, Splittet Kondoresonans, Guld-coatet STM-spids, Frit positionerbart Kondosystem, To-urenheds Kondosystem, crossover, Antiferromagnetisk kobling*

Tildækningen af koboltøer på Cu(111) med sølv er undersøgt med STM og fotoemissionsspektroskopi. Det er vist at ved lav dækning nukleerer sølvet fortrinsvist ovenpå de dobbeltlags høje koboltøer i stedet for direkte på Cu(111) substratet. Ydermere danner sølvet en kombination af en rekonstruktion og et Moirémønster, hvilket er undersøgt med lav-energi elektrondiffraktion (LEED) og med spektroskopisk STM kortlægning ved 6 K. Det er vist at heterostrukturen har meget interesante elektroniske egenskaber. Den d-relaterede tilstand fra den nu begravede koboltø er synlig igennem det dækkende sølvlag, men sølvets Moirémønster modulerer den spinpolariserede kobolt d-tilstand i amplitude, energiposition og bredde. Dette er relateret til d-båndsmodellen for katalytiske reaktioner. Det største skifte er i amplituden af tilstanden, men den omvendte struktur med kobolt på Ag(111) viser lignende egenskaber, dog med et stort skifte i energiposition i stedet for amplitude af tilstanden.

Kondoeffekten er brugt til at probe magnetisk interaktion mellem de førnævnte sølvdækkede koboltøer (og ydermere guld-dækkede koboltøer) og enkelte koboltatomer placeret på Moirémønstret. Der er observeret en splittet Kondoresonans på grund af exchange-vekselvirkningen mellem øen og atomerne.

I et mere teknisk afsnit af afhandlingen vises det hvordan en guld-dækket STM-spids gøres modtagelig for enkelte koboltatomer. Spidsen dyppes enten direkte i en Au(111) overflade eller flager af guld samles op fra koboltøerne på Cu(111). En ændring i den lokale barrierehøjde (arbejdsfunktion) af spids-prøve forbindelsen indikerer at det yderste af spidsen er guld-dækket og at enkelte koboltatomer kan samles op. Et koboltatom påhæftet STM-spidsen viser en Kondoresonans dannet mellem atomet og spidsen meget lig resonansen, der dannes når et koboltatom er på overfladen og der måles med en ren spids.

Her bruges dette til at vise hvordan et to-urenheds-Kondosystem bestående af to koboltatomer (den ene på STM-spidsen og den anden på Au(111)-prøven) gennemgår et kontinuert crossover fra en fase med Kondoskærmede atomer til en fase med antiferromagnetisk koblede atomer når afstanden mellem atomerne ændres fra

ikke-vekselvirkende til stærkt vekselvirkende. I det Kondoskærmede regime er Kondotemperaturen konstant og kun Fano linjeformen ændrer sig fra et dyk til en top. I det antiferromagnetiske regime ses en opsplitning af de inelastiske spinflip eksitationer. Dette understøttes af numerisk renormaliseringsgruppeteori. Dette crossover mellem de to regimer er ydermere interessant fordi det foregår i et område af fasediagrammet tæt på det kvantekritiske punkt, hvor faseovergangen møder det absolutte nulpunkt i temperatur.

Dette frit positionerbare Kondosystem på STM-spidsen repræsenterer en ny måde at probe magnetisk vekselvirkning på, med muligheden for kontinuert at ændre positionen af det probende Kondosystem. Eksperimentet fremstår som ét blandt mange anvendelsesmuligheder med et frit positionerbart Kondosystem påhæftet STM-spidsen og metoden kan åbne op for et nyt felt indenfor STM. Vi forventer at vores forskning har direkte indflydelse på andre forskningsområder såsom tunge fermion materialer, hvilket er en klasse af materialer hvis egenskaber er styret af konkurrencen mellem Kondoskærmning og lokal antiferromagnetisk moment, samt indenfor kvanteinformationsbehandling.

Growth and structure of Ag on bilayer Co nanoislands on Cu(111)

A

Jakob Bork, Jens Onsgaard, and Lars Diekhöner.
"Growth and structure of Ag on bilayer Co nanoislands on Cu(111)", Accepted in Journal of Physics: Condensed Matter (2010).

arXiv:0904.4170v3 [cond-mat.mtrl-sci] 15 Feb 2010

Growth and structure of Ag on bilayer Co nanoislands on Cu(111)

Jakob Bork, Jens Onsgaard, and Lars Diekhöner*
Institut for Fysik og Nanoteknologi, and Interdisciplinary Nanoscience Center (iNANO),
Aalborg Universitet, Skjernvej 4A, DK–9220 Aalborg, Denmark

We have studied the growth of Ag on bilayer high Co nanoislands on Cu(111) using Scanning Tunneling Microscopy. Noble metal capping of magnetic nanostructures is known to influence the magnetism and knowledge of the growth is therefore important. We find that Ag preferentially nucleates on the Co nanoislands initially leaving the free Cu sites clean. Furthermore we observe, that those Co islands which are capped with Ag are almost completely capped thus making a perfect multilayered system of Ag/Co/Cu(111). We observe a (9×9) reconstruction of the Ag overlayer on Co/Cu(111).

PACS numbers: 61.46.-w, 68.35.bd, 68.37.Ef, 68.65.Ac

I. INTRODUCTION

The properties of metallic thin films and nanostructures on crystalline surfaces are strongly interlinked with the morphology and chemical composition of the structures. Epitaxial growth of in particular homoepitaxial and bimetallic systems have therefore been studied extensively[1–3]. When growing multilayered heterostructures of several materials it becomes more complicated to control the growth and ensure that the desired structures are fabricated during deposition of the constituents of interest. Besides diffusion on terraces also interlayer mass transport becomes decisive for the growth[4–8]. Multilayered systems of magnetic and non-magnetic metallic layers, which we have studied, are in particular interesting for their technological applications in the area of data storage and processing[9–11]. It has recently been shown that capping a ferromagnetic thin film with a noble metal can influence the magnetic properties[12–17].

We report here on the capping of ferromagnetic Co nanoislands with Ag thus producing Ag/Co/Cu(111) nanostructures. The growth of Co on Cu(111) is well known and the structural, electronic and magnetic properties have been studied in great detail[18–25]. Important for the work presented here is that for lower coverages at room temperature Co forms bilayer high islands of triangular shape and a width of 3–25 nm[18,25]. We have deposited Ag on top and found that there is a preference for covering the Co islands before the Cu-terraces and we observe that the Ag capped Co islands, with few exceptions, are always fully covered with Ag. We conclude that interlayer mass transport plays an important role where Ag atoms, which have landed on the Cu-terrace, must be allowed to ascend the bilayer high step edges of the Co-island.

II. EXPERIMENT

Experiments have been performed in an ultra high vacuum system (5×10^{-11} mbar) using a scanning tunneling microscope (STM) operated at room temperature and low energy electron diffraction (LEED). We have used WSxM to analyze and display STM images[26]. A Cu(111) crystal was cleaned by sputter/anneal (500°C) cycles. Co was deposited with a flux of 0.14 ML/min at T=27°C . Next, Ag was deposited at room temperature (or 70°C in one case) with a flux of 0.44 ML/min or 3.6 ML/min. The area Co coverage in all experiments is 0.15–0.36 ML and the Ag overlayer coverage is varied from 0 to ∼1.6 ML. Note that for the Co islands the term monolayer (ML) is used for the visible area coverage, meaning that the deposited amount of Co is twice the visible coverage since the Co islands are of bilayer height.

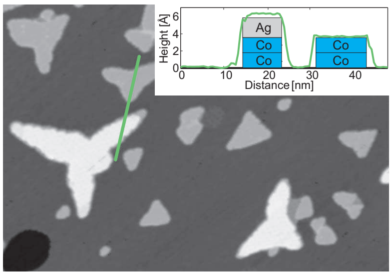

FIG. 1: STM image after depositing 0.07 ML Ag on 0.2 ML Co/Cu(111). The image is taken at a bias voltage of 0.35 V, the size is 157×108 nm and the z-scale spans 0.91 nm. The inset shows a linescan.

III. RESULTS AND DISCUSSION

A. Growth

After depositing Co on Cu(111) we observe the well-known bilayer high (3.9 Å) islands[18,19,22–25] mostly of triangular shape as well as star-shaped islands (which is known to be a kinetic effect[25]). An STM image of 0.07 ML Ag deposited on a Cu surface with a low coverage of Co islands (Θ_{Co} = 0.20, where only bilayer high Co islands are formed) is shown in Figure 1. The bright islands are consisting of 2 ML Co with 1 ML Ag on top. Although Co islands of 3 ML height are never observed at these Co coverages we note for comparison that the height of islands consisting of 2 ML Co + 1 ML Ag is 1 Å larger than 3 ML Co. Furthermore the Ag cap layer shows a reconstruction (discussed later). The less bright islands are 2 ML Co islands that are not capped with Ag. The heights are illustrated by the inset in Figure 1. It is remarkable that those Co islands which *do contain* Ag on top are almost *completely covered* with a Ag layer. On the other hand, the amount of Ag on the Cu surface is minimal although Ag has been deposited homogeneously. Ag thus accumulates on top of some of the Co islands leaving the other Co islands and the Cu terrace clean. We note that occasionally it might happen that narrow corners of islands are not filled with Ag (as observable at the upper right corner of the largest star shaped island in Figure 1). As the Ag coverage is increased to 0.35 ML we observe, besides fully capped Co islands, that some of the Co islands are surrounded by Ag instead (Figure 2a). At 0.8 ML Ag (Figure 2b) most of the Cu surface and all Co islands are filled with Ag, except from some of the smaller Co islands. In Figure 2c we have plotted the fraction of Co islands that are capped with Ag as a function of island size and see that larger islands have a higher probability of being capped.

Before analyzing the data in more detail we will briefly discuss the growth in the areas containing Cu step edges. Co deposition on clean Cu(111) leads to islands on the terraces as well as a decoration of both sides of the Cu step edges[18]. On the other hand, deposition of Ag on clean Cu(111) at room temperature never leads to nucleation on the terraces but only to decoration of the lower side of Cu step edges resulting in "step flow growth"[27]. In agreement with this we find here that Ag deposited on a partially Co covered Cu(111) surface nucleates at step edges but also on top of Co islands. This is shown in an overview STM image in Figure 3. We avoid the complexity at the Cu step edges and concentrate our further analysis on Cu terraces.

We will now quantify the preference of Ag nucleating on top of Co islands vs. nucleating on Cu. For fabrication of Ag/Co/Cu structures nucleation on top of Co islands would be preferred. We have determined the partial coverage of Ag on Co islands, Y_{AgCo}, and Ag directly on Cu(111), Y_{AgCu}, from STM images of surfaces with variable Ag coverage and a Co coverage of 0.25±0.1 ML. The partial coverage of Ag on Co (Cu) is defined as the relative area of Co (Cu), that is covered with Ag. In this way we normalize the Ag coverage to the available area of Co (Cu). Whereas Y_{AgCo} is sensitive to Θ_{Co} it is notable that the free Cu area plays a less important role for how much of the Ag nucleates on Cu sites since nucleation of Ag never occurs on Cu terrace sites away from Co island steps. We have used the Flooding function of the WSxM program[26] to determine coverages. The images used for the analysis are sized approximately 200 nm × 200 nm.

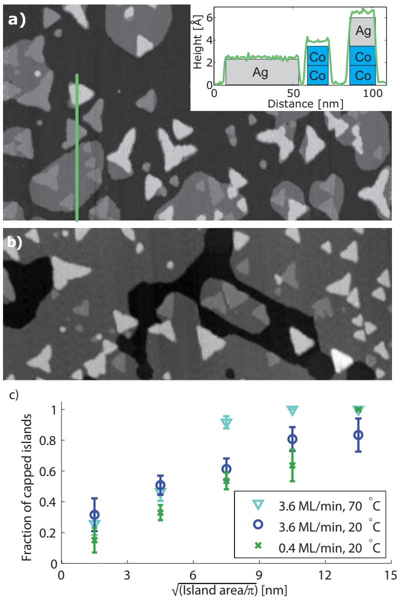

FIG. 2: (Color online) STM images for a) 0.35 ML Ag on 0.2 ML Co/Cu(111). The image is 300×167 nm and the z-scale spans 0.94 nm. The linescan runs through a Ag capped Co island, an uncapped Co island and a layer of Ag directly on Cu(111). b) 0.80 ML Ag on 0.2 ML Co/Cu(111). The image is 300×118 nm and the z-scale spans 0.94 nm. c) The fraction of capped islands as a function of approximate island radius grouped in 3 nm bins for two Ag-deposition rates and two temperatures. $\Theta_{Co} \approx 0.17$ and $\Theta_{Ag} \approx 0.4$. In total 598 islands were analyzed to produce the 3 data sets.

For each datapoint in Figure 4 we have analyzed 1–4 different areas on the surface for a given preparation. In Figure 4a and 4b we plot Y_{AgCo} and Y_{AgCu} as a function of Θ_{Ag} for two different Ag deposition fluxes of 0.44 ML/min and 3.6 ML/min, respectively. At low Ag doses Y_{AgCo} increases faster than Y_{AgCu}. This preference disappears above $\Theta_{Ag} \sim 0.7$ML. The effect is more clearly demonstrated by plotting the ratio $\frac{Y_{AgCo}}{Y_{AgCu}}$ (Figure 4c), which thus is a measure of the preference of Ag nucleating on Co vs. on Cu[38]. In agreement with the qualitative discussion earlier we observe indeed that at low Ag coverage there is an increased preference of Ag nucleating on Co islands. At higher Ag coverage this decreases since Co islands which are already capped and those with a Ag rim are no longer available and the ratio approaches unity. Furthermore we note that a higher Ag flux initially leads to a slightly increased preference for nucleation on Co (see Figure 4c). We observe no significant dependance on Θ_{Co} in the range we have used (Θ_{Co}: 0.15–0.36

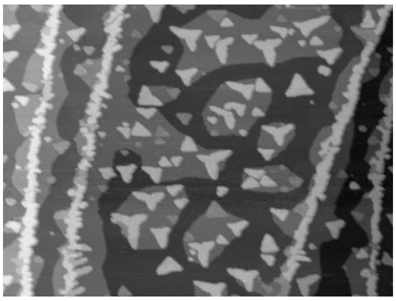

FIG. 3: Overview STM image of 0.48 ML Ag deposited on 0.25 ML Co on Cu(111). For the analysis only terrace sites are used and the areas around Cu-steps are neglected. The image size is 400×300 nm.

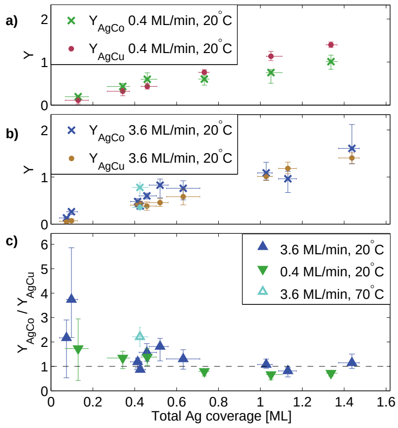

FIG. 4: (Color online) a) The partial coverage (Y) of Ag on Co and Cu respectively at low Ag-deposition rate (0.44 ML/min). b) The partial coverage (Y) of Ag on Co and Cu respectively at high Ag-deposition rate (3.6 ML/min). c) The ratio of the partial coverages of Ag on Co-islands and Ag on Cu(111) as a function of deposited Ag for the two Ag-rates. At a ratio above 1, indicated by the horizontal dashed line, there is preference for Ag-nucleation on Co. All data are for deposition at T=20°C except for the light-blue data point (T=70°C).

ML).

There have been a number of studies investigating nucleation on a surface with pre-grown islands[4–8]. Atoms landing directly on an island will diffuse around until they either descend and disappear from the island or meet other adatoms finally forming a stable cluster. This can then act as nucleation site for further adatoms. The additional Erlich-Schwoebel barrier at the step edge[28,29] increases the time an adatom stays on the island and thereby the probability of meeting another adatom. With this in mind we can rationalize our experimental findings. We observed that larger Co islands have a larger probability of being capped with Ag (see Figure 2c). This has also been seen in other systems[5] and is due to a larger probability of finding two adatoms at the same time on a larger island. There was a more sharp transition between capped an uncapped islands, compared to the results presented here, and it was possible to identify a so-called critical radius (R_c), where islands having a radius larger than R_c would experience 2. layer nucleation on top[4,5]. The varying and in part irregular shape of the Co islands makes it difficult to identify a radius but we used $\sqrt{A/\pi}$, where A is the island area[39]. We found that a higher Ag flux lead to increased nucleation on top of Co islands. This is seen as a slight shift towards smaller islands in Figure 2c but more clearly in Figure 4c, where the trend is that the ratio $\frac{Y_{AgCo}}{Y_{AgCu}}$ (and thereby the preference for nucleation on Co) is largest for the high Ag deposition rate, 3.6 ML/min. A higher Ag-flux makes it more likely that another atom necessary for making a stable cluster lands on the island in time. We also studied the effect of increased surface temperature. The simple expectation would be that a higher temperature leads to a higher diffusivity of Ag adatoms on the island and a higher descend rate thus reducing the residence time and the chance of nucleation[4,5] (especially visible in the experimental data presented in Ref[5]). We find on the contrary that T=70°C results in an *increased* nucleation rate on the islands compared to T=20°C. This can be seen in Figure 2c (as a function of island size) and in the ratio of relative coverages (Figure 4c). The explanation presented in Ref[4,5] does not take into account that atoms landing on the bare surface (not on the islands) may *ascend* the islands and thereby lead to an increased nucleation probability on the islands. Apparently this is a prerequisite in this case and is very surprising since the Ag atoms need to ascend steps of 2 ML height. In contrast, Ag atoms never ascend monatomic Cu steps[27] or steps at Ag islands. This peculiarity is illustrated in Figure 5. The reason is likely to be found in Co being chemically more reactive than the more noble Cu[35] and the binding of Ag is therefore expected to be stronger to Co than to Cu. This could give rise to asymmetric rates of step edge crossing, i.e. the diffusion rate for atoms moving up is higher than for moving down, but also to a smaller critical cluster size on Co than on Cu. Both effects lead to a preference for nucleation and an accumulation on Co compared to Cu as observed.

Another reason for the preference of capping Co with Ag can possibly be found in the gain of free energy[1]. Most simply there are three free energy parameters to take into account, where γ_S is the surface free energy of the substrate (Cu or Co), γ_D is the surface free energy of the deposit (Ag in this case) and γ_i is the interface free energy. The values for the surface energies

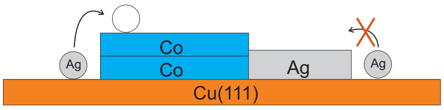

FIG. 5: (Color online) We here illustrate the peculiar growth, where Ag atoms ascend bilayer high Co islands but do not ascend monolayer high Ag islands (or Cu step edges).

are $\gamma_{Ag(111)} = 1.17\ J/m^2$, $\gamma_{Cu(111)} = 1.95\ J/m^2$ and $\gamma_{Co(0001)} = 2.78\ J/m^2$[36]. Note that the latter value is for Co(0001) and not for 2 ML Co/Cu(111), where it may be different due to the strained Co adlayer, which has adapted to the Cu lattice. The criterion for layer-growth, $\gamma_D + \gamma_i < \gamma_S$ seems to be fulfilled for both Ag on Cu(111) and Ag on Co/Cu(111) since in both cases a complete adlayer of Ag is formed. The change in free energy, $\Delta\gamma = (\gamma_D + \gamma_i) - \gamma_S$ is difficult to evaluate exactly since, to our knowledge, $\gamma_{i,Ag/Co}$ is not available for Ag on Co/Cu(111). The interface energy is strongly interlinked with the lattice mismatch and there is therefore reason to believe that $\gamma_{i,Ag/Co}$ and $\gamma_{i,Ag/Cu}$ are similar in this particular case and the gain in free energy will therefore be larger for capping the Co islands, since $\gamma_{Cu} < \gamma_{Co}$. This argument is in agreement with our finding of increased preference for capping Co.

Although the mobility of single atom diffusion on (111) surfaces is very high it does not always lead to Ag-covered Co islands. This can be explained by an apparent high critical cluster size for nucleation, i.e. only if a sufficient number of Ag atoms meet and form a stable immobile cluster on top of the Co island the Ag adlayer will be formed. Otherwise, Ag atoms diffuse down on to the Cu surface. If, on the other hand, a stable cluster has been formed, attachment of further Ag atoms occurs frequently due to the high mobility of Ag atoms and a complete adlayer is formed. At very low Ag coverages it might happen that there is not sufficient Ag to form a complete capping layer on an island, but the Ag coverages used here (all above 0.07 ML) lead to either capped or empty Co islands. This is in contrast to findings for Au or Cu growth on Co/Cu(111), where only part of a Co island is capped[30]. Those Co-islands which are not capped are mostly completely surrounded with Ag (see Figures 2a and 2b). This can be due to a simple blocking effect, where a Ag-rim at the Co-island border prevents further atoms from ascending the island or that the rim reduces the Erlich-Schwoebel barrier and the confinement of Ag atoms landing on top of an island is then less effective. It is known that Co islands on Cu(111) grow in two general orientations[18]. We note that this had no influence on the Ag-capping.

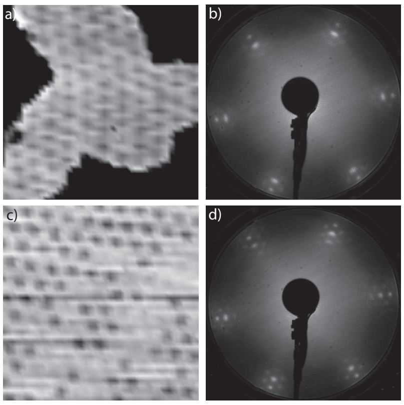

FIG. 6: a) Closeup STM image of a Ag capped Co island on Cu(111) with b) corresponding LEED pattern. The observed Moiré pattern has a corrugation of 25 pm and a periodicity of ca. 24 Å taken with the bias voltage of 0.35 V. c) Closeup STM image of the (9×9) reconstruction of Ag grown directly on Cu(111) with the bias voltage at 0.23 V and d) corresponding LEED pattern. The image size is 24×24 nm in both a) and c). The electron energy used for the LEED images was 65 eV.

B. Structure

Finally, we will address the atomic structure of Ag on Co/Cu(111) by STM and LEED measurements. Figure 6a shows an STM image of bilayer thick Co island which subsequently has been capped with Ag. We observe a Moiré pattern with a periodicity of ca. 24 Å and an apparent corrugation of 25 pm. For the diffraction experiments we deposited 3 ML Co and subsequently 1.3 ML Ag at room temperature. The LEED image in Figure 6b show six main spots from the Cu(111) substrate (or the Co islands which grow pseudomorphically[22]). At each main spot there are six satellites due to the Ag layer. This symmetry is identical to what is seen for a Ag overlayer on Cu(111)[27,31–34] where the atomic structure depends on deposition temperature[27,34], but in any case the periodicity is ca. (9×9) originating from the lattice mismatch between Cu and Ag. For comparison we have deposited 1.3 ML Ag on Cu(111) and recorded an STM and a LEED image (shown in Figure 6c and d). Since Co grows pseudomorphically on Cu a similar reconstruction is expected for Ag grown on Co/Cu(111). This is indeed observed here, although the Ag-related LEED pattern is more blurry for Ag/Co/Cu(111) compared to Ag/Cu(111). We believe this is due to edge effects at Co islands where the periodicity of the Ag Moiré pattern may change and the relatively smaller "coherence areas" for LEED taken on Ag/Co/Cu(111) than on the much larger Ag areas directly on Cu(111), since Ag grows almost layer by layer on Cu(111)[27] and the size of Ag domains is therefore only limited by the terrace size of the Cu(111) crystal. The Moiré pattern of Ag on Co/Cu(111) has recently been shown to exhibit interesting electronic properties, where the electronic structure of the Co islands is modulated with the same periodicity as the Ag overlayer Moiré superstructure[37].

IV. CONCLUSION

We have studied the growth of a Ag overlayer on Co nanoislands on Cu(111) at room temperature. The atomic structure of Ag on Co/Cu(111) shows a (9×9) periodicity due to the mismatch of lattice parameter. We find that there is a preferred nucleation for Ag on top of Co compared to Cu(111) terrace sites, especially at low Ag doses. This is quite remarkable since the Co islands are all of bilayer height and an accumulation on top of the islands thus involves ascending steps of 2 ML height. We furthermore find that Co islands are either completely free of Ag or almost completely capped with Ag. These nearly perfect multilayers can be expected to act as a model system for magnetic multilayer studies.

References

---

[*] Electronic address: ld@nano.aau.dk

[1] J.A. Venables, G. D. T. Spiller, and M. Hanbrücken. Nucleation and growth of thin films. *Rep. Prog. Phys.*, 47:399, 1984.

[2] H. Brune. Microscopi view of epitaxial metal growth: nucleation and aggregation. *Surf. Sci. Rep.*, 31:121, 1998.

[3] C. Ratsch and J.A. Venables. Nucleation theory and the early stages of thin film growth. *J. Vac. Sci. Technol. A*, 21:S96, 2003.

[4] J. Tersoff, A. W. Denier van der Gon, and R. M. Tromp. Critical island size for layer-by-layer growth. *Phys. Rev. Lett.*, 72(2):266–269, Jan 1994.

[5] Karsten Bromann, Harald Brune, Holger Röder, and Klaus Kern. Interlayer mass transport in homoepitaxial and heteroepitaxial metal growth. *Phys. Rev. Lett.*, 75(4):677–680, Jul 1995.

[6] Zhenyu Zhang and Max G. Lagally. Atomistic processes in the early stages of thin-film growth. *Science*, 276(5311):377–383, 1997.

[7] Jörg Rottler and Philipp Maass. Second layer nucleation in thin film growth. *Phys. Rev. Lett.*, 83(17):3490–3493, Oct 1999.

[8] Joachim Krug, Paolo Politi, and Thomas Michely. Island nucleation in the presence of step-edge barriers: Theory and applications. *Phys. Rev. B*, 61(20):14037–14046, May 2000.

[9] Gary A. Prinz. Magnetoelectronics. *Science*, 282:1660–1663, 1998.

[10] S. A. Wolf, D. D. Awschalom, R. A. Buhrman, J. M. Daughton, S. von Molnar, M. L. Roukes, A. Y. Chtchelkanova, and D. M. Treger. Spintronics: A spin-based electronics vision for the future. *Science*, 294:1488, 2001.

[11] I. Zutic, J. Fabian, and S. Das Sarma. Spintronics: Fundamentals and applications. *Rev. Mod. Phys.*, 76:323, 2006.

[12] W. Weber, C.H. Back, A. Bischof, D. Pescia, and R. Allenspach. Magnetic switching in cobalt films by adsoprtion of copper. *Nature*, 374:788, 1995.

[13] J.S. Tsay, Y.D. Yao, J.Y. Lin, and C.S. Yang. Oscillation of the coercive force for ultrathin ag/co/cu(111) films. *Journal of Applied Physics*, 89:7377, 2001.

[14] M. Kisielewski, A. Maziewski, M. Tekielak, A. Wawro, and L. T. Baczewski. New possibilities for tuning ultrathin cobalt film magnetic properties by a noble metal overlayer. *Phys. Rev. Lett.*, 89(8):087203, Aug 2002.

[15] F. C. Chen, Y. E. Wu, C. W. Su, and C. S. Shern. Ag-induced spin-reorientation transition of co ultrathin films on pt(111). *Phys. Rev. B*, 66(18):184417, 2002.

[16] Y. J. Chen, M. H. Kuo, and C. S. Shern. Ag-induced spin-reorientation transition of ultrathin fe films on pt(111). *Applied Physics Letters*, 93(1):012503, 2008.

[17] Farid El Gabaly, Kevin F. McCarty, Andreas K. Schmid, Juan de la Figuera, M. Carmen Munoz, Laszlo Szunyogh, Peter Weinberger, and Silvia Gallego. Noble metal capping effects on the spin-reorientation transitions of co/ru(0001). *New Journal of Physics*, 10(7):073024, 2008. 1367-2630.

[18] J. de la Figuera, J. E. Prieto, C. Ocal, and R. Miranda. Scanning-tunneling-microscopy study of the growth of cobalt on Cu(111). *Phys. Rev. B*, 47(19):13043–13046, 1993.

[19] J. de la Figuera, J. E. Prieto, C. Ocal, and R. Miranda. Surface etching and enhanced diffusion during the early stages of the growth of cobalt on Cu(111). *Surface Science*, 307-309:538–543, 1994.

[20] K Heinz, S Müller, and L Hammer. Crystallography of ultrathin iron, cobalt and nickel films grown epitaxially on copper. *J. Phys. Cond. Matt.*, 11:9437–9454, 1999.

[21] U. Alkemper, C. Carbone, E. Vescovo, W. Eberhardt, O. Rader, and W. Gudat. Exchange-split electronic states of ultrathin co layers on cu(111). *Phys. Rev. B*, 50:17496–17501, 1994.

[22] J. de la Figuera, J. E. Prieto, G. Kostka, S. Müller, C. Ocal, R. Miranda, and K. Heinz. Crystallography and morphology of the early stages of the growth of co/cu(111) by leed and stm. *Surface Science*, 349:L139–L145, 1996.

[23] L. Diekhöner, M. A. Schneider, A. N. Baranov, V. S. Stepanyuk, P. Bruno, and K. Kern. Surface states of cobalt nanoislands on cu(111). *Phys. Rev. Lett.*, 90:236801, 2003.

[24] O. Pietzsch, A. Kubetzka, M. Bode, and R. Wiesendanger. Spin-polarized scanning tunneling spectroscopy of nanoscale cobalt islands on cu(111). *Phys. Rev. Lett.*, 92:057202, 2004.

[25] N. N. Negulyaev, V. S. Stepanyuk, P. Bruno, L. Diekhöner, P. Wahl, and K. Kern. Bilayer growth of nanoscale co islands on cu(111). *Phys. Rev. B*, 77(12):125437, 2008.

[26] I. Horcas, R. Fernández, J. M. Gómez-Rodríguez, J. Colchero, J. Gómez-Herrero, and A. M. Baro. Wsxm: A software for scanning probe microscopy and a tool for nanotechnology. *Review of Scientific Instruments*,

78(1):013705, 2007.

[27] W. E. McMahon, E. S. Hirschorn, and T. C. Chiang. Scanning tunneling microscopy study of a ag monolayer on cu(111). *Surface Science*, 279(3):L231–L235, 1992.

[28] Gert Ehrlich and F. G. Hudda. Atomic view of surface self-diffusion: Tungsten on tungsten. *The Journal of Chemical Physics*, 44(3):1039–1049, 1966.

[29] Richard L. Schwoebel. Step motion on crystal surfaces. ii. *Journal of Applied Physics*, 40(2):614–618, 1969.

[30] L. Diekhöner *et al. unpublished*, 2009.

[31] E. Bauer. Multiple scattering versus superstructures in low energy electron diffraction. *Surface Science*, 7:351 – 364, 1967.

[32] K. A. R. Mitchell, D. P. Woodruff, and G. W. Vernon. A test of energy averaging in leed: The coincidence lattice structure formed by ag on cu(111). *Surface Science*, 46(2):418 – 426, 1974.

[33] Bernard Aufray, Mats Göthelid, Jean-Marc Gay, Christine Mottet, Erik Landemark, Gerald Falkenberg, Lars Lottermoser, Lorenz Seehofer, and Robert L. Johnson. An incommensurate reconstruction studied with scanning tunnelling microscopy and surface x-ray diffraction. *Microsc. Microanal. Microstruct.*, 8:167–174, 1997.

[34] A. Bendounan, H. Cercellier, Y. Fagot-Revurat, B. Kierren, V. Yu Yurov, and D. Malterre. Modification of shockley states induced by surface reconstruction in epitaxial ag films on cu(111). *Phys. Rev. B*, 67:165412, 2003.

[35] J. H. Larsen, and I. Chorkendorff. Increased dissociation probability of CH4 on Co/Cu(111). *Surface Science*, 405:62, 1998.

[36] L. Vitos, A. V. Ruban, H. L. Skriver and J. Kollár. The surface energies of metals. *Surface Science*, 411:186, 1998.

[37] J. Bork, P. Wahl, L. Diekhöner, and K. Kern. Potential energy landscape of metallic Moiré patterns. *New Journal of Physics*, 11:113051, 2009.

[38] Although the absolute errorbars in Figure 4a and b are comparable, the relative errors are larger for low Ag coverage. This explains the large errorbars seen at low coverage of the ratio between Y_{AgCo} and Y_{AgCu} in Figure 4c

[39] The geometry of the step in general influences diffusion barriers[25] and the island shape may therefore play a role in the interlayer mass transport. It was therefore necessary to use relatively large bin sizes to achieve reasonable statistics and could explain why the capping fraction vs. island size in Figure 2c is so broad compared to the more step like distribution seen e.g. in Ref[5], where the islands varied in size but where much more uniformly shaped. We note that the size distribution of the Co islands ranges from 3-25 nm in width showing a smooth and broad distribution, peaking at ca 10 nm width.

Study of the Pt/Ru(0001) Interface

B

P. J. Godowski, Z. S. Li, J. Bork, and J. Onsgaard.
"Study of the Pt/Ru(0001) Interface", Surface Review and Letters, Vol. **14**, No. **5**
911914 (2007).

Surface Review and Letters, Vol. 14, No. 5 (2007) 911–914

STUDY OF THE Pt/Ru(0001) INTERFACE

P. J. GODOWSKI
Institute of Experimental Physics, University of Wrocław,
Pl. Maxa Borna 9, 50-204 Wrocław, Poland
pjg@ifd.uni.wroc.pl

Z. S. LI
Institute of Storage Ring Facilities, University of Aarhus,
DK-8000 Aarhus, Denmark

J. BORK and J. ONSGAARD
Department of Physics and Nanotechnology, Aalborg University,
DK-9220 Aalborg East, Denmark

Received 17 March 2007

The growth process of platinum on Ru(0001) near room temperature was characterized using photoelectron spectroscopy of high resolution. The binding energy position and intensity of the Pt $4f_{7/2}$ and Ru $3d_{5/2}$ core levels as well as the shape and structure of the valence band spectra corresponding to the different stages of the deposition were analyzed. Up to ca. two adsorbate monolayers, the intensity changes of the peaks indicated layer-by-layer growth mode. The surface core level shifts of Ru and Pt levels were evaluated as −0.33 and −0.476 eV, respectively. The valence band spectra show a rather weak interaction between the d-bands of Pt and Ru.

Keywords: Platinum; ruthenium; photoelectron spectroscopy; surface core level shift; surface structure.

1. Introduction

The study of Pt and Pt-containing bi-metallic systems is important in areas of catalysis and electrochemistry.[1–3] Particularly, the Pt/Ru(0001) interface can serve as a model system because of its considerable catalytic activity for the methanol oxidation reaction.[4] The element–element distance within Pt and Ru is 277.5 and 270.59 pm, respectively,[5] which gives the misfit, calculated relatively to the substrate, of $m = 2.6\%$ for the Pt/Ru interface. In consequence, Pt deposition on Ru(0001) near room temperature (RT) produces two-dimensional (2D) islands with a characteristic, relaxed dendritic shape. As it was shown by STM, for the 0.42 adsorbate monolayer, AML, the islands are homogeneously distributed over the terraces with an island density of $2.0 \times 10^{15}\,\mathrm{m}^{-2}$. Subsequent annealing to 800 K causes these islands to collapse, resulting in large, compact platinum islands with no Pt/Ru intermixing. The surface Pt–Ru alloy formation was detected on the high-resolution STM images (with chemical contrast) of the interface after annealing at 1250 K.[4] More recent STM investigations showed that at 600 K platinum grows pseudomorphically on Ru(0001) up to 4 AML and then gradually releases strain by forming large scale dislocation networks.[6] Similarly, for the $m = 2.6\%$ a semi-empirical theory[7] predicts that deposition up to over four monolayers near RT leads to layer-by-layer growth mode.

In this paper the growth of thin platinum layers on Ru(0001) was thoroughly re-examined with the help of high resolution photoelectron spectroscopy based on the use of synchrotron radiation. The layers were characterized by the parameters characteristic of the deposit and substrate core level peaks as well as the valence band spectra.

2. Experimental

The measurements were carried out on the beamline SGM1 at the ASTRID storage ring, ISA, Aarhus, Denmark. Full details of the experiment are described elsewhere.[8–10] Platinum was evaporated from a rod with a diameter of 1 mm and the evaporation rate was 8.0×10^{-2} AML/min. All binding energies (BE's) obtained in the photoemission experiment are expressed relative to the Fermi level. The spectra were fitted using a Doniach–Šunjić approximation of a peak shape with the parameters: Gaussian width, GW, of $0.32 - 0.38$ eV, Lorenzian width, LW, of $0.40 - 0.50$ eV and singularity index, α, (where it is not indicated) of 0.120 for the Pt $4f_{7/2}$ level. The parameters of the Ru $3d_{5/2}$ feature were as follows: GW $= 0.30$ eV, LW $= 0.22 - 0.26$ eV, and $\alpha = 0.050 - 0.060$. The accuracy of the BE determination was established as ± 0.018 eV.[8–10]

3. Results and Discussion

The Pt $4f_{7/2}$ and Ru $3d_{3/2}$ core-level spectra obtained during deposition are collected in Fig. 1. A typical fitting procedure used in the analysis is presented in the bottom.

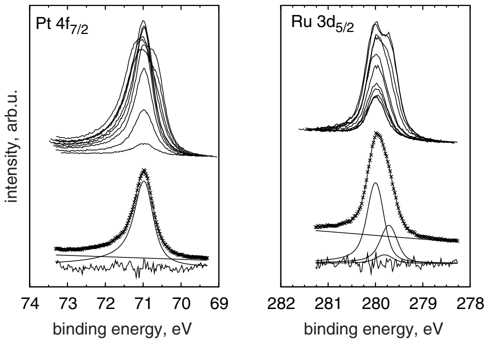

Fig. 1. Collection of the Pt $4f_{7/2}$ and Ru $3d_{5/2}$ spectra (top part) obtained during platinum deposition on the Ru(0001) substrate at 350 K. Examples of fitting procedure of peaks (0.56 AML, bottom part) with residuals magnified 5 times for clarity.

The intensities of the Pt $4f_{7/2}$ (circles) and Ru $3d_{5/2}$ (crosses) peaks as a function of deposition time are plotted in Fig. 2. Straight lines, approximated to the appropriate set of data, show breaks around 12.5 min. At that time, the platinum coverage corresponding to 1 AML is expected.

At the beginning of the deposition the Pt $4f_{7/2}$ region consists of a single feature which represents the interface $\mathrm{Pt}^{\mathrm{V}}_{\mathrm{Ru}}$ peak (Fig. 3). For coverages greater than one monolayer the spectrum consists of two contributions: the interface, now $\mathrm{Pt}^{\mathrm{Pt}}_{\mathrm{Ru}}$, and the simple surface peak, $\mathrm{Pt}^{\mathrm{V}}_{\mathrm{Pt}}$. For small coverages, the BE energy of the interface $\mathrm{Pt}^{\mathrm{V}}_{\mathrm{Ru}}$ peak remains

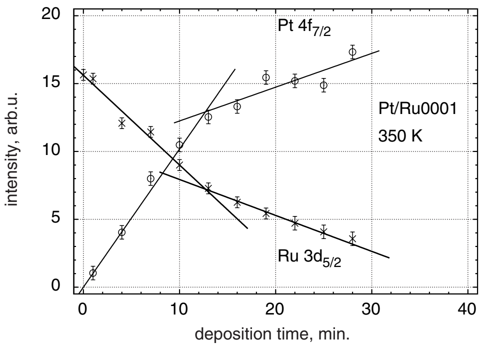

Fig. 2. Intensities of the Pt $4f_{7/2}$ and Ru $3d_{5/2}$ peaks as a function of deposition time. The break point, corresponding to the completion of the first monolayer, appears at $12\frac{1}{2}$ min.

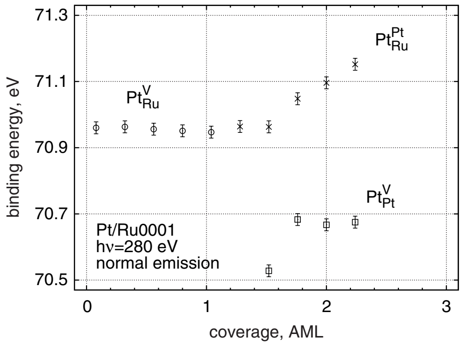

Fig. 3. Binding energy positions of the Pt $4f_{7/2}$ components as a function of platinum coverage.

at the same level (a small shift toward lower value is negligible). After the first layer becomes complete, the BE of the $\mathrm{Pt}^{\mathrm{Pt}}_{\mathrm{Ru}}$ increases. At the same time, the BE of the surface peak, $\mathrm{Pt}^{\mathrm{V}}_{\mathrm{Pt}}$, shows a jump to a certain value and then it is constant. Although "the jump" lies outside the uncertainty level, the analytical difficulties of the peak parameters determination of that point are quite large so that coverage and the first point could be excluded from further treatment.

For coverages less than 1 AML the α (not presented here) is close to zero, then increases up to $\alpha = 0.120$. The singularity index of the surface contribution at coverages greater than 1 AML was found as very small (around 0.030) through the rest of deposition. Such a dependence could be expected for disordered systems of atoms.

The BE's of the $\mathrm{Pt}^{\mathrm{V}}_{\mathrm{Ru}}$, $\mathrm{Pt}^{\mathrm{V}}_{\mathrm{Pt}}$ and $\mathrm{Pt}^{\mathrm{Pt}}_{\mathrm{Ru}}$ were determined equal to 70.955, 70.675, and 71.151 eV, respectively. The values indicate a surface core level shift (SCLS) of negative sign which could be evaluated as ≥ -0.476 eV. It is a consequence of narrowing of the valence bandwidth of platinum surface atoms which in turn leads to the increase of the density of states where the band center is higher than bulk.

Results of the analysis of BE of the Ru $3d_{5/2}$ feature are presented in Fig. 4. We performed deconvolution into two components, remembering that the third one, i.e., the second surface peak, lies at a BE slightly higher that the bulk one.[10] The bulk contribution, $\mathrm{Ru}^{\mathrm{Ru}}_{\mathrm{Ru}}$, seems to be constant during platinum depositon. The negligible variations in the BE of the interface, $\mathrm{Ru}^{\mathrm{Pt}}_{\mathrm{Ru}}$, are inside the range of experimental error. The only (simple) surface peak, $\mathrm{Ru}^{\mathrm{V}}_{\mathrm{Ru}}$ shows a small shift toward higher BE with coverage.

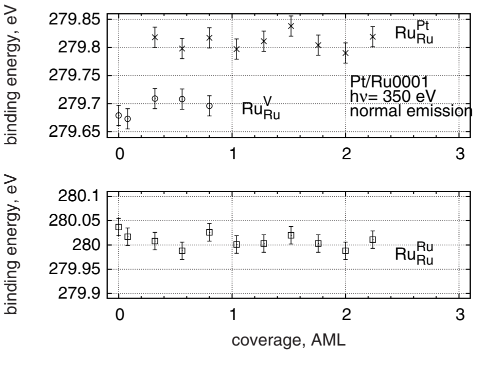

Fig. 4. Binding energy positions of the Ru $3d_{5/2}$ components as a function of platinum coverage.

The BE of the bulk $\mathrm{Ru}^{\mathrm{Ru}}_{\mathrm{Ru}}$ peak was determined as equal to 280.009 eV and the negative SCLS changes from -0.333 to -0.300 eV for this case. The BE of the interface peak is equal to 279.810 eV, i.e., it is shifted by -0.199 eV from the main bulk contribution.

Figure 5 shows selected valence band (VB) spectra obtained during deposition of platinum on Ru(0001) at 350 K. The VB of the clean substrate consists of several features: a steep increase in the BE range of 0.00–0.24 eV, the main broadband with a maximum at 2.35 eV, a feature at 5.75 eV, and a small structure at 7.70 eV. Deposition of Pt (at coverages less than 1 AML) gives rise to a small feature at 0.85 eV, a relatively big and sharp peak near 4.00 eV accompanied by a smaller structure near 6.55 eV shifting toward 6.30 eV with coverage. Larger amounts of Pt give rise to an increase of density of states at 0.85 eV followed by a reduction as observed in the difference spectra. For the highest investigated coverages a peak appears close to the Fermi level at 0.37 eV. At higher BE's large features are observed at 4.30 and 6.70 eV. Neglecting attenuation of the substrate signal, the difference spectra could be treated as the Pt valence bands. At a coverage of 0.32 AML the step function characteristic for the metallic Fermi level is not found, whereas it is noticeable at higher coverages. Therefore, the spectrum

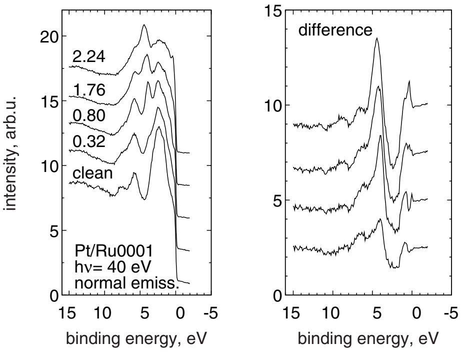

Fig. 5. Selected valence band (left) and difference ("overlayer" minus "clean") spectra (right) of the Pt/Ru(0001) interface obtained at 350 K. The parameter of the curve is the platinum coverage.

resembles atomic-like Pt 5d states. With increasing coverage, the valence band features develop into the ones corresponding to a bulk Pt sample.[11,12] The VB obtained here could be thought of as the sum of separate ruthenium and platinum contributions.

In summary, the growth of a subnanometer thick platinum film on Ru(0001) has been characterized by means of photoelectron spectroscopy as a layer-by-layer growth. Considerable surface core level shifts, of the order −300 meV, have been measured. The changes in the valence band energy distribution curves indicate a weak interaction between the d-bands of Pt and Ru.

Acknowledgments

This work was supported by the European Community — Research Infrastructure Action under the FP6 Structuring the European Research Area programme (through the Integrated Infrastructure Initiative Activity on Synchrotron and Free Electron Laser Science, contract number RII3-CT-2004-506008). Two of us (JB and JO) want to acknowledge the support from The Danish National Scientific Research Council and NordForsk.

References

1. S. R. Brankovic, J. McBreen and R. R. Adžić, *J. Electroanal. Chem.* **503** (2001) 99.
2. M. S. Zei, T. Lei and G. Ertl, *Z. Phys. Chem.* **217** (2003) 447.
3. K. W. Park and Y. E. Sung, *J. Phys. Chem. B* **109** (2005) 13585.
4. F. Buatier de Mongeot, M. Scherer, B. Gleich, E. Kopatzki and R. J. Behm, *Surf. Sci.* **411** (1998) 249.
5. http://www. webelements. com/.
6. A. Schlapka, M. Lischka, A. Groß, U. Käsberger and P. Jakob, *Phys. Rev. Lett.* **91** (2003) 016101.
7. I. Daruka and A.-L. Barabási, *Phys. Rev. Lett.* **79** (1997) 3708.
8. T. H. Andersen, L. Bech, Z. S. Li, S. V. Hoffmann and J. Onsgaard, *Surf. Sci.* **559** (2004) 111.
9. P. J. Godowski, J. Onsgaard, M. Trzebiatowska-Gusowska, K. Pater and Z. S. Li, *Phys. Rev. B* **73** (2006) 193403.
10. P. J. Godowski, J. Onsgaard, M. Trzebiatowska-Gusowska, K. Pater and Z. S. Li, *Acta Phys. Pol. A*, **111** (2007) 263.
11. K. A. Mills, R. F. Davis, S. D. Kevan, G. Thornton and D. A. Shirley, *Phys. Rev. B* **22** (1980) 581.
12. V. Murgai, S. Raaen, M. Strongin and R. F. Garrett, *Phys. Rev. B* **33** (1986) 4345.

Electronic structure and ordering of multilayers of Co and Ag on Cu(111) investigated by photoelectron spectroscopy

C

J. Bork, L. Diekhöner, Z. Li, and J. Onsgaard.
"Electronic structure and ordering of multilayers of Co and Ag on Cu(111) investigated by photoelectron spectroscopy", Submitted (2010).

Electronic structure and ordering of multilayers of Co and Ag on Cu(111) investigated by photoelectron spectroscopy

J. Bork[a], *L.Diekhöner*[a], *Z. Li*[b], *and J. Onsgaard*[a]
[a]Department of Physics and Nanotechnology, and Interdisciplinary Nanoscience Center (iNANO), Aalborg University, DK-9220 Aalborg, Denmark
[b]Institute of Storage Ring Facilities, University of Aarhus, DK-8000 Aarhus C, Denmark

Abstract

The growth and the electronic structure of multilayers of Co and Ag on Cu(111) at room temperature has been studied with photoelectron spectroscopy and low-energy electron diffraction (LEED). The coverage range spans from Co and Ag layers between one monolayer (ML) to stacking of several monolayers. Surface states and ordered structures have been identified at room temperature. A Ag-related surface state with a binding energy of 0.20 eV is identified in normal emission in the ultraviolet photoelectron spectra when silver constitutes the top layer. Core level binding energy shifts of Ag $3d_{5/2}$ reflect the changing surroundings of Ag. Hexagonal diffraction patterns are observed for sandwiches of consecutive layers of Co and Ag up to 5 layers. Since no interlayer diffusion is observed in the layer-by-layer formation of the films, multilayers of consecutive silver and cobalt on Cu(111) offer preparation of sandwiched magnetic–non-magnetic structures.

Key words: *Multilayers, surface state, photoelectron spectroscopy, LEED, Cu(111), Ag, Co.*

1. Introduction

Multilayers of ultrathin metallic films grown on top of a metallic substrate can exhibit new physical and chemical properties compared to those characteristic of the bulk. Surface relaxation, superstructures, induced strain and the reduced dimensionality are among the phenomena that influence the electronic structure of the multilayer films and the interfaces. Catalysis and magnetism are currently active research fields where newfound effects can be beneficial for processes and devices [1-2].

Ultrathin films made of alternating layers of magnetic and nonmagnetic metals can exhibit oscillatory magnetic coupling and the giant-magnetoresistance effect. Variation of the magnetic properties of ultrathin films of Co on metal substrates and the effect of introducing a cap of a noble metal has been much studied. Araki *et al.* [3] reported on a large and oscillating magnetoresistance in evaporated Ag/Co multilayers and Loloee *et al.* confirmed these observations [4]. Kohlhepp *et al.* observed that whereas the free Co(0001) surface supports in-plane magnetization, capping with Ag supports perpendicular magnetization with a maximum in the magnitude of magnetic surface anisotropy for 1 mono layer (ML) Ag [5]. It was found by Chen *et al.* that 1 ML of Ag deposited on a Co(5ML)/Pt surface causes a reorientation of the easy axis of the magnetization from the in-plane to the out-of-plane direction [6]. Tsay *et al*. studied the variation of the magnetic properties of Co/Cu(111) films upon Ag deposition up to a few ML and observed a Ag overlayer-induced oscillation of the coercive force as the thickness of the Ag overlayer increases [7]. Noble metal capping effects on the spin-reorientation transitions of Co/Ru(0001) were studied by El Gabaly *et al.*, who found that the noble metal capping results in spin reorientation transitions that depend on the atomic layer thickness of the capping layer [8].

Accordingly, there is a need for a detailed understanding of the geometrical and the electronic structures of multilayer films consisting of a magnetic metal and a noble metal capping, from the submonolayer coverage to thicknesses of the order of a few nanometers.

There is a substantial amount of literature on the electronic and morphological structures of ultrathin

Co layers on Cu(111). The reports on the electronic structure include photoemission, angle resolved ultraviolet photoemission spectroscopy [9-10] and inverse photoemission measurements [11]. Quantitative low energy electron diffraction (LEED), photoelectron diffraction and Fermi surface mapping of Co/Cu(111) [12-14]. Scanning tunneling spectroscopy (STS) was used for the study of the electronic structure around the Fermi level [15-16].

The room-temperature growth of Co on Cu(111) in the low-coverage regime, $\theta < 2$ ML, is characterized by the formation of islands of triangular shape and bilayer height above the Cu(111) surface[17-18]. With increasing coverage, single layers of Co grow on top of the Co islands and 3-dimensional growth is observed [17]. The ultrathin Co film is dominated by continuation of the fcc stacking dictated by the copper [19]. A 5 ML thick Co film exhibits a hexagonally close-packed structure [20].

Recently the initial stages of the room-temperature growth of Ag on bilayer high Co nanoislands on Cu(111) have been studied by scanning tunneling microscopy (STM) [21]. It was found that there is a preferred nucleation for Ag on top of Co compared to Cu(111) terrace sites, particularly at low Ag doses. Furthermore, it was observed that the Co islands are either completely free of Ag or completely capped with Ag. The Ag adlayer formed a 9x9 reconstruction due to the lattice mismatch [21]. In a recent STS-study, it was shown how the deposition of Ag on Co/Cu(111) modulates the electronic landscape around the Fermi level of the heterostructured interface. By spectroscopic mapping of the local density of states it was observed that a modulation of the energy position, width and intensity of the Co d-state is correlated with the morphology of the silver Moiré pattern [22].

The purpose of the present report is to characterize the electronic structure of multilayers, consisting of the magnetic element, Co, and the noble metal, Ag, on the Cu(111) surface in the coverage range of 1 ML to 6 ML. It is found that the successive build up of the layers at room temperature takes place without interlayer diffusion. LEED shows ordering and a Ag associated surface state is identified when Ag forms the topmost layer. The experimental evidence is based on photoelectron spectroscopy in the form of core-level spectroscopy (CLS) and energy distribution curves (EDCs) of the valence electrons.

2. Experimental

The experiments were performed in an ultrahigh-vacuum (UHV) chamber, with a base pressure < 4×10^{-8} Pa, attached to the SGM1/Scienta beamline at the storage ring ASTRID at Aarhus University. The beamline consists of a spherical grating monochromator and the end-station is equipped with a hemispherical Scienta SES-200 electron energy analyzer and a channelplate as a detector. The photon beam incidence angle was 40^o relative to the sample normal and the spectra were collected with the electron emission parallel to the normal of the surface. Concerning the EDCs of the valence band (VB) electrons and the Ag $3d_{5/2}$ core electrons, the total instrumental resolution was better than 100 meV and 300 meV, respectively. VB EDCs were recorded either in a small-angle mode with an analyzer acceptance angle of $\pm 1^o$ or in an integral mode with an acceptance angle of $\pm 9^o$. Further, X-ray photoelectron spectroscopy (XPS) could be performed via a Mg-K_α X-ray source in connection with the analyzer. A LEED facility allows detection of ordered overlayer structures. Cleaning of the Cu sample was carried out by repeated cycles of Ar^+ sputtering followed by annealing at 500^oC. Overlayers of Ag were prepared by evaporation from an electron bombarded crucible and Co was evaporated by electron bombardment from a high-purity Co wire; the Cu(111) sample was kept at room temperature. The Co flux was 0.22 ML/min and the deposition rate of Ag was 0.24 ML/min. Calibrations of the sources were carried out using the photoemission intensities versus dose curves and an oscillating quartz crystal thickness monitor. The photoemission spectra were recorded at room temperature. STM experiments have been performed in a different UHV-system as described in [21]. We note that the same metal-evaporator was used in both systems making it easier to compare and calibrate doses.

In the following the compositions of the multilayers on the Cu(111) substrate are written as Ag(m)/Co(n)/Cu(111) where m and n indicate the number of Ag and Co monolayers, respectively, deposited on the Cu(111) surface, here with Co as the first deposit material. The term monolayer is used as the atomic amount deposited. Analysis and fitting of the core level spectra of Cu 2p$_{3/2}$, Co 2p$_{3/2}$ and Ag 3d$_{5/2}$ were based on a Doniach-Sunjic line shape [23] convoluted with a Gaussian distribution function using the program FitXPS [24].

3. Results and discussion

Growth curves

Co was evaporated on Cu(111) at room temperature and the growth was followed using CLS of Cu 2p$_{3/2}$ and Co 2p$_{3/2}$. The growth curves shown in Fig. 1 exhibit linear segments, where the Cu 2p$_{3/2}$ curve has a knee-point at 2.7 ML Co and the Co 2p$_{3/2}$ curve has a less pronounced cutting point at 2.4 ML Co. Thus, keeping the island growth of Co in mind, the break points on the growth curves, corresponds to an almost fully covered Cu(111) surface. This is corroborated by STM images (Fig. 1), which have been recorded in a different UHV-system using the same doses of Co. It was found that the STM image with a cobalt coverage of θ_{Co} = 2.2 ML corresponds to a 15% free copper substrate. From the intensity decay curve of Cu 2p$_{3/2}$ a reduction in intensity to 53% of the intensity of the uncovered surface is read at this Co coverage. This number can be compared with the intensity reduction estimated in a simplistic attenuation model where the measured Cu 2p intensity is a sum of the contribution from the free Cu surface (15%) and the contribution from the Co covered part. According to the STM results (Fig. 1) the Co covered part of the surface is characterized by mostly bilayer (3.9 Å high) islands as well as some in the third layer. The attenuation of the Cu 2p intensity by passage of the 2.2 ML Co is determined by the electron mean free path in the Co layers, which is λ_{Co} = 3.0 ML for electrons with a kinetic energy of 320 eV as is the case for 2p-electrons emitted from the copper substrate [25]. This results in a Cu 2p$_{3/2}$ intensity reduction of 55% in good agreement with the attenuation in intensity found above.

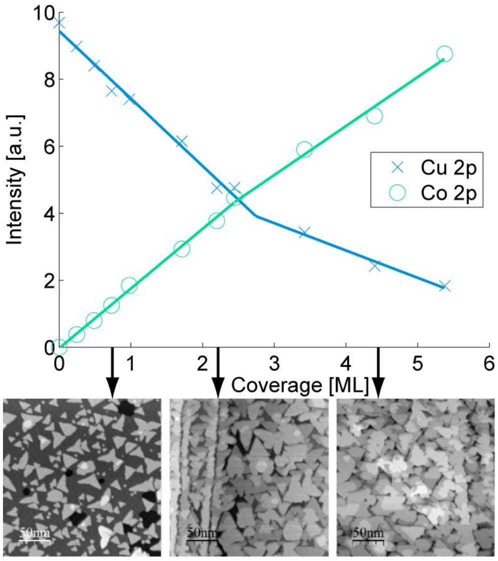

Figure 1 The evolution of the Co 2p$_{3/2}$ and Cu 2p$_{3/2}$ intensities as a function of deposited Cobalt. In order to correlate photoelectron data and STM results for the same system three STM inserts, recorded for coverages of 1.1, 2.2 and 4.4 ML Co, show the evolution of the triangular Co islands distributed on the Cu(111) terraces. Note that initially the visible coverage of the Cu(111) surface with bilayer islands of Co is half the deposited amount.

*Ag 3d$_{5/2}$ core-level spectra for Ag/Co/Cu(111***)**

Next Ag is evaporated on a Co pre-covered Cu(111) sample at room temperature and Ag 3d$_{5/2}$ EDCs are measured. The Co coverage was kept constant at 0.66 ML whereas the Ag coverage ranged from 0.75 ML to 2.0 ML. The spectra (Ag 3d$_{5/2}$) are shown in Fig. 2. It is observed that the Ag 3d$_{5/2}$ peaks have more than one component reflecting that different surroundings of the silver atoms result in a chemical shift. A decomposition of the peak for θ_{Ag} = 0.75 ML results in a low-binding energy component, $E_{\mathrm{B,L}}$ at 367.70 eV and a high-binding energy component, $E_{\mathrm{B,H}}$ at 368.03 eV. For comparison a Ag(0.7ML)/Cu(111) interface, without Co, with silver was prepared at room temperature. The Ag 3d$_{5/2}$ curve is displayed as the lower curve in Fig. 2, showing an E_{B} = 367.87 eV. This finding supports an interpretation of silver mostly occupying the top of the Co islands [21].

For the Ag/Cu(111) interface an increasing E_{B} for Ag 3d$_{5/2}$ with increasing silver coverage was observed corresponding to +270 meV for the 3.3 ML thick silver film. The present determined binding energy E_{B} = 368.15 eV for the 3.3 ML thick Ag film coincides with the Ag bulk E_{B} = 368.19 eV determined by Citrin et al. [26] and it is close to the E_{B} = 368.00 eV for a 20 ML Ag film

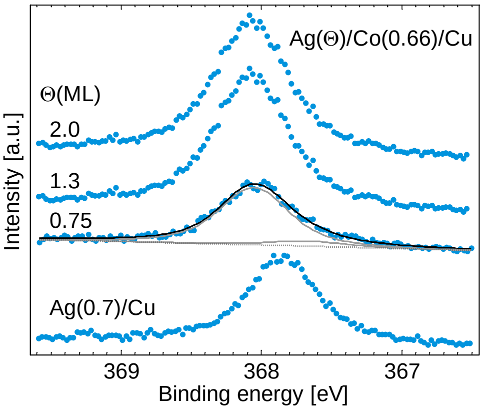

Figure 2 The bottom curve shows a Ag 3d$_{5/2}$ core-level spectrum for 0.7 ML of Ag deposited on a Cu(111) surface at room temperature. The next three curves display Ag 3d$_{5/2}$ spectra for 0.75 ML, 1.3 ML and 2.0 ML of Ag deposited on a Co(0.66 ML)/Cu(111) interface at room temperature. A decomposition of the spectrum for 0.75 ML Ag is included.

deposited on Ru(0001) measured by Rodriguez [27]. In ref. [28] it was reported that the surface core-level shift in Ag(111) is below 100 meV.

Deposition of different amounts of Ag on a Co(2.2ML)/Cu(111) surface at room temperature result in the Ag 3d$_{5/2}$ spectra shown in Fig. 3. A fitting procedure based on a single peak approach gives rise to a Lorentzian line-width around 0.36 eV and a Gaussian line-width around 0.39 eV. It is seen, taking the uncertainty in the energy determination into consideration, that E_B is constant, 368.05 eV. This observation is on line with the STM findings in ref. [21] where the silver caps the bilayer high cobalt islands. Another observation from the present results is the constancy of E_B for Ag 3d$_{5/2}$ with θ_{Ag} above 1 ML.

Valence band energy distribution curves, integral and small-angle measurements

Valence band EDCs for multilayer films recorded in the integral mode, shown in Figs.4 - 5, clearly illustrate that the VB energy range is divided in intervals representing Co, Cu and Ag, as read from the Fermi edge. All overlayers were formed at room temperature and the VB spectra were recorded for incoming photon energy of 40 eV. At this photon energy the cross sections for the 3d electrons of Co and Cu, and the 4d electrons of Ag are 8.7, 9.9 and 38 Mbarn, respectively [29].

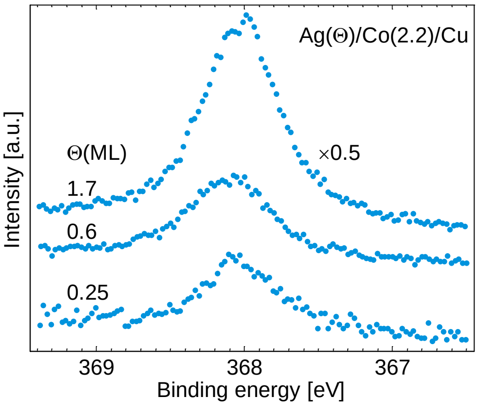

Figure 3 Ag 3d$_{5/2}$ core-level spectra for different coverages of Ag on a Co(2.2ML)/Cu(111) interface. From bottom and upwards the Ag coverages are 0.25 ML, 0.6 ML and 1.7 ML.

Deposition of 2.2 ML Co on the Cu(111) substrate gives rise to the EDC shown in Fig. 4a as the upper curve (i). A 2 eV broad structure with a maximum E_B of 0.50 eV occurs near the Fermi level well separated from the Cu 3d main structure. Alkemper *et al.* observed maximum intensity at E_B = 0.7 eV for 1.7 ML Co on Cu(111) in normal emission and hυ = 25 eV [10]. Addition of 1.7 ML Ag changes the density of states (DOS) in the low-binding energy range with a shift of the maximum towards lower E_B, curve (ii). The changes are observable in the difference curve, (ii)-(i), where a small structure at the Fermi level indicates a Ag induced surface or interface state. The negative excursions in the E_B -ranges, 0.2 – 1.5 eV, and 2 - 3 eV, reflect the damping influence of the Ag layers on the photoelectron intensity from the underlying Co and Cu layers.

The effects of adding a 2.2 ML thick Co layer on top of a Ag(1.8ML)/Co(2.2ML)/Cu(111) interface are demonstrated in Fig. 4b, where we show valence band curves for Ag(1.8ML)/Co(2.2ML)/Cu(111) and Co(2.2)/Ag(1.8ML)/Co(2.2ML)/Cu(111) together with the difference curve. Co 3d constitutes the VB in the E_B -range 0-2 eV, and the surface state due to Ag is removed when Co constitutes the top layer. For E_B's higher than 2 eV the difference spectrum is negative reflecting the attenuation of photoelectrons originating from the Ag and Cu subsurface layers.

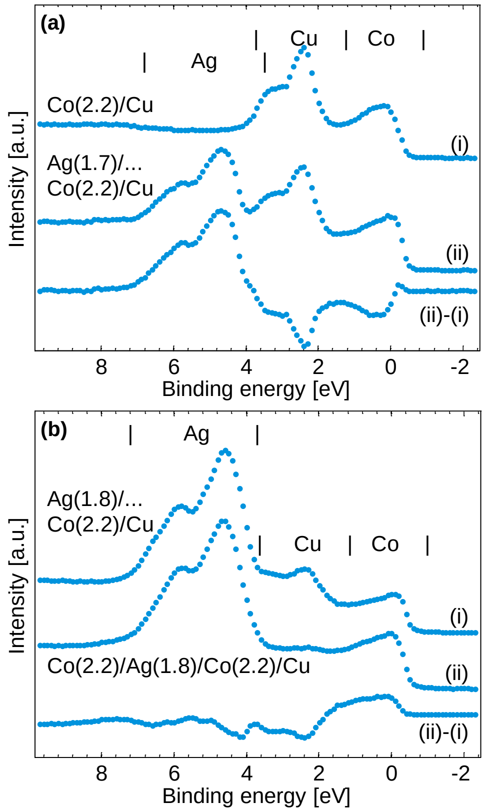

Figure 4 (a) Valence band spectra obtained with photons of energy 40 eV. The upper spectrum, (i), represents an interface with 2.2 ML Co deposited on Cu(111) at room temperature. Next spectrum, (ii), displays the VB spectrum after deposition of 1.8 MLs of Ag at room temperature and the lowest curve shows the difference spectrum, (ii) – (i). (b) Valence band spectra demonstrating the effect of adding 2.2 ML Co to a sandwich consisting of Ag(1.8)/Co(2.2)/Cu(111). Co 3d becomes the dominant component in the structure near the Fermi level and the maximum intensity is observed at a 100 meV higher E_B.

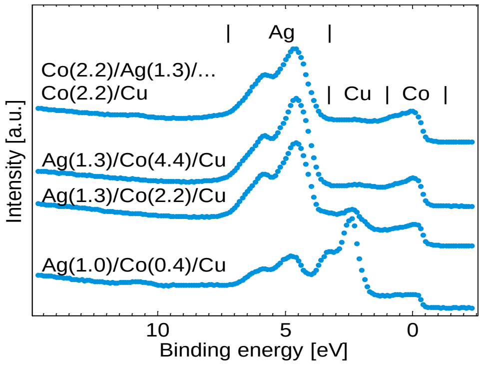

Figure 5 Valence band PES spectra of multilayers of Ag and Co, deposited on Cu(111) at room temperature, obtained with a photon energy of 40 eV. From below, the spectrum is recorded from a Cu(111) surface after deposition of 0.33 ML Co and further deposition of 1.0 ML Ag. The next two spectra are recorded for 2.2 and 4.4 ML of Co covered with 1.3 ML of Ag. A VB spectrum of a 5 ML sandwich of changing Co and Ag is displayed as the upper curve.

In Fig. 5 we present valence band spectra of a sample prepared with varying Co coverages and constant Ag coverage. The three upper EDCs in Fig. 5 are dominated by Ag, and the Cu(111) substrate is hardly recognizable in the two upper spectra where 5 overlayers are present. In the case of a submonolayer coverage of Co, the lowest curve in Fig.5, the EDC exhibits pronounced contributions from Ag and the Cu substrate. Thus, the attenuation of the Cu 4d spectrum, and further, the relative intensities of Co and Ag demonstrate that interlayer mixing does not take place in any significant way. Again, the evolution of the EDC close to the Fermi level, 0 eV < E_B < 2eV, is informative. For the interface spectrum, shown as the bottom curve, with a low Co coverage, 0.4 ML, the band is flat in contrast to curve two and three from below, where 1.3 ML of Ag is deposited on 2.2 and 4.4 ML of Co, respectively. A maximum in the EDC is observed at an increasing E_B due to the growing influence of Co. For 1.3 ML Ag embedded in 2 ML thick Co layers, the maximum is shifted to a E_B which is 180 meV compared to that characteristic of the Ag(1.3ML)/Co(4.4ML)/Cu(111) interface.

To summarize the integral measurements of the VB EDCs it is deduced that the layers grow as deposited at room temperature and a Ag-related surface state on Ag(1.8)/Co(2.2)/Cu(111) can be assigned.

Small-angle photoemission and LEED

We now reduce the acceptance angle of the detector from ± 9^o to ± 1^o. The normal emission spectra, θ = 0, for the Ag(1.3)/Co(0.4)/Cu(111) surface and the Ag(1.3)/Cu(111) surface are shown in Fig. 6 as the lowest curve and the top curve, respectively. Compared to the Ag(1.3)/Cu(111) spectrum a slightly increased intensity for binding

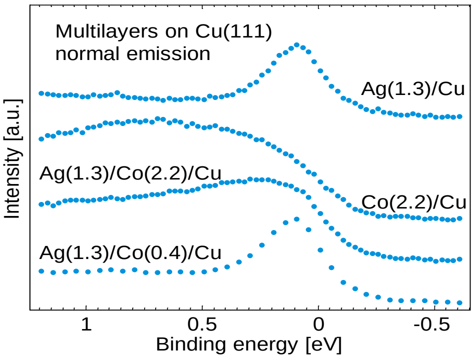

Figure 6 Small-angle photoemission spectra in normal emission for multilayers of Ag and Co on Cu(111). Spectra of one-component overlayers with Ag and Co on the substrate are shown as the two upper curves. EDCs of sandwiches with 1.3 ML Ag as the top-layer and different coverages, 0.4 ML and 2.2 ML, of Co as the intermediate layer are shown as the lowest and next-lower curves, respectively.

energies higher than 0.4 eV is observed in the Ag(1.3)/Co(0.4)/Cu(111) spectrum. This is due to the presence of the bilayer Co islands. Thus, the photoemission spectrum of the last mentioned surface is composed of contributions partly from areas where Cu(111) is covered by Ag and partly from areas where bilayer high Co islands are covered by Ag.

It is instructive to observe the effect of adding 1.3 ML of Ag on the photoemission spectra of a Cu(111) surface covered with 2.2 ML of Co, Fig. 6, where the spectra are recorded in normal emission. The spectrum of the Co(2.2)/Cu(111) surface, second curve from above, is characterized by a broad feature with a maximum at 0.8 eV and a broad shoulder around 0.5 eV. The present Co(2.2)/Cu(111) spectrum shows much resemblance to the angular-resolved EDC of photoelectrons using s-polarized light for the Co(2.2)/Cu(111) interface reported in ref. [9]. As determined from spin-resolved photoemission spectra the Co 3d emission peak positioned close to the Fermi level is a composite of spin-up and spin-down photoelectrons [10]. For a coverage of 2.8 ML Co on Cu(111), a photon energy of 25 eV and normal emission, the spin-up and spin-down emission peak at 0.80 eV and the spin-up electrons exhibit a slow decay at higher binding energies.

The deposition of 1.3 ML of Ag, the third curve from above, causes a strong change of the spectrum with an energy shift towards the Fermi level and a broad peak around a binding energy of 0.30 eV. A difference spectrum (not shown), formed by subtraction of the Co(2.2)/Cu spectrum from the Ag(1.3)/Co(2.2)/Cu spectrum, displays a narrow peak at 0.2 eV binding energy and a broad negative excursion with a minimum at 0.9 eV binding energy. These energy positions confirm that the composite spectrum can be interpreted as a superposition of the Ag component in the uppermost layer and the Co component beneath the surface layer.

A more pronounced surface (or interface) state is observed for a 2 ML thick Ag film on a Co(4.4)/Cu(111) substrate, Fig. 7. Finally, for a double Ag-Co sandwich film, the upper curve in Fig. 7, the peak at 0.20 eV E_B is not present.

It is possible in the ultraviolet photoemission spectra of multilayer samples of Ag and Co on Cu(111) to identify a Ag-related surface state in normal emission provided silver constitutes the top layer. The E_B of the surface state observed at 0.20 eV for the Ag(1.3)/Co(2.2)/Cu(111) sample coincides with that of a 1.3 ML Ag directly deposited on Cu(111) [30].

It was demonstrated by LEED in ref. [21] that 1.3 ML Ag deposited on a Co(2.2)/Cu(111) sample exhibits a 6-spot pattern, where each spot is surrounded by 6 satellites due to the Ag overlayer. A periodicity of approximately (9x9) as in the case of 1.3 ML Ag on Cu(111) was observed.

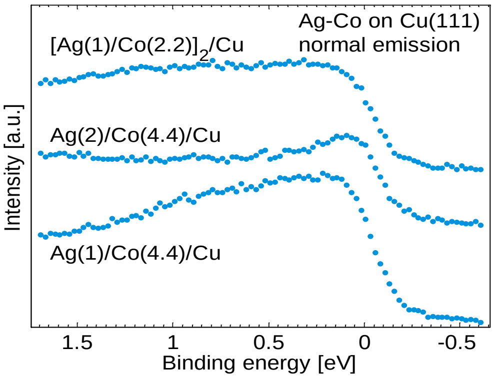

Figure 7 The build-up of the Ag-related surface state on a Co(4.4)/Cu(111) substrate is shown in the lower photoemission spectra recorded in normal emission and with a photon energy of 40 eV. A spectrum of a 6 layers sandwich with alternating Co and Ag layers is displayed as the upper curve.

In Fig. 8 we present a sequence of LEED patterns of Co(2.2)/Cu(111), Ag(1.3)/Co(2.2)/Cu(111), Co(2.2)/Ag(1.3)/Co(2.2)/Cu(111) and Ag(1.3)/Co(2.2)/Ag(1.3)/Co(2.2)/Cu(111). The primary kinetic energy (E_p) of incident electrons was in the range 115-143 eV (see figure caption for details). For 2.2 ML Co on Cu(111) we observe a LEED image (Fig. 8a) with hexagonal structure originating from the Co islands, that grow pseudomorphically on the Cu(111) surface, and from the Cu(111) substrate. Addition of one layer of Ag results in an image (Fig. 8b) that agrees with the pattern measured in ref. [21]. The latter was recorded with a different E_p, 66 eV. A well-ordered sandwich, as judged by LEED, is thus obtainable. Further deposition of 2 ML Co at room temperature, Fig. 8c, gives rise to two concentric and hexagonal patterns with a 9% change in distance from the (00) beam. We assign the inner spots to Cu and the outer spots to Co. Apparently, the topmost Co layer is ordered but exhibits a different lattice constant than the Cu-substrate (compare with Fig. 8a). Finally, repeated deposition of Ag, 1.3 ML (Fig. 8d) leads to an increasing diffusivity, reflecting that no diffraction ordering occurs in the last deposited Ag layer.

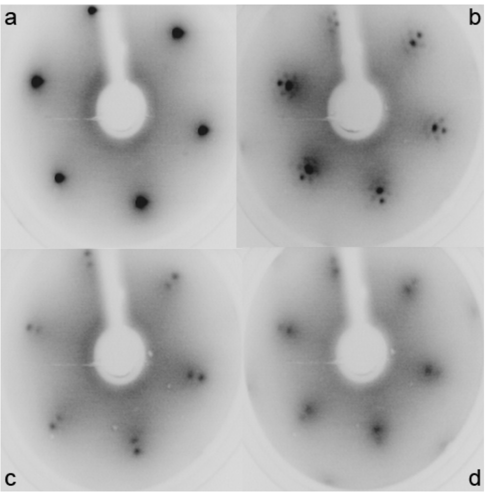

Figure 8 LEED images from a series of multilayers deposited at room temperature on Cu(111). (a) represents Co(2.2)/Cu(111) recorded with E_p = 136 eV; (b) Ag(1.3)/Co(2.2)/Cu(111) with E_p = 115 eV; (c) Co(2.2)/Ag(1.3)/Co(2.2)/Cu(111) with E_p = 121 eV and (d) Ag(1.3)/Co(2.2)/Ag(1.3)/Co(2.2)/Cu(111) with E_p = 143 eV.

4. Conclusions

In conclusion, multilayers of Co and Ag deposited on a Cu(111) substrate at room temperature have been characterized in terms of electronic structure and ordering. In combination with a recent work on the growth and atomic structure of Ag on bilayer Co nanoislands on Cu(111) [21] the following picture emerges. It is possible to prepare sandwiched magnetic-nonmagnetic Co-Ag structures. The E_B of Ag $3d_{5/2}$ is sensitive to the surroundings of the Ag causing a core-level shift between Ag positioned on top of Co and Ag covering free Cu sites. Valence band energy distribution curves for consequtive layers of Co and Ag show layer by layer growth and exhibit a Ag associated surface state when Ag is the last deposited component. The binding energy of the surface state is 0.20 eV for the Ag(1.3)/Co(0.4)/Cu(111), the Ag(1.3)/Co(2.2)/Cu(111) and the Ag(2.2)/Co(4.4)/Cu(111) sandwiches. Concerning ordering, it is demonstrated by LEED that hexagonal ordering for up to 5 monolayers takes place. The Ag(*m*)/Co(*n*)/Cu(111) multilayer system has a potential for magnetic studies of Co embedded between noble metals even at room temperature.

References

1. G. Ertl, H. Knözinger, F. Schüth, and J. Weitkamp, *Handbook of Heterogeneous Catalysis, 2. ed*. 2008: Wiley.
2. J. Stöhr and H. Siegmann, *Magnetism: From Fundamentals to Nanoscale Dynamics* Springer Series in Solid State Sciences. Vol. 152. 2006, Berlin: Springer.
3. S. Araki, K. Yasui, and Y. Narumiya, J. Phys. Soc. Japan **60** (1991) 2827.
4. R. Loloee, P.A. Schroeder, W.P.P. Jr., J. Bass, and A. Fert, Physica B, **204** (1995) 274.
5. J. Kohlhepp and U. Gradmann, Journal of Magnetism and Magnetic Materials, **139** (1995) 347.
6. F.C. Chen, Y.E. Wu, C.W. Su, and C.S. Shern, Physical Review B, **66** (2002) 184417.
7. J.S. Tsay, J.Y. Lin, C.S. Yang, Y.D. Yao, and Y. Liou, Surface Science, **482-485** (2001) 1040.
8. F.E. Gabaly, K.F. McCarty, A.K. Schmid, J.d.l. Figuera, Mu, M.C. oz, L. Szunyogh, P. Weinberger, and S. Gallego, New Journal of Physics, **10** (2008) 073024.
9. R. Miranda, F. Ynduráin, D. Chandesris, J. Lecante, and Y. Petroff, Phys. Rev. B, **25** (1983) 527-530.
10. U. Alkemper, C. Carbone, E. Vescovo, W. Eberhardt, O. Rader, and W. Gudat, Phys. Rev. B, **50** (1994) 17496-17501.
11. G.J. Mankey, R.F. Willis, and F.J. Himpsel, Phys. Rev. B, **47** (1993) 190-196.
12. K. Heinz, S. Müller, and L. Hammer, J. Phys. Cond. Matt., **11** (1999) 9437-9454.
13. V. Scheuch, K. Potthast, B. Voigtländer, and H.P. Bonzel, Surf. Sci., **318** (1994) 115-128.
14. J. Osterwalder, T. Greber, E. Wetli, J. Wider, and H.J. Neff, Progress in Surface Science, **64** (2000) 65-87.
15. L. Diekhöner, M.A. Schneider, A.N. Baranov, V.S. Stepanyuk, P. Bruno, and K. Kern, Phys. Rev. Lett., **90** (2003) 236801.
16. O. Pietzsch, A. Kubetzka, M. Bode, and R. Wiesendanger, Phys. Rev. Lett., **92** (2004) 057202.
17. J.d.l. Figuera, J.E. Prieto, C. Ocal, and R. Miranda, Phys. Rev. B, **47** (1993) 13043-13046.
18. N.N. Negulyaev, V.S. Stepanyuk, P. Bruno, L. Diekhöner, P. Wahl, and K. Kern, Physical Review B (Condensed Matter and Materials Physics), **77** (2008) 125437.
19. J.d.l. Figuera, J.E. Prieto, G. Kostka, S. Müller, C. Ocal, R. Miranda, and K. Heinz, Surf. Sci., **349** (1996) L139-L145.
20. C. Rath, J.E. Prieto, S. Müller, R. Miranda, and K. Heinz, Phys. Rev. B, **55** (1997) 10791-10799.
21. J. Bork, J. Onsgaard, and L. Diekhöner, J. Phys. Cond. Matt. (and arXiv:0904.4170[cond.-mat]), **accepted** (2009.
22. J. Bork, P. Wahl, L. Diekhöner, and K. Kern, New Journal of Physics, **11** (2009) 113051.
23. S. Doniach and M. Sunjic, J. Phys. C, **3** (1970) 285.
24. D.L. Adams, *FitXPS*: Aarhus University.
25. M.P. Seah and W.A. Dench, Surface and Interface Analysis, **1** (1979) 2.
26. P.H. Citrin, G.K. Wertheim, and Y. Baer, Phys. Rev. B, **27** (1983) 3160.
27. J.A. Rodriguez, Surf. Sci., **296** (1993) 149.
28. J.N. Andersen, D. Hennig, E. Lundgren, M. Methfessel, R. Nyholm, and M. Scheffler, Phys. Rev. B, **50** (1994) 17525.
29. J.J. Yeh and I. Lindau, At. Data Nucl. Data Tables **32** (1985) 1.
30. M. Wessendorf, C. Wiemann, M. Bauer, M. Aeschlimann, M.A. Schneider, H. Brune, and K. Kern, Appl. Phys. A, **78** (2004) 183.

Potential energy landscape of metallic Moiré patterns

D

Jakob Bork, Peter Wahl, Lars Diekhöner, and Klaus Kern.
"Potential energy landscape of metallic Moiré patterns", New Journal of Physics **11** 113051 (2009).

New Journal of Physics
The open-access journal for physics

Potential energy landscape of metallic Moiré patterns

Jakob Bork[1,2,4], **Peter Wahl**[1], **Lars Diekhöner**[2] **and Klaus Kern**[1,3]
[1] Max-Planck-Institut für Festkörperforschung, Heisenbergstrasse 1,
D-70569 Stuttgart, Germany
[2] Institut for Fysik og Nanoteknologi, and Interdisciplinary Nanoscience Center
(iNANO), Aalborg Universitet, Skjernvej 4A, DK-9220 Aalborg, Denmark
[3] Institut de Physique des Nanostructures, Ecole Polytechnique Fédérale de
Lausanne (EPFL), CH-1015 Lausanne, Switzerland
E-mail: ld@nano.aau.dk

New Journal of Physics **11** (2009) 113051 (9pp)
Received 21 August 2009
Published 30 November 2009
Online at http://www.njp.org/
doi:10.1088/1367-2630/11/11/113051

Abstract. The modulation of the electronic structure of cobalt islands on Cu(111) by the Moiré pattern of an Ag overlayer is investigated. Acquisition of tunneling spectroscopy maps reveals a local modification of both the energy and the amplitude of the cobalt-related *d*-states on the length scale of the periodicity of the Moiré superstructure. The modulation of the energy can be rationalized by the spatially varying hybridization of the cobalt atoms with the silver *sp*-bands. We propose that Moiré modulated *d*-states at metal interfaces with a periodicity of a few nanometers may provide a novel route to manipulate the chemical reactivity of surfaces and might serve as a template which modulates magnetic properties such as the spin density.

The ability to precisely control the electronic structure of solids and their surfaces is crucial for the engineering of materials and devices with properties and functionalities tailored to specific needs. A number of strategies have been developed in the past to tune the electronic structure of metal surfaces globally and locally [1], including the growth of pseudomorphic thin films [2] and bimetallic surface alloys [3]. The reactivity of a transition metal surface is strongly dependent on the energetic position, relative to the Fermi level, of the localized *d*-states [4]. Whereas flat metallic films lead to an overall shift of the electronic states [2], alloying creates sites where the reactivity is locally enhanced, e.g. sees molecules preferentially adsorbing at specific sites of the alloy [3]. The latter thus represents a structured surface with an atomically varying local electronic structure across the surface. Many surfaces in nature

---

[4] Author to whom any correspondence should be addressed.

1367-2630/09/113051+09$30.00

show large-scale reconstructions, either in their clean state or during growth. In heteroepitaxial growth this restructuring is driven by strain often inducing complex patterns of ordered surface dislocations or Moiré structures [5, 6]. At these surfaces, bonding and diffusion energies change on a much larger length scale than for individual atomic sites. The periodically patterned surfaces can thus serve as nanotemplates to guide nanostructure formation via predefined nucleation sites or energetic sinks. The directed self-ordering growth strategy has very successfully been used for the fabrication of highly ordered nanostructure arrays [7]–[11]. Surprisingly, the spatial modulation of the electronic structure that inherently must accompany the structural inhomogeneity of the interface has only been studied for non-metallic systems so far [9], [11]–[15]. In this paper, we demonstrate how a silver adlayer, forming a Moiré pattern, modulates the electronic structure of an underlying cobalt layer on the nanometer scale. The local electronic structure is measured using scanning tunneling spectroscopy and the analysis of spectroscopic maps acquired over areas on the order of $10 \times 10\,\mathrm{nm}^2$. A prominent feature from a d-derived surface state is tracked over the unit cell of the Moiré pattern to detect local changes in the electronic structure. To this end, we have investigated silver-capped cobalt islands on a Cu(111) surface.

The growth of silver on bilayer cobalt nanoislands on Cu(111) has recently been investigated [16]. It was found that at room temperature silver preferentially nucleates on top of cobalt islands and that these are either completely capped with 1 ML Ag or remain uncovered. Thus cobalt islands with a closed Ag cap layer can be investigated. It was furthermore found that the low-energy electron diffraction pattern of Ag/Co/Cu(111) shows the same symmetry as Ag/Cu(111), evidence of a similar reconstruction or Moiré pattern due to the lattice mismatch between the silver overlayer and the cobalt island to that between Ag and Cu(111) [17]. The growth and electronic structure of cobalt on Cu(111) are well known: cobalt grows pseudomorphic on Cu(111) and forms triangular islands of bilayer height [20, 21]. The cobalt islands exhibit a very pronounced electronic feature in the local density of states, which can be easily probed by tunneling spectroscopy. This feature has been characterized both experimentally [22, 23] and theoretically [22, 24] and has been shown to be a spin-polarized state related to the d-states of cobalt. The cobalt islands are found to expose a stable out-of-plane magnetization at 14 K [23].

Scanning tunneling microscopy (STM) measurements have been performed in a purpose-built low-temperature ultra-high vacuum (UHV) STM which operates at 6 K. Tunneling spectra have been acquired with an open feedback loop recording the $\mathrm{d}I/\mathrm{d}V$ signal from a lock-in amplifier (frequency 3.8 kHz and 3 mV modulation). For spectroscopic maps, spectra have been taken on a regular grid at each point of the grid. The tip–sample distance has been stabilized at each point and the spectrum has been measured after opening the feedback loop. The Cu(111) single-crystal substrate has been prepared by cycles of argon sputtering and annealing to 800 K. Silver and cobalt have been evaporated from a commercial electron-beam heated evaporator. To prevent ions from the deposition source from hitting the sample and damaging it, either a counter-voltage or a high voltage on a deflection shield has been applied.

A typical topography after deposition of a sub-monolayer coverage of cobalt and subsequently silver at room temperature is shown in figure 1. The Ag-capped Co island exhibits a Moiré pattern due to the lattice mismatch between the silver overlayer and the cobalt island. The apparent corrugation of the Moiré pattern amounts to 0.4 Å at a bias of 100 mV, but varies only a little in the range ±1 V around the Fermi level. Three distinct points of high symmetry can be found as marked in figure 2(b). By comparison with the Moiré pattern formed by

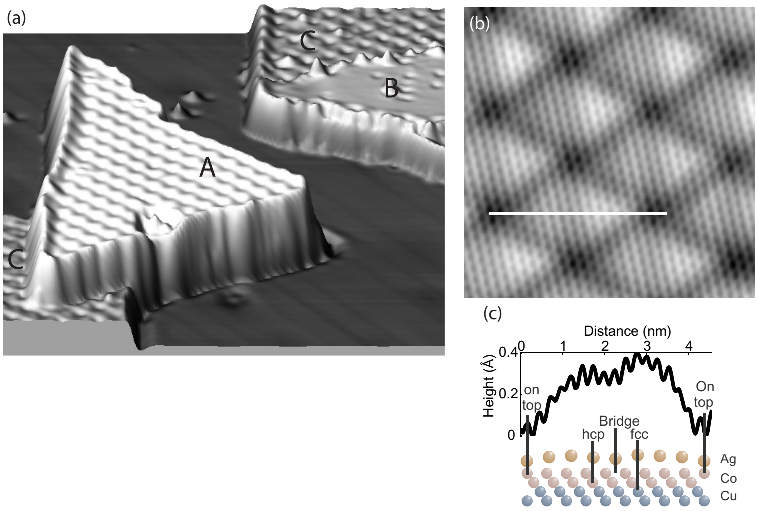

Figure 1. (a) Overview STM topography (54 × 54 nm^2) showing triangular cobalt islands either capped with Ag (**A**) or free of Ag (**B**). Ag directly on Cu(111) (**C**) can also be seen next to the islands. (b) Close-up image of an Ag-covered bilayer high Co island on Cu(111) acquired with a bias voltage of 50 mV [25]. (c) Line cut through the topography in (b) with an atomic model of the Moiré pattern along the same cut. The model is a sketch to illustrate the positions of the atoms and some of the atoms are therefore omitted for clarity.

silver on Cu(111), as well as by symmetry arguments, we can assign these to the silver atoms sitting in fcc, hcp and on-top sites of the underlying cobalt island. Calculations for the Moiré pattern of Ag on Cu(111) [26, 27] reveal in agreement with experiments [17] that the vertical positions of the silver atoms above the substrate are modulated with the periodicity of the Moiré pattern, i.e. the surface is reconstructed. It turns out that the silver atoms in on-top sites of the substrate are the ones that exhibit the strongest displacement towards the surface and are also imaged with the smallest apparent height by STM. The silver-covered cobalt islands expose a strong spectroscopic feature in tunneling spectroscopy similar to that of bare cobalt islands on Cu(111) [22]. This feature is shown in comparison with that of an uncovered cobalt island in figure 2(a). The peak position shifts towards the Fermi energy when going from a bare cobalt island to a silver-covered one and the peak energy depends on where in the Moiré pattern the spectrum is measured; fcc, hcp or on-top. This can be seen from the point spectra in figure 2(b). The designation of the positions is explained in the model in figure 1(c) and defines whether the Ag atoms of the overlayer reside in on-top, fcc or hcp positions of the two cobalt layers. Furthermore, a second peak (labelled peak B in figure 2(b)) appears with lower or comparable amplitude depending on the position in the Moiré pattern. It becomes evident that the two peaks exhibit their maximum amplitude at different locations. No similarly position-dependent feature is found on the Moiré pattern formed by silver on Cu(111), where only the onset of the

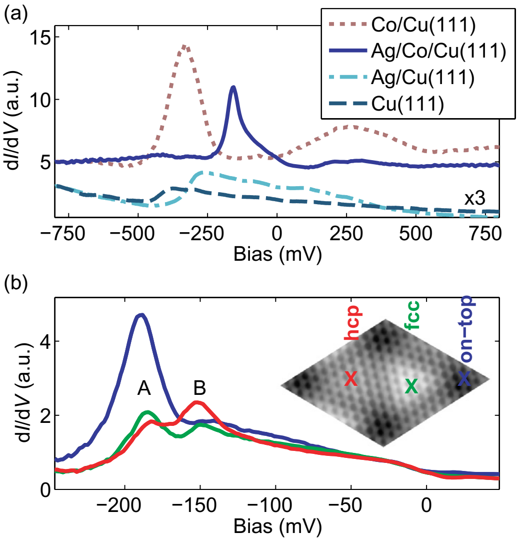

Figure 2. (a) Spectra acquired on the bare Cu(111) surface, on Ag-covered Cu(111) on cobalt islands on Cu(111) and on an Ag-covered cobalt island on Cu(111) in the on-top site. The spectra are normalized at −800 mV, the spectra for Cu(111) and Ag/Cu(111) are stretched vertically by a factor of 3 and the spectra for Co/Cu(111) and Ag/Co/Cu(111) are vertically displaced. (b) Spectra on the fcc, hcp and on-top positions in the Moiré pattern formed by the silver cap layer on a cobalt island on Cu(111).

delocalized two-dimensional (2D) surface state of Cu(111) is shifted towards the Fermi energy by the silver overlayer, as can be seen in figure 2(a) [17]–[19]. Thus we conclude that both features stem from the cobalt island underneath the silver layer.

In order to gain insight into the local modifications of the electronic structure and the origin of the two peaks, we have acquired spectroscopic maps of the silver-covered cobalt islands. For the spectroscopic maps, spectra have been taken at each point of a grid of 64×64 lattice points. These maps, consisting of $\approx$4000 spectra, allow a detailed analysis of the behavior of the two features as a function of position in the Moiré pattern. We used a set point bias value of +50 mV to stabilize the tip in each position. In this region above the Fermi level there is only very little corrugation in the local density of states (LDOS) across the unit cell, which could otherwise influence the amplitude distribution of the spectra across the surface. For the analysis, we have fitted the two peaks by the sum of two Lorentzians and a slowly varying background consisting of another two Lorentzians, which are much wider and have a smaller peak height compared to those describing peaks A and B (see figure 3(a)). Each spectrum in a map has been fitted by this function, allowing us to analyze the behavior of the two peaks separately. We have also attempted to describe the background by a polynomial up to the sixth order, which however did not describe the data as well.

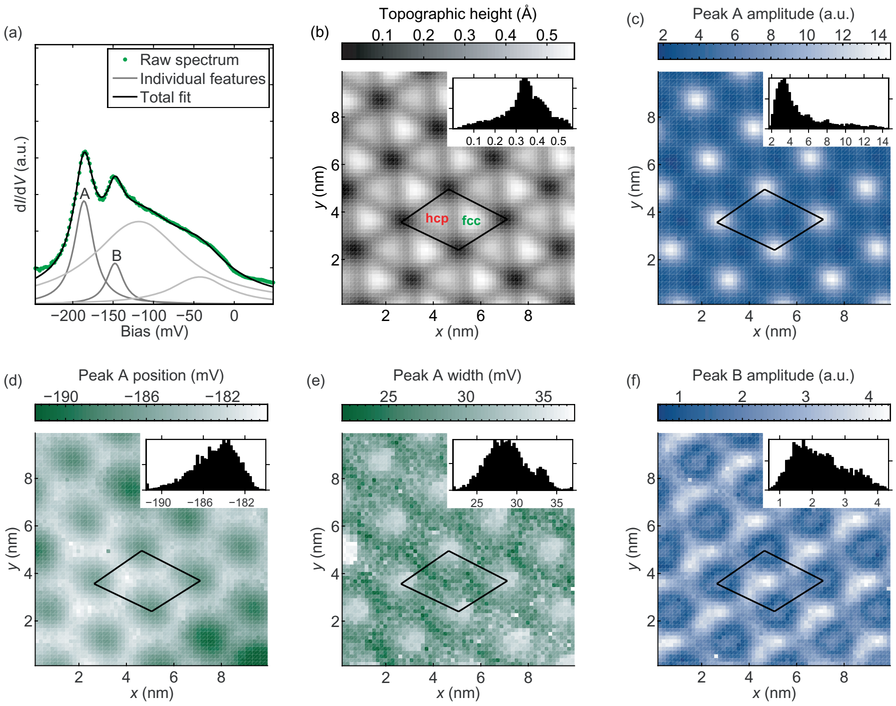

Figure 3. (a) An example fit to a spectrum acquired at an fcc site of the Moiré pattern. The fit function consists of two Lorentzians to describe the two pronounced peaks at −150 and −180 mV plus two broader Lorentzians to account for the background. (b) Topographic image of the area in which the spectroscopic map has been acquired from which the following maps have been extracted. (c) Map of the amplitude of the lower energy peak (A) as extracted from the spectra acquired at each position in the shown area. (d) Map of the energy position and (e) of the FWHM. (f) Amplitude of the higher energy peak (B). The inset in each panel shows a histogram of the respective quantity. All data maps consist of 64 × 64 points.

The images in figures 3(b)–(f) display the topography and the maps resulting from the analysis of the spectroscopy map. Figure 3(c) shows the amplitude distribution of the lower energy peak (peak A) as a function of position within the Moiré pattern. It is evident that the amplitude of the peak is strongly enhanced in on-top positions. Figures 3(d) and (e) show the energy position and width of the peak. Both turn out to be correlated with the morphology of the Moiré pattern. The peak position shifts by up to 10 mV between fcc and on-top positions, whereas the full-width at half-maximum (FWHM) varies between 24 and 35 mV. The amplitude map of the higher energy peak (peak B) shown in figure 3(f) also exhibits a modulation with the periodicity of the Moiré pattern. However, in contrast to the lower energy peak (peak A) its maxima appear in positions that correspond to silver atoms in hcp positions of the cobalt island[5]. The parameters of the two Lorentzians which describe the background of the tunneling spectra are only weakly correlated with the topography. The strong peak found in the tunneling spectrum on bare cobalt islands is a d_{z^2}-state of the cobalt [22], hence the strong peaks on the silver-covered cobalt islands can be assumed to be derived from this d_{z^2}-state. This is supported by the fact that a spectrum on a monolayer of silver on Cu(111), which forms a very similar Moiré pattern if deposited at low temperature, does not show a similar feature in the tunneling spectrum (cf the spectra in figure 2(a)). Instead of only one strong peak as on the cobalt islands we find two peaks on the Ag-covered cobalt islands. The amplitude of the one at lower energy is directly anti-correlated with the apparent height and shows a huge increase in the $\mathrm{d}I/\mathrm{d}V$ signal; by more than a factor of two in on-top sites compared to the adjacent fcc and hcp regions. The strong increase in amplitude in on-top sites (see figure 3(c)) means that the wave function extends much further into the vacuum at these sites. It is therefore likely to have substantial overlap with wave functions of atomic or molecular adsorbates and could play an important role in bond formation at the surface. The peak is fairly narrow with a FWHM of only 24–35 mV, which is much narrower than the d-resonance of the bare cobalt island, which is 100 mV wide [22]. The peak found at higher energy has its maximum amplitude in positions where the silver atoms occupy hcp sites of the cobalt island. From symmetry arguments, this amplitude distribution cannot be rationalized by the presence of only two layers, the silver layer and the upper cobalt layer, where fcc and hcp cannot be defined for the silver atoms. Thus the difference between the spectra at the two positions as seen in figure 3(f) must be related to the influence of the lower cobalt layer, i.e. we ascribe this state to the inner interfacial layer at the Co/Cu interface. Note that a modulation of the morphology does not necessarily lead to a spatial modulation in the electronic structure. We have also measured spectroscopic maps on Ag/Cu(111), where a similar Moiré pattern as on Ag/Co/Cu(111) is seen. The electronic structure across the unit cell shows only very weak variations (roughly an order of magnitude smaller corrugation in the LDOS), which we mainly attribute to a setpoint effect.

As can be seen from figure 3(d), the lower energy peak is shifting down in energy at positions where atoms in the silver adlayer are imaged at a lower height, while it is moving towards higher energies when the topography shows a larger apparent height. This finding becomes more evident from a two-dimensional histogram (see figure 4(a)), in which the energy of the peak is plotted against the apparent height from the topography. The darkness of each pixel in the histogram represents the number of occurrences within the spectroscopic map of the specific combination of peak energy and height. Although there is some scatter, a clear trend can be observed. We find a similar correlation between the width of the peak and the apparent height as that displayed in figure 4(b). For lower apparent height, meaning the silver atoms are closer to the substrate, we observe a larger width of the peak. We note that also for the reversed case, cobalt grown on an Ag(111) surface, a Moiré pattern with a similar periodicity but reversed contrast in the topography is observed [28]. In this case, we see a similar behavior of the cobalt-related peak [29]. The behavior observed in the correlation plots can be rationalized by the so-called d-band model originally developed by Ruban *et al* [2] to explain the reactivity of bimetallic surfaces. In their model, the d-band center of an adlayer shifts away from the Fermi energy with increased hybridization, with the bulk sp-bands to maintain a constant occupation

---

[5] The pattern could come from the topography as the hcp and fcc sites are imaged with different heights. We made sure that the same contrast is observed in quantities that do not depend on the setup condition [33].

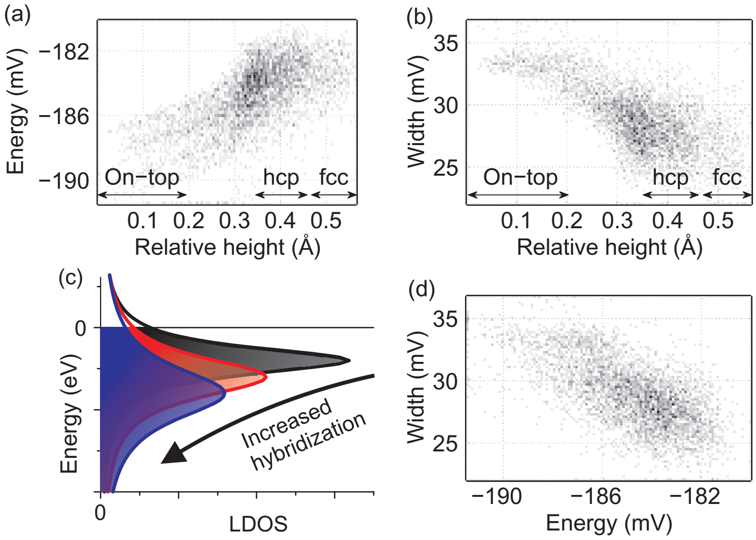

Figure 4. (a) 2D histogram of the energy position of peak A against the height extracted from figures 3(d) and (a), (b) 2D histogram of the FWHM of peak A against the height extracted from figures 3(e) and (a). (c) Sketch of the model by Ruban and coworkers [2] for a *d*-band hybridizing with the *sp*-states of a host metal. (d) 2D histogram of the FWHM against the energy position. The histogram shows a trend consistent with the model by Ruban and coworkers.

of the *d*-band (cf sketch in figure 4(c)). Specifically, the model proposes a linear relationship between the energy position of the *d*-band center and the width of the *d*-band. Transferred to our system, we apply the model to the d_{z^2}-state which is found in tunneling spectra. If we hypothesize that the hybridization between the cobalt *d*-states and the silver *sp*-states increases with the silver atoms moving closer to the cobalt layer, as evident from the measured lower apparent height of the silver adlayer (see figure 1(c)), the peak should get wider due to the increased hybridization and move further away from the Fermi energy. This is consistent with the correlation plots displayed in figures 4(a) and (b). To allow a direct comparison, in figure 4(d) the correlation between energy position and width of state is shown. A trend that is consistent with the model discussed above is found, where the state shifts away from the Fermi energy as it becomes wider. Note that the amplitude of the measured spectra does not follow the model sketch of figure 4(c), where a decrease in amplitude with increasing hybridization is expected. In figure 3(c) it can be seen that the amplitude increases at the on-top sites where the hybridization is strongest. Although the LDOS at the Ag–Co interface may behave as in figure 4(c), the difference to the measured spectra at the surface–vacuum interface could be explained by a decrease in distance between tip and Co-layer, but also by varying tunneling matrix elements across the unit cell originating from the varying atomic geometries of the first layers (see figure 1(c)). These would affect the amplitude but not the energy position or width of the resonance.

The formation of Moiré patterns is observed for a number of metallic heteroepitaxial systems with a lattice mismatch between the substrate and the deposited material (see e.g. [5, 17, 28]). It can be expected that quite generally a modulation of the electronic structure occurs in these systems similar to the one reported here. For example, we have also investigated Co islands on Ag(111) [29], where we have observed similar effects to those found on Ag/Co/Cu(111). We thus believe that our results can be generalized by varying the metal adlayer on top of the Co, but also expect to see similar effects in other metallic Moiré systems. This is also corroborated by the recently observed correlations between morphology and electronic structure in non-metallic Moiré systems like FeO(111), NaCl/Ag(100), boron nitride/Rh(111) and graphene/Ru(0001) [9], [11]–[15].

The observed modulation of the cobalt-related d-state invoked by the silver adlayer can be expected to result in a modulation of the local reactivity at the surface due to the change in the energy position, but also due to the spill-out of the state towards the vacuum making it more accessible for adsorbates. It should be mentioned that the observed changes in energy position on the order of tens of mV are most likely too small to significantly change the reactivity [4], and the variation in amplitude is therefore expected to be more important for this particular system. Besides the interesting local modifications of reactivity of these nanostructures, we can expect to observe modulations of the spin density across the surface. If some of the elements in the multilayered structures are magnetic and involve spin-polarized electronic states, a variation in local density of states will lead to a modulation of magnetic properties. The effects of the modulation can range from a locally modulated spin polarization at the Fermi energy to complicated spin structures. Such influences on magnetic properties have been discussed in terms of a modulation of the density of states by quasiparticle scattering from subsurface defects [30], or by the interaction of an overlayer with a substrate [31]. Since the prominent resonance found on bare cobalt islands is known both from theory [22] and spin sensitive STM measurements [23] to be spin polarized and of minority spin character, the magnetic properties of the cobalt/silver heterostructure will be modulated on a nanometer scale. This might be useful for the fabrication of novel magnetic phases or the self-assembly of ordered arrays of magnetic nanostructures or molecules [8, 32].

In conclusion, we have shown how the deposition of a metallic adlayer can modulate the electronic landscape of a heterostructured interface consisting of Ag/Co/Cu(111). By spectroscopic mapping of the local density of states we measure the electronic structure of the silver-capped cobalt nanoislands on Cu(111). We observe a modulation of the energy position, width and amplitude of the cobalt d-state which is correlated directly with the morphology of the silver Moiré pattern. Analysis of the amplitude distribution of the electronic states allows us to relate them to the inner and outer cobalt interface layers. By choosing a different metallic Moiré system, we expect that it is possible to shape the periodicity of the potential energy landscape.

References

[1] Nørskov J K, Bligaard T, Rossmeisl J and Christensen C H 2009 *Nat. Chem.* **1** 37
[2] Ruban A *et al* 1997 *J. Mol. Catal.* A **115** 421
[3] Gauthier Y *et al* 2001 *Phys. Rev. Lett.* **87** 036103
[4] Hammer B and Nørskov J K 1995 *Nature* **376** 238
[5] Müller U *et al* 1992 *Phys. Rev.* B **46** 12899
[6] Brune H, Röder H, Boragno C and Kern K 1994 *Phys. Rev.* B **49** 2997

[7] Brune H, Giovannini M, Bromann K and Kern K 1998 *Nature* **394** 451
[8] Barth J V, Costantini G and Kern K 2005 *Nature* **437** 671
[9] Nilius N, Rienks E D L, Rust H-P and Freund H-J 2005 *Phys. Rev. Lett.* **95** 066101
[10] N'Diaye A T, Bleikamp S, Feibelman P J and Michely T 2006 *Phys. Rev. Lett.* **97** 215501
[11] Berner S *et al* 2007 *Angew. Chem. Int. Ed. Engl.* **46** 5115
[12] Pivetta M, Patthey F, Stengel M, Baldereschi A and Schneider W-D 2005 *Phys. Rev.* B **72** 115404
[13] Marchini S, Günther S and Wintterlin J 2007 *Phys. Rev.* B **76** 075429
[14] Vázques de Parga A L *et al* 2008 *Phys. Rev. Lett.* **100** 056807
[15] Wang B, Bocuet M-L, Marchini S, Günther S and Wintterlin J 2008 *Phys. Chem. Chem. Phys.* **10** 3530
[16] Bork J, Onsgaard J and Diekhöner L 2009 arXiv:0904.4170 [cond.-mat]
[17] Bendounan A *et al* 2003 *Europhys. Lett.* **64** 392
[18] Wessendorf M *et al* 2004 *Appl. Phys.* A **78** 183
[19] Bendounan A *et al* 2005 *Phys. Rev.* B **72** 075407
[20] de al Figuera J, Prieto J E, Ocal C and Miranda R 1993 *Phys. Rev.* B **47** 13043
[21] Negulyaev N N *et al* 2008 *Phys. Rev.* B **77** 125437
[22] Diekhöner L *et al* 2003 *Phys. Rev. Lett.* **90** 236801
[23] Pietzsch O, Kubetzka A, Bode M and Wiesendanger R 2004 *Phys. Rev. Lett.* **92** 057202
[24] Barral M A, Weissmann M and Llois A M 2005 *Phys. Rev.* B **72** 125433
[25] Horcas I *et al* 2007 *Rev. Sci. Instrum.* **78** 013705
[26] Foiles S 1993 *Surf. Sci.* **292** 5
[27] Meunier I, Tréglia G, Gay J-M, Aufray B and Legrand B 1999 *Phys. Rev.* B **59** 10910
[28] Morgenstern K, Kibsgaard J, Lauritsen J, Lægsgaard E and Besenbacher F 2007 *Surf. Sci.* **601** 1967
[29] Bork J, Wahl P, Diekhöner L and Kern K 2009 unpublished
[30] Weismann A *et al* 2009 *Science* **323** 1190
[31] von Bergmann K *et al* 2006 *Phys. Rev. Lett.* **96** 167203
[32] Gambardella P *et al* 2009 *Nat. Mater.* **8** 189
[33] Kohsaka Y *et al* 2008 *Nature* **454** 1072

Technical Setup

E

E.1 Aalborg STM

STM and LEED measurements for the article in appendix A and STM measurements for the article in appendix C are carried out at the Omicron STM at the Department of Physics and Nanotechnology, Aalborg University in Denmark. The system consist of a standard UHV chamber (base pressure $1 \cdot 10^{-11}$ mbar) with separated preparation and analysis chamber containing a sputter gun with neon gas, annealing possibilities, E-beam evaporator from Oxford Scientific, two mass spectrometers for different mass-ranges, a combined LEED/Auger system and a variable-temperature STM with tip-exchange from Omicron.

E.2 Aarhus synchrotron

ARPES and LEED measurements for the articles in appendices B and C are done at the SGM-1 beamline [126] at the ASTRID synchrotron at the Institute of Storage Ring Facilities, Aarhus University in Denmark. The monochromator for the beamline gives a usable energy range from 30 eV to 400 eV and the end station is a RT-UHV chamber with separated preparation and analysis chamber. The preparation chamber contains a sputter gun, LEED optics, mass spectrometer and the same E-beam evaporator as in the Aalborg STM (installed when needed). The analysis chamber contains access to the synchrotron radiation as well as an Mg-K_α X-ray tube and a Scienta 200 mm mean radius spherical electron analyser (Scienta SES-200) with a channelplate detector.

E.3 Stuttgart 4K–STM

The STM/S measurements done for the article in appendix D and for chapter 4 are done at the 4K–STM at the Nanoscale Science Department, MPI-FKF in Stuttgart, Germany. It is a UHV chamber split in a preparation and analysis chamber with a 4 K cryostat containing a home-build STM head.

The preparation chamber contains an argon sputter gun, sample annealing and cooling to ∼50 K, a mass spectrometer and two single Omicron evaporators together with the possibility to mount an extra evaporator on the load lock. In the analysis chamber, the cryostat is a liquid helium cryostat with a liquid nitrogen shield and a 5 T superconducting magnet perpendicular to the sample. The STM head allows for direct optical access to the sample so single Co atoms can be evaporated from a Co wire wound around a tungsten wire onto the sample at 15–20 K.

The operating temperature of the STM head is 6–8 K and the hold time of the cryostat is limited by the nitrogen shield to maximum 40 hours.

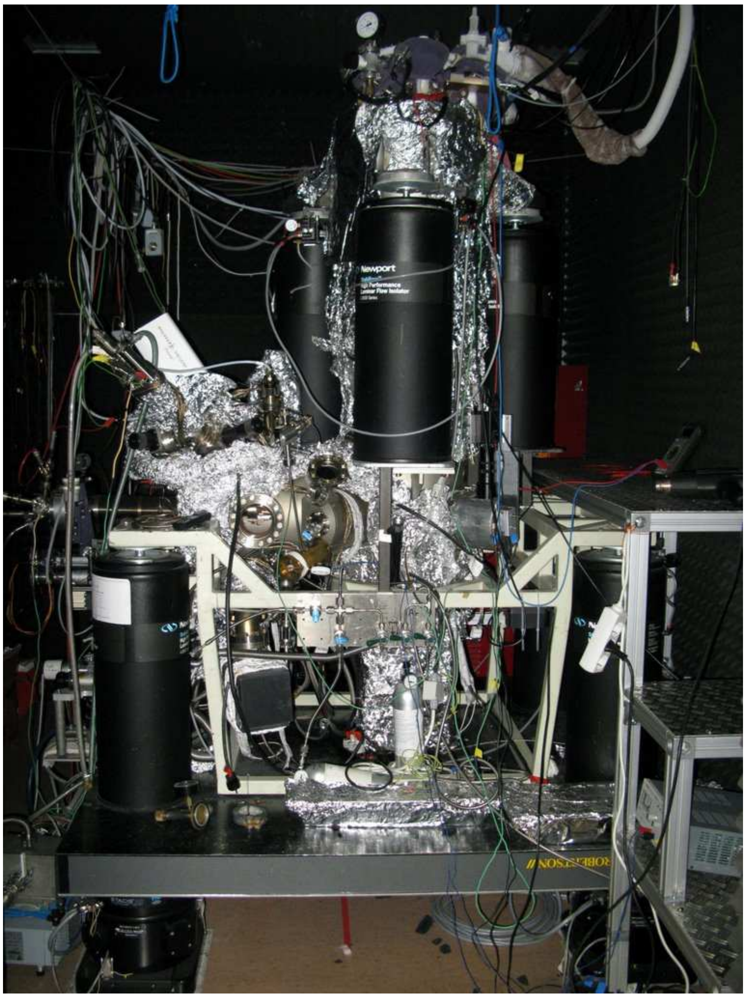

Figure E.1: The 4K–STM in MPI-FKF Stuttgart